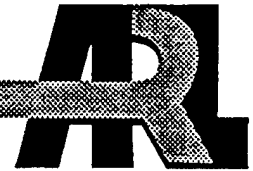


**ARMY RESEARCH LABORATORY**



**EOSAEL92  
Aerosol Phase Function  
Data Base PFNDAT**

**By**

**D. H. Tofsted, B. T. Davis,  
A. E. Wetmore, J. Fitzgerrel,  
R. C. Shirkey, and R. A. Sutherland**

**Battlefield Environment Directorate**

**ARL-TR-273-9**

**June 1997**

**[DTIC QUALITY INSPECTED 8]**

Approved for public release; distribution unlimited.

**19970902 100**

## **NOTICES**

### **Disclaimers**

The findings in this report are not to be construed as an official Department of the Army position, unless so designated by other authorized documents.

The citation of trade names and names of manufacturers in this report is not to be construed as official Government indorsement or approval of commercial products or services referenced herein.

| REPORT DOCUMENTATION PAGE   |  | Form Approved<br>OMB No. 0704-0188              |                            |
|---|--|---|----------------------------|
| <p>Public reporting burden for this collection of information is estimated to average 1 hour per response, including the time for reviewing instructions, searching existing data sources, gathering and maintaining the data needed, and completing and reviewing the collection of information. Send comments regarding this burden estimate or any other aspect of this collection of information, including suggestions for reducing the burden to Washington Headquarters Services, Directorate for Information Operations and reports, 1215 Jefferson Davis Highway, Suite 1204, Arlington, VA 22202-4302 and to the Office of Management and Budget, Paperwork Reduction Project (0704-0188), Washington, DC 20503.</p>  |  |   |                            |
| 1. AGENCY USE ONLY (Leave Blank)  | 2. REPORT DATE                           | 3. REPORT TYPE AND DATES COVERED                |                            |
|   | June 30, 1995                            | Final August 1993 - June 1995                   |                            |
| 4. TITLE AND SUBTITLE   |  | 5. FUNDING NUMBERS                              |                            |
| EOSAEL 92, Aerosol Phase Function Data Base PFNDAT  |  |   |                            |
| 6. AUTHOR(S)  |  |   |                            |
| T. H. Tofsed, B. T. Davis, A. E. Wetmore, J. Fitzgerrel,<br>R. C. Shirkey, and R. A. Sutherland   |  |   |                            |
| 7. PERFORMING ORGANIZATION NAMES(S) AND ADDRESS(E)  |  | 8. PERFORMING ORGANIZATION REPORT NUMBER        |                            |
| U.S. Army Research Laboratory<br>Battlefield Environment Directorate<br>ATTN: AMSRL -BE-S<br>White Sands Missile Range, NM 88002-5513   |  | ARL-TR-273-9                                    |                            |
| 9. SPONSORING/MONITORING AGENCY NAMES(S) AND ADDRESS(E)   |  | 10. SPONSORING/ MONITORING AGENCY REPORT NUMBER |                            |
| U.S. Army Research Laboratory<br>2800 Powder Mill Road<br>Adelphi, MD 20783-1145  |  |   |                            |
| 11. SUPPLEMENTARY NOTES   |  |   |                            |
| 12a. DISTRIBUTION/AVAILABILITY STATEMENT  |  | 12b. DISTRIBUTION CODE                          |                            |
| Approved for public release; distribution unlimited   |  | A   |                            |
| 13. ABSTRACT (Maximum 200 words)  |  |   |                            |
| <p>The Electro-Optical Systems Atmospheric Effects Library (EOSAEL) Phase Function DATabase (PFNDAT) consists of a series of phase functions and extinction and scattering coefficient data for 30 naturally occurring and 8 manmade aerosols associated with the near surface atmosphere. These phase functions are useful in characterizing the near surface atmosphere for propagation and scattering studies where typical scattering species are required. Models using this database include several EOSAEL modules. The naturally occurring aerosols consist of the maritime, urban, and rural aerosol sizedistributions at eight relative humidities each, two fog distributions, three rain distributions, and one snow distribution. The manmade aerosols consist of three dust types and five smoke types. The dusts include a high-explosive dust distribution and light and heavy loading dust distributions. The smokes consist of white phosphorous results for three different relative humidities; hexachloroethane; and fog oil smoke. The database includes information at a variety of wavelengths for each scattering species (dependent on availability of index of refraction data). Wavelengths range from 0.35 to 40.0 <math>\mu\text{m}</math>. This report contains brief descriptions of the aerosol size distribution characteristics, aerosol index of refraction data used to generate the phase functions, information on the contents of the PFNDAT database, and graphs of the phase functions. This version of PFNDAT improves on the original database by increasing the resolution of visible band phase function results. Previous versions only included a 0.55 <math>\mu\text{m}</math> result. Improvements in the AGAUS code used to generate the Mie scattering results used has also resulted in more accurate phase functions.</p> |  |   |                            |
| 14. SUBJECT TERMS   |  | 15. NUMBER OF PAGES                             |                            |
| aerosols, scattering, phase function, transmission  |  | 124   |                            |
| 16. PRICE CODE  |  |   |                            |
| 17. SECURITY CLASSIFICATION OF REPORT   | 18. SECURITY CLASSIFICATION OF THIS PAGE | 19. SECURITY CLASSIFICATION OF ABSTRACT         | 20. LIMITATION OF ABSTRACT |
| UNCLASSIFIED  | UNCLASSIFIED                             | UNCLASSIFIED                                    | SAR                        |

## PREFACE

The Electro-Optical Systems Atmospheric Effects Library (EOSAEL) was developed to assist the characterization of the battlefield environment. One component of that characterization focuses on the quantification of the scattering properties of various natural boundary-layer aerosols, battlefield dusts, and inventory smoke munitions. This report documents the improved aerosol scattering phase property data incorporated in the 1992 version of EOSAEL.

The aerosol phase function database (PFNDAT) is a continuation of previous phase function databases released with the 1980, 1982, and 1987 versions of EOSAEL (c.f., Duncan (ed.), 1980; Shirkey et al., 1987).

## ABSTRACT

The Electro-Optical Systems Atmospheric Effects Library (EOSAEL) Phase Function DATabase (PFNDAT) consists of a series of phase functions and extinction and scattering coefficient data for 30 naturally occurring and 8 manmade aerosols associated with the near surface atmosphere. These phase functions are useful in characterizing the near surface atmosphere for propagation and scattering studies where typical scattering species are required. Models using this database include several EOSAEL modules. The naturally occurring aerosols consist of the maritime, urban, and rural aerosol size distributions at eight relative humidities each, two fog distributions, three rain distributions, and one snow distribution. The manmade aerosols consist of three dust types and five smoke types. The dusts include a high-explosive dust distribution and light and heavy loading dust distributions. The smokes consist of white phosphorus results for three different relative humidities; hexachloroethane; and fog oil smoke. The database includes information at a variety of wavelengths for each scattering species (dependent on availability of index of refraction data). Wavelengths range from 0.35 to 40.0  $\mu\text{m}$ . This report contains brief descriptions of the aerosol size distribution characteristics, aerosol index of refraction data used to generate the phase functions, information on the contents of the PFNDAT database, and graphs of the phase functions. This version of PFNDAT improves on the original database by increasing the resolution of visible band phase function results. Previous versions only included a 0.55  $\mu\text{m}$  result. Improvements in the AGAUS code used to generate the Mie scattering results used has also resulted in more accurate phase functions.

**This page left intentionally blank.**

# CONTENTS

|   |     |
|---|-----|
| PREFACE . . . . .                                       | 1   |
| EXECUTIVE SUMMARY . . . . .                             | 9   |
| 1. INTRODUCTION . . . . .                               | 11  |
| 1.1 PFNDAT Overview . . . . .                           | 11  |
| 1.2 Availability . . . . .                              | 13  |
| 1.2.1 Mailing Address . . . . .                         | 13  |
| 1.2.2 Phone and Electronic Mail . . . . .               | 13  |
| 2. TECHNICAL DOCUMENTATION . . . . .                    | 15  |
| 2.1 EOSAEL Application – PFNDAT . . . . .               | 15  |
| 2.1.1 Phase Function Production . . . . .               | 16  |
| 2.1.2 Particle Size Distribution Models Used . . . . .  | 17  |
| 2.2 Maritime, Urban, and Rural Aerosol Models . . . . . | 19  |
| 2.3 Fog Models . . . . .                                | 23  |
| 2.4 Rain and Snow Models . . . . .                      | 23  |
| 2.5 Dust Aerosol Models . . . . .                       | 26  |
| 2.6 Aerosol Smoke Models . . . . .                      | 31  |
| 2.7 EOSAEL92 Improvements . . . . .                     | 35  |
| 3. USER'S GUIDE . . . . .                               | 37  |
| 3.1 Introduction . . . . .                              | 37  |
| 3.2 Usage . . . . .                                     | 37  |
| 3.3 Structure . . . . .                                 | 37  |
| REFERENCES . . . . .                                    | 41  |
| ACRONYMS and ABBREVIATIONS . . . . .                    | 45  |
| APPENDICES . . . . .                                    | 47  |
| Appendix A. Indices of Refraction . . . . .             | 47  |
| Appendix B. Graphs . . . . .                            | 59  |
| Appendix C. EOSAEL Modules . . . . .                    | 99  |
| DISTRIBUTION . . . . .                                  | 101 |

**This page left intentionally blank.**

# FIGURES

|   |    |
|---|----|
| 1. Measured/modeled snow distribution. . . . .                | 26 |
| B-1. Maritime aerosol, 0 percent relative humidity . . . . .  | 60 |
| B-2. Maritime aerosol, 50 percent relative humidity . . . . . | 61 |
| B-3. Maritime aerosol, 70 percent relative humidity . . . . . | 62 |
| B-4. Maritime aerosol, 80 percent relative humidity . . . . . | 63 |
| B-5. Maritime aerosol, 90 percent relative humidity . . . . . | 64 |
| B-6. Maritime aerosol, 95 percent relative humidity . . . . . | 65 |
| B-7. Maritime aerosol, 98 percent relative humidity . . . . . | 66 |
| B-8. Maritime aerosol, 99 percent relative humidity . . . . . | 67 |
| B-9. Urban aerosol, 0 percent relative humidity . . . . .     | 68 |
| B-10. Urban aerosol, 50 percent relative humidity . . . . .   | 69 |
| B-11. Urban aerosol, 70 percent relative humidity . . . . .   | 70 |
| B-12. Urban aerosol, 80 percent relative humidity . . . . .   | 71 |
| B-13. Urban aerosol, 90 percent relative humidity . . . . .   | 72 |
| B-14. Urban aerosol, 95 percent relative humidity . . . . .   | 73 |
| B-15. Urban aerosol, 98 percent relative humidity . . . . .   | 74 |
| B-16. Urban aerosol, 99 percent relative humidity . . . . .   | 75 |
| B-17. Rural aerosol, 0 percent relative humidity . . . . .    | 76 |
| B-18. Rural aerosol, 50 percent relative humidity . . . . .   | 77 |
| B-19. Rural aerosol, 70 percent relative humidity . . . . .   | 78 |
| B-20. Rural aerosol, 80 percent relative humidity . . . . .   | 79 |
| B-21. Rural aerosol, 90 percent relative humidity . . . . .   | 80 |
| B-22. Rural aerosol, 95 percent relative humidity . . . . .   | 81 |
| B-23. Rural aerosol, 98 percent relative humidity . . . . .   | 82 |
| B-24. Rural aerosol, 99 percent relative humidity . . . . .   | 83 |
| B-25. Fog (heavy advection) . . . . .                         | 84 |
| B-26. Fog (moderate radiation) . . . . .                      | 85 |
| B-27. Rain (drizzle) . . . . .                                | 86 |
| B-28. Rain (widespread) . . . . .                             | 87 |

|   |    |
|---|----|
| <b>B-29.</b> Rain (thunderstorm) . . . . .                                    | 88 |
| <b>B-30.</b> Snow . . . . .   | 89 |
| <b>B-31.</b> Dust (light aerosol loading) . . . . .                           | 90 |
| <b>B-32.</b> Dust (heavy aerosol loading) . . . . .                           | 91 |
| <b>B-33.</b> Dust (high explosive (HE)) . . . . .                             | 92 |
| <b>B-34.</b> Smoke (white phosphorus), 17 percent relative humidity . . . . . | 93 |
| <b>B-35.</b> Smoke (white phosphorus), 50 percent relative humidity . . . . . | 94 |
| <b>B-36.</b> Smoke (white phosphorus), 90 percent relative humidity . . . . . | 95 |
| <b>B-37.</b> Smoke (fog oil), 50 percent relative humidity . . . . .          | 96 |
| <b>B-38.</b> Smoke (hexachloroethane), 85 percent relative humidity . . . . . | 97 |

# TABLES

|     |  |    |
|-----|--|----|
| 1.  | Mode radii ( $\mu\text{m}$ ), spread, and number densities ( $\text{cm}^{-3}$ ) as functions of relative humidity for the small (S) and large (L) modes of the AFGL maritime haze aerosol model. . . . . | 20 |
| 2.  | Extinction coefficients ( $\text{km}^{-1}$ ) versus wavelength ( $\mu\text{m}$ ) for the maritime aerosol model. . . . .   | 20 |
| 3.  | Mode radii ( $\mu\text{m}$ ), spread, and number densities ( $\text{cm}^{-3}$ ) as functions of relative humidity for the small (S) and large (L) modes of the AFGL urban haze aerosol model. . . . .    | 21 |
| 4.  | Extinction coefficients ( $\text{km}^{-1}$ ) versus wavelength ( $\mu\text{m}$ ) for the urban aerosol model. . . . .  | 21 |
| 5.  | Mode radii ( $\mu\text{m}$ ), spread, and number densities ( $\text{cm}^{-3}$ ) as functions of relative humidity for the small (S) and large (L) modes of the AFGL rural haze aerosol model. . . . .    | 22 |
| 6.  | Extinction coefficients ( $\text{km}^{-1}$ ) versus wavelength ( $\mu\text{m}$ ) for the rural aerosol model. . . . .  | 22 |
| 7.  | Liquid water content ( $\mu\text{g}/\text{m}^3$ ) as functions of relative humidity for small mode, large mode, and total content for rural, urban, and maritime aerosols. . . . .                       | 23 |
| 8.  | Extinction coefficients ( $\text{km}^{-1}$ ) versus wavelength ( $\mu\text{m}$ ) for various fogs. . . . .   | 24 |
| 9.  | Liquid water content ( $\mu\text{g}/\text{m}^3$ ) as a function of the type of precipitation. . . . .  | 24 |
| 10. | Extinction coefficients ( $\text{km}^{-1}$ ) versus wavelength ( $\mu\text{m}$ ) for various natural aerosol models. . . . .   | 27 |
| 11. | Values of lognormal particle size distribution parameters (mode radius $r_g$ and geometric standard deviation $\sigma_g$ ). . . . .  | 28 |
| 12. | Real ( $n$ ) and imaginary ( $k$ ) indices of refraction for light dust constituents ammonium sulfate and carbon. . . . .  | 29 |
| 13. | Real ( $n$ ) and imaginary ( $k$ ) indices of refraction for heavy dust constituents quartz and montmorillonite. . . . .   | 29 |
| 14. | Derived real ( $n$ ) and imaginary ( $k$ ) indices of refraction for high explosive dust. . . . .  | 30 |
| 15. | Extinction coefficients ( $\text{km}^{-1}$ ) versus wavelength ( $\mu\text{m}$ ) for various manmade aerosol models. . . . .   | 31 |

|  |    |
|--|----|
| <b>16.</b> Representative parameters for determining phase functions of inventory smokes at various relative humidities. . . . .   | 32 |
| <b>17.</b> Real ( <i>n</i> ) and imaginary ( <i>k</i> ) indices of refraction for the smoke aerosol models at indicated relative humidities. . . . .   | 33 |
| <b>18.</b> Comparison of theoretical (from the AGAUS model) and experimentally measured (Exp) mass extinction coefficients ( $m^2/g$ ) at 50 percent relative humidity for various smoke aerosols. . . . . | 34 |
| <b>19.</b> Average single-scattering albedo for the inventory smokes as calculated by AGAUS. . . . .   | 34 |
| <b>20.</b> Phase function data base for EOSAEL92. . . . .  | 38 |
| <b>21.</b> Structure for aerosol phase function data file PFNDAT.nnn. . . . .  | 40 |
| <b>A-1.</b> Index of refraction as a function of relative humidity (0-80 percent) for small urban aerosols. . . . .  | 48 |
| <b>A-2.</b> Index of refraction as a function of relative humidity (90-99 percent) for small urban aerosols. . . . .   | 49 |
| <b>A-3.</b> Index of refraction as a function of relative humidity (0-80 percent) for large urban aerosols. . . . .  | 50 |
| <b>A-4.</b> Index of refraction as a function of relative humidity (90-99 percent) for large urban aerosols. . . . .   | 51 |
| <b>A-5.</b> Index of refraction as a function of relative humidity (0-80 percent) for small rural aerosols. . . . .  | 52 |
| <b>A-6.</b> Index of refraction as a function of relative humidity (90-99 percent) for small rural aerosols. . . . .   | 53 |
| <b>A-7.</b> Index of refraction as a function of relative humidity (0-80 percent) for large rural aerosols. . . . .  | 54 |
| <b>A-8.</b> Index of refraction as a function of relative humidity (90-99 percent) for large rural aerosols. . . . .   | 55 |
| <b>A-9.</b> Index of refraction as a function of relative humidity (0-80 percent) for oceanic aerosols. . . . .  | 56 |
| <b>A-10.</b> Index of refraction as a function of relative humidity (90-99 percent) for oceanic aerosols. . . . .  | 57 |

# EXECUTIVE SUMMARY

## Introduction

The Aerosol Phase Function Database (PFNDAT) is the primary repository of aerosol scattering property data provided within the Electro-Optical Systems Atmospheric Effects Library (EOSAEL). EOSAEL is designed to provide detailed atmospheric effects models of the battlefield environment. Often these environmental effects include the influences of extinction, absorption, and scattering due to aerosols. The PFNDAT database provides the necessary information to characterize a wide variety of battle-induced and natural aerosols. Included in this collection are data sets describing the three main classes of hazes (rural, maritime, and urban) at varying relative humidity levels. Two types of fog (radiation and advection) are provided. Rain properties are provided at three precipitation rates (drizzle (1 mm/h), moderate (5 mm/h), and heavy (10 mm/h)). One class of snow is considered, along with several battlefield induced contaminants: Dusts are treated under three categories: light, heavy advection, and high explosive munition caused. Inventory smokes include white phosphorus at three relative humidities, hexachloroethane, and fog oil.

## Purpose

Providing scattering information in a database format allows aerosol scattering species to be used within larger radiative transfer models without large runtime calculational costs. The Mie scattering codes used to assess the scattering properties of these aerosols require long processing times. When preprocessed, the resulting propagation characteristics can readily be used within the radiative transfer codes under a variety of conditions without again incurring these costs. Several EOSAEL modules require input from PFNDAT to perform radiative transfer calculations. Also, aerosols are often mixed, requiring a weighted addition of multiple scattering species.

## Overview

Previous versions of PFNDAT have focused on characterizing scattering properties within infrared (IR) bands associated with midband and far IR sensor systems. The current calculations extend the previous results to a higher resolution in the visible band, and extend the IR calculations to  $40\text{ }\mu\text{m}$ . This allows PFNDAT results to be used in other radiative transfer applications such as for solar loading and energy balance calculations.

An updated version of the AGAUS Mie scattering routine was also used in the calculations. This model was introduced to improve the accuracy of forward scattered radiation predictions for large size parameter aerosols.

Documentary improvements include additional tables detailing the net aerosol densities used in the phase function calculations, tables of the real and imaginary indices of refraction used in the calculations, and an updated snow particle size distribution.

## Conclusions

The PFNDAT database is an accurate description of aerosol scattering properties of a wide range of particulates to be encountered on the dirty battlefield. This upgraded version provides significantly more resolution and detail concerning these aerosols of interest to Army systems developers and radiative transfer specialists than previous editions.

# 1. INTRODUCTION

## 1.1 PFNDAT Overview

The propagation of electro-magnetic energy within the Earth's atmosphere depends on the wavelength of the radiation and on the nature of the medium being traversed. This medium consists of various molecular species and aerosol particles. In this report we describe the nature of a particular set of aerosol scatterer classes related to near-ground propagation issues relevant to the Army.

To characterize an aerosol species we must be able to identify the number, size, shape, composition, and distribution of the aerosol particles. In general a given aerosol species will consist of a statistical distribution of particle sizes and mean real and imaginary indices of refraction. Some species are considered to be composed of weighted sums of more than one particle type, as in the case of various dusts.

Once the nature of the scatterer particles is known, a model can be used to determine the effect of this species on atmospheric propagation. However, in general it is not realistic to rely on the direct properties of the scattering species in most radiative transfer models. Instead, an intermediate procedure is used. This procedure determines the overall scattering properties of each class of scatterer. Since each atmospheric constituent scatters or absorbs the incident radiation according to its own properties, and the incident radiation may have been previously scattered by another constituent, in order to make the atmospheric propagation problem tractable, a preprocessing step is often needed where the single scattering properties of a class are determined. These single scattering results can then be used in the more general code to determine multiple scattering problems.

To evaluate the single scattering properties of a given scattering species a number of simplifying assumptions are often made:

- The particles are assumed spaced far enough apart that radiation scattered by one particle does not affect how radiation is scattered from another particle. Each scattering event is therefore independent.
- A Mie scattering code is assumed valid for predicting the behavior of each scattering species. The usage of a Mie scattering method assumes that the particles can be approximated as spherical in shape. This assumption is often made even for nonspherical particles, since in most cases the orientation of the particles is random because no external influences such as strong

magnetic fields or hydrodynamic forces are present. Orientation averaging then produces nearly the same result as the assumption of sphericity.

- The scattering properties of a given type of particulate distribution can be represented by a weighted integral over the particle size distribution. This approach is dependent on the assumption of independent scattering above.
- The particulate size distribution divided by the density (though not necessarily the density itself) is constant over the volume concerned.

Having preprocessed the scattering properties of various aerosol species, one can then accurately describe the scattering and absorption of radiation of a given wavelength as it passes through the atmosphere. The relevant information needed to determine these radiation results includes the angular scattering probability distribution, the volume extinction coefficient ( $\beta$ ), and the single scattering albedo ( $\varpi$ ). The volume extinction coefficient  $\beta$  that determines the attenuation of the incident radiation, is composed of two parts:

- a scattering coefficient  $\beta_s$ , that describes the radiation scattered out of the line of sight (LOS) without a change in wavelength
- the absorption coefficient  $\beta_a$  that describes the amount of radiation along the LOS converted into other forms of energy or that undergoes a change in wavelength.

These two quantities are related to  $\beta$  and  $\varpi$  by

$$\varpi = \beta_s / (\beta_s + \beta_a), \quad \beta_s = \varpi \beta, \quad \beta_a = (1 - \varpi) \beta. \quad (1)$$

$\varpi$  represents the probability that interacting radiation will be scattered rather than absorbed: for pure scattering,  $\varpi = 1$ ; for total absorption,  $\varpi = 0.0$ . The angular scattering distribution (the phase function) gives the directional distribution of radiation scattered by the aerosol under consideration: the phase function  $P$  is proportional to the probability that incoming radiation that scatters is scattered through an angle  $\theta$  into an element of solid angle  $d\Omega$ . The phase function for incident unpolarized radiation used here is normalized as,

$$\begin{aligned} \frac{1}{4\pi} \int_{4\pi} P(\theta) d\Omega &= \frac{1}{4\pi} \int_0^{2\pi} d\phi \int_0^\pi P(\theta) \sin(\theta) d\theta \\ &= \frac{1}{2} \int_0^\pi P(\theta) \sin(\theta) d\theta \\ &= 1.0, \end{aligned} \quad (2)$$

where  $\theta$  is the scattering angle.

## **1.2 Availability**

EOSAEL is available to U.S. Government Agencies, specified allied organizations, and their authorized contractors at no cost. U.S. Government agencies needing EOSAEL should send a letter of request, signed by a branch chief or division director, to the U.S. Army Research Laboratory (ARL). Contractors should have their Government contract monitor send the letter of request. Allied nation organizations must request EOSAEL through their national representative. Please include, within security restrictions, a short description of your intended use(s).

Release of EOSAEL requires a Memorandum of Agreement (MOA) between ARL and the recipient's organization. We will send an MOA to you for signature, when you return that to us we sign it and return a copy of the MOA to you. EOSAEL is currently distributed through the DoD TECNET facility; this Test and Evaluation Community NETwork system is located at Patuxent River Maryland. If you do not already have an account on TECNET we will sponsor an account for you and include an application for you to fill out. Return the application to ARL and we will complete the account application process for you. You will receive information about how to log onto the TECNET (through the Internet, or dial-up) directly from TECNET. If you need additional help locating or downloading EOSAEL files after you get your account, contact ARL.

On TECNET, the EOSAEL source code, DOS executables, sample input and output files are available. Documentation for the modules is included as postscript files suitable for viewing or printing.

Specific technical questions concerning PFNDAT should be directed to David Tofsted at U.S. Army Research Laboratory, (505) 678-3039 commercial and 258-3039 DSN, or via e-mail at dtosted@arl.mil.

The EOSAEL point of contact at ARL is Dr. Alan Wetmore.

### ***1.2.1 Mailing Address***

U.S. Army Research Laboratory  
ATTN: AMSRL-IS-ES (Dr. Wetmore)  
2800 Powder Mill Road  
Adelphi, MD 20783-1197

### ***1.2.2 Phone and Electronic Mail***

COM:(301) 394-2499  
FAX:(301) 394-4797  
DSN: 290-2499  
email:awetmore@arl.mil

**This page left intentionally blank.**

## 2. TECHNICAL DOCUMENTATION

### 2.1 EOSAEL Application – PFNDAT

The Electro-Optical Systems Atmospheric Effects Library (EOSAEL) is a coordinated set of databases and models that allow for characterization of numerous atmospheric effects on electro-optical systems. Because of the pervasive nature of aerosol scattering effects in all aspects of propagation problems, and due to the desire to not have to compute atmospheric scattering properties on a case-by-case basis, it is reasonable to accumulate a collection of scattering phase functions for a wide variety of atmospheric conditions in one place. The collection is called PFNDAT, the Phase Function DATabase. PFNDAT contains many commonly encountered aerosol types within the atmospheric boundary layer, including the main haze aerosols (rural, urban, and maritime), two classes of fog (radiative and advective), as well as precipitation classes (drizzle, rain, and one type of snow) and battlefield induced contaminant aerosols (fog oil, hexachloroethane (HC), white phosphorous (WP), and dusts). This set covers the scattering effects of the majority of cases of aerosols encountered by the Army within the near surface environment, up to approximately 1000 m above ground level. Various scattering models for upper air aerosols (most cloud types) are not included in this database; databases developed by the Air Force address this area.

As a result of the development of this common database, many models utilize PFNDAT as model input. Some EOSAEL modules use the volume extinction coefficients to determine transmission along lines of sight; two EOSAEL modules (the Approximate Multiple Scattering Module (ASCAT) and the Finite CLOUD contrast transmission module (FCLOUD)) deal with aspects of the scattered radiation and therefore use the phase function information. The Weather and Atmospheric Visualization Effects for Simulation suite of codes accesses the PFNDAT phase function and extinction information when computing scattering effects in the Boundary Layer Illumination and Radiation Balance radiative transfer model.

Scattering results for 38 different aerosol distributions have been included in the data base to cover the aerosol environments expected for Army purposes. The extinction coefficients and phase functions produced were generated with the computer code AGAUS (Miller 1983), that uses the classical Mie scattering theory approach.

Phase functions and extinction coefficients for the fogs, rains, snow, and maritime, urban and rural aerosols were generated at wavelengths of 0.35, 0.40,

0.45, 0.50, 0.55, 0.60, 0.65, 0.70, 0.75, 1.06, 3.0, 3.5, 4.0, 4.5, 5.0, 8.0, 8.5, 9.0, 9.5, 10.0, 10.5, 11.0, 11.5, 12.0, 14.0, 16.0, 18.0, 20.0, 25.0, 30.0, 35.0, and 40.0  $\mu\text{m}$ . The manmade aerosols were generated at wavelengths of 0.55, 1.06, 3.0, 3.5, 4.0, 4.5, 5.0, 8.0, 8.5, 9.0, 9.5, 10.0, 10.5, 11.0, 11.5, and 12.0  $\mu\text{m}$ . The phase functions were computed at 65 angles spaced unequally between 0.0 and 180.0 degrees. The selection of output angles for each aerosol case provides more values of the phase function in which the variation is most rapid, particularly in the forward and backward peak directions ( $0^\circ$  and  $180^\circ$ , respectively). The phase functions for all of the distributions described here are presented graphically in appendix B.

### 2.1.1 Phase Function Production

The following symbology and terms are used in the remainder of this report. The calculation of phase function information for natural aerosols usually entails a combination of effects from more than one scattering substance type, for which each type may have its own relative density distribution and refractive index properties. For example, dusts are composed of various component quantities of quartz, montmorillonite, and ammonium sulfate particles. Each particle type has a particulate bulk density  $\rho$  (in units of  $\text{g}/\text{cm}^3$ ) for a given volume of the scattering substance. However, each species must also be characterized by a given mass concentration  $C$ , also given in units of density ( $\text{g}/\text{cm}^3$ ), representing the weight of lofted material mixed within a unit volume of air.  $C$  is often referred to by the term liquid water content from a meteorological standpoint. The term mass concentration is used to describe both effects in this text.

Relating the quantities  $\rho$  and  $C$ , the particle size distribution is denoted by  $n(r)$ , where  $r$  is the radius of a particle (using Mie theory all particles are considered spherical). The total number of particles per unit volume is denoted by the number density  $N$ , which relates to the particle size distribution through

$$N = \int_0^\infty n(r) \, dr; \quad n(r) = \frac{dN}{dr}. \quad (3)$$

$n(r)$  has units of particles per  $\text{cm}^3\text{-}\mu\text{m}$ .

Writing the mass concentration as a function of the particle size distribution,

$$C = \int n(r) \frac{4}{3} \pi r^3 \rho \, dr, \quad (4)$$

where  $(4/3)\pi r^3 \rho$  is the mass of a particle of radius  $r$ .

The particle size distributions are comprised of the Air Force Geophysics Laboratory (AFGL) maritime, urban, and rural models at relative humidities of 0, 50, 70, 80, 90, 95, 98, and 99 percent, the AFGL fog models for heavy advection and radiation types (Shettle and Fenn 1979); three rain models (drizzle, widespread, and thunderstorm), a snow model, moderate and heavy

aerosol dust models, a high-explosive (HE) dust model, and three smoke types. The WP smoke type is calculated at three relative humidities (17, 50, and 90 percent). The rain models use the Marshall-Palmer (MP) distribution based on the work of Marshall and Palmer (1948). The snow and fog models use the modified gamma (MG) distribution. The smoke distributions are lognormal. The dust, rural, urban, and maritime distributions are bimodal lognormal (large and small particle component lognormal distributions).

### 2.1.2 Particle Size Distribution Models Used

The following aerosol particle size distributions are used in evaluating the phase functions contained in the PFNDAT database.

#### Marshall-Palmer Rain Distribution

The MP distribution is given in the AGAUS documentation (The 1982 AGAUS documentation lists  $B$  incorrectly as  $8.2 \times 10^{-4}$ , while the value in equation (5) is consistent with Pruppacher and Klett (1980).) by the equation

$$n(r) = \frac{dN}{dr} = A \exp(-Br) \quad (5)$$

$$A = 1.6 \times 10^{-5} \text{ cm}^{-3} \mu\text{m}^{-1}, \quad (6)$$

$$B = 8.2 \times 10^{-3} R^{-0.21} \mu\text{m}^{-1}, \quad (7)$$

where  $R$  is the rain rate in mm/hr. Using this form and equation (3) yields the relationship,

$$N = A/B = 1951 \times 10^{-6} R^{0.21} \text{ cm}^{-3}. \quad (8)$$

The mass concentration for this distribution is given by,

$$C = \frac{8\pi\rho A}{B^4} = 8\pi\rho \frac{N}{B^3} = 89 \times 10^{-3} R^{0.84} \text{ g/m}^3, \quad (9)$$

where  $\rho = 1 \text{ g/cm}^3$  is used for the bulk density of water.

#### Modified Gamma Distribution

The modified gamma (MG) distribution is given in Shettle and Fenn (1979) by the equation

$$n(r) = \frac{dN}{dr} = Ar^\alpha \exp[-br^\gamma], \quad (10)$$

where  $A$ ,  $b$ ,  $\alpha$  and  $\gamma$  are fit coefficients of the distribution.  $A$  has units of number of particles per cubic centimeter per  $\mu\text{m}^{\alpha+1}$ . A similar equation is used by AGAUS:

$$n(r) = \frac{dN}{dr} = r_c r^\alpha \exp\left[\frac{-\alpha}{\gamma}\left(\frac{r}{r_c}\right)^\gamma\right], \quad (11)$$

where  $b$  must equal  $\alpha/(\gamma r_c^\gamma)$  to convert from the form of the exponential argument in equation (10) to the form in equation (11).

Equation (11) is the distribution contained within the AGAUS program. The equation in the 1983 AGAUS documentation incorrectly contained an  $r$  instead of a  $\gamma$  in the denominator of the first term of the exponential argument. However this equation is in error, since it does not contain any particle density dependence as in Pruppacher and Klett (1980). A direct integration of the particle size distribution, using definition 3.478.1 from Gradshteyn and Ryzhik (1980), allows us to substitute a function for  $A$ , which depends on  $N$ ,  $b$ ,  $\alpha$ , and  $\gamma$ . The resulting equation matches that listed in Pruppacher and Klett (1980):

$$N = \int_0^\infty n(r) dr \quad (12)$$

$$= A \int_0^\infty dr r^\alpha \exp(-b r^\gamma) \quad (13)$$

$$= A \frac{b^{-\vartheta}}{\gamma} \Gamma(\vartheta); \quad \vartheta = \frac{\alpha+1}{\gamma}. \quad (14)$$

Solving this equation for  $A$  and substituting the function in  $r_c$ ,  $\alpha$ , and  $\gamma$  for  $b$ , a new equation for the particle size distribution equation is obtained,

$$n(r) = \frac{dN}{dr} = A' \left( \frac{r}{r_c} \right)^\alpha \exp \left[ \frac{-\alpha}{\gamma} \left( \frac{r}{r_c} \right)^\gamma \right], \quad (15)$$

where,

$$A' = \frac{N}{r_c} \frac{\gamma \left( \frac{\alpha}{\gamma} \right)^\vartheta}{\Gamma(\vartheta)}. \quad (16)$$

The mass concentration for this distribution can be expressed by

$$C = \frac{4}{3} \pi \rho N r_c^3 \frac{\Gamma[\vartheta + (3/\gamma)]}{\left( \frac{\alpha}{\gamma} \right)^{3/\gamma} \Gamma(\vartheta)}. \quad (17)$$

### Lognormal Distribution

The lognormal distribution is given in Shettle and Fenn (1979) by the equation

$$n(r) = \frac{dN}{dr} = \left[ \frac{N}{\ln(10) r \sqrt{2\pi} \sigma_{SF}} \right] \exp \left[ -\frac{(\log_{10} r - \log_{10} r_g)^2}{2 \sigma_{SF}^2} \right]. \quad (18)$$

$N$  is the aerosol particle number density (particles per cm<sup>3</sup>),  $r_g$  is the distribution geometric mean radius (or mode radius) in  $\mu\text{m}$ , and  $\sigma_{SF}$  is the width of the distribution measured in  $\log_{10}$  space.

A similar equation is used for the lognormal distribution in the AGAUS program, but with a different meaning for the  $\sigma$  term. In AGAUS

$$n(r) = \frac{dN}{dr} = \left[ \frac{N}{r \sqrt{2\pi} \ln(\sigma_g)} \right] \exp \left[ -\frac{(\ln r - \ln r_g)^2}{2 \ln(\sigma_g)^2} \right], \quad (19)$$

where  $\sigma_g$  is called the geometric mean standard deviation. The relationship between  $\sigma_g$  and  $\sigma_{SF}$  is

$$\sigma_{SF} = \log_{10}(\sigma_g); \quad \sigma_{SF} \ln(10) = \ln(\sigma_g). \quad (20)$$

The above lognormal distribution equation is correct for the code contained within the AGAUS program. (The equation contained in the 1983 AGAUS documentation was missing the appropriate normalization terms. Perhaps this is intentional, since AGAUS appears to use a different method of normalization.) The mass concentration equation for this distribution is given by

$$C = \frac{4}{3} \pi \rho N r_g^3 \exp \left[ \frac{9}{2} (\ln \sigma_g)^2 \right]. \quad (21)$$

## 2.2 Maritime, Urban, and Rural Aerosol Models

The maritime, urban, and rural aerosol models are identical to those found in Shettle and Fenn (1979) and are bimodal lognormal, with the mode radius varying as a function of relative humidity. The rural aerosol model consists of small and large rural distributions with correspondingly different indices of refraction. Similarly, the urban aerosol model consists of small and large urban distributions. The maritime aerosol model consists of the small rural distribution along with a large particle continental oceanic distribution.

The indices of refraction for the individual aerosols are in Appendix A.

The number densities (rounded) for each mode of the distribution type along with the mode radius and variance data, the resulting extinction coefficient data, and the related liquid water content information are provided for the user who may wish to change the visibilities. The number density, mode radius ( $r_g$ ), and variance ( $\sigma_g$ ) information for the maritime aerosols are contained in table 1 and the extinction data is contained in table 2. The same information for the urban aerosols is in tables 3 and 4. The same information for the rural aerosols is contained in tables 5 and 6. The liquid-water-content (mass concentration) data is contained in table 7. The latter information is derived using equation (21) for each aerosol type. The extinction coefficients in these tables were generated for a 5.0-km visibility, with number densities corresponding to those found in tables 8 through 10 of Shettle and Fenn (1979).

Table 1. Mode radii ( $\mu\text{m}$ ), spread, and number densities ( $\text{cm}^{-3}$ ) as functions of relative humidity for the small (S) and large (L) modes of the AFGL maritime haze aerosol model.

| Qty            | Relative Humidity(%) |         |         |         |         |         |         |         |
|----------------|----------------------|---------|---------|---------|---------|---------|---------|---------|
|                | 0                    | 50      | 70      | 80      | 90      | 95      | 98      | 99      |
| $N$ (S)        | 38251                | 35129   | 27757   | 13902   | 9697    | 6976    | 4360    | 2948    |
| $N$ (L)        | 386.4                | 354.8   | 280.4   | 140.4   | 98.0    | 70.5    | 44.0    | 29.8    |
| $r_g$ (S)      | 0.02700              | 0.02748 | 0.02846 | 0.03274 | 0.03884 | 0.04238 | 0.04751 | 0.05215 |
| $r_g$ (L)      | 0.1600               | 0.1711  | 0.2041  | 0.3180  | 0.3803  | 0.4606  | 0.6024  | 0.7505  |
| $\sigma_g$ (S) | 2.239                | 2.239   | 2.239   | 2.239   | 2.239   | 2.239   | 2.239   | 2.239   |
| $\sigma_g$ (L) | 2.512                | 2.512   | 2.512   | 2.512   | 2.512   | 2.512   | 2.512   | 2.512   |

Table 2. Extinction coefficients ( $\text{km}^{-1}$ ) versus wavelength ( $\mu\text{m}$ ) for the maritime aerosol model

| $\lambda$<br>( $\mu\text{m}$ )      | Relative Humidity(%) |         |         |        |        |        |        |        |
|-------------------------------------|----------------------|---------|---------|--------|--------|--------|--------|--------|
|                                     | 0                    | 50      | 70      | 80     | 90     | 95     | 98     | 99     |
| 0.35                                | 0.9605               | 0.9499  | 0.9163  | 0.8549 | 0.8582 | 0.8412 | 0.8217 | 0.8117 |
| 0.40                                | 0.8991               | 0.8953  | 0.8700  | 0.8257 | 0.8325 | 0.8200 | 0.8045 | 0.7970 |
| 0.45                                | 0.8530               | 0.8478  | 0.8341  | 0.8057 | 0.8078 | 0.8018 | 0.7925 | 0.7872 |
| 0.50                                | 0.8083               | 0.8076  | 0.7969  | 0.7849 | 0.7874 | 0.7861 | 0.7797 | 0.7780 |
| 0.55                                | 0.7696               | 0.7718  | 0.7711  | 0.7691 | 0.7714 | 0.7721 | 0.7695 | 0.7694 |
| 0.60                                | 0.7324               | 0.7383  | 0.7439  | 0.7581 | 0.7566 | 0.7569 | 0.7565 | 0.7600 |
| 0.65                                | 0.7049               | 0.7105  | 0.7201  | 0.7414 | 0.7425 | 0.7494 | 0.7540 | 0.7576 |
| 0.70                                | 0.6768               | 0.6867  | 0.6977  | 0.7285 | 0.7306 | 0.7397 | 0.7531 | 0.7571 |
| 0.75                                | 0.6559               | 0.6596  | 0.6743  | 0.7208 | 0.7216 | 0.7301 | 0.7398 | 0.7460 |
| 1.06                                | 0.5430               | 0.5566  | 0.5946  | 0.6738 | 0.6783 | 0.6995 | 0.7198 | 0.7321 |
| 3.00                                | 0.3265               | 0.3414  | 0.3900  | 0.5236 | 0.5541 | 0.5992 | 0.6563 | 0.6881 |
| 3.50                                | 0.2410               | 0.2618  | 0.3234  | 0.4937 | 0.5325 | 0.5975 | 0.6742 | 0.7248 |
| 4.00                                | 0.2119               | 0.2273  | 0.2747  | 0.4271 | 0.4700 | 0.5397 | 0.6301 | 0.6943 |
| 4.50                                | 0.1917               | 0.2040  | 0.2440  | 0.3815 | 0.4242 | 0.4950 | 0.5902 | 0.6621 |
| 5.00                                | 0.1631               | 0.1747  | 0.2119  | 0.3436 | 0.3879 | 0.4594 | 0.5598 | 0.6368 |
| 8.00                                | 0.07913              | 0.08616 | 0.1096  | 0.2003 | 0.2377 | 0.2974 | 0.3930 | 0.4768 |
| 8.50                                | 0.09768              | 0.1018  | 0.1177  | 0.1902 | 0.2215 | 0.2751 | 0.3646 | 0.4464 |
| 9.00                                | 0.1207               | 0.1229  | 0.1317  | 0.1844 | 0.2099 | 0.2564 | 0.3369 | 0.4147 |
| 9.50                                | 0.09504              | 0.09732 | 0.1067  | 0.1586 | 0.1828 | 0.2266 | 0.3023 | 0.3761 |
| 10.00                               | 0.08018              | 0.08099 | 0.08988 | 0.1371 | 0.1592 | 0.1981 | 0.2671 | 0.3350 |
| 10.50                               | 0.06671              | 0.06866 | 0.07741 | 0.1206 | 0.1403 | 0.1741 | 0.2340 | 0.2935 |
| 11.00                               | 0.05683              | 0.05982 | 0.07113 | 0.1186 | 0.1379 | 0.1704 | 0.2240 | 0.2767 |
| 11.50                               | 0.05261              | 0.05690 | 0.07234 | 0.1295 | 0.1981 | 0.1848 | 0.2382 | 0.2878 |
| 12.00                               | 0.04529              | 0.05268 | 0.07668 | 0.1519 | 0.2072 | 0.2165 | 0.2747 | 0.3276 |
| 14.00                               | 0.03274              | 0.04895 | 0.09399 | 0.2116 | 0.2488 | 0.2992 | 0.3717 | 0.4335 |
| 15.00                               | 0.03824              | 0.05470 | 0.1002  | 0.2208 | 0.2596 | 0.3126 | 0.3881 | 0.4526 |
| 18.00                               | 0.05800              | 0.07020 | 0.1070  | 0.2184 | 0.2571 | 0.3125 | 0.3944 | 0.4654 |
| 20.00                               | 0.05147              | 0.06235 | 0.09504 | 0.1968 | 0.2338 | 0.2882 | 0.3709 | 0.4448 |
| 25.00                               | 0.04225              | 0.05017 | 0.07445 | 0.1557 | 0.1880 | 0.2369 | 0.3152 | 0.3886 |
| 30.00                               | 0.04105              | 0.04662 | 0.06401 | 0.1265 | 0.1534 | 0.1956 | 0.2667 | 0.3361 |
| 35.00                               | 0.04729              | 0.05128 | 0.06379 | 0.1120 | 0.1336 | 0.1696 | 0.2321 | 0.2950 |
| 40.00                               | 0.06735              | 0.07085 | 0.07976 | 0.1150 | 0.1320 | 0.1631 | 0.2195 | 0.2773 |
| Number density ( $\text{cm}^{-3}$ ) | 38637                | 35484   | 28037   | 14042  | 9795   | 7047   | 4404   | 2978   |

Table 3. Mode radii ( $\mu\text{m}$ ), spread, and number densities ( $\text{cm}^{-3}$ ) as functions of relative humidity for the small (S) and large (L) modes of the AFGL urban haze aerosol model.

| Qty            | Relative Humidity(%) |         |         |         |         |         |         |         |
|----------------|----------------------|---------|---------|---------|---------|---------|---------|---------|
|                | 0                    | 50      | 70      | 80      | 90      | 95      | 98      | 99      |
| $N$ (S)        | 87204                | 83354   | 64829   | 42776   | 27693   | 18217   | 10516   | 7286    |
| $N$ (L)        | 10.9                 | 10.4    | 8.1     | 5.4     | 3.5     | 2.3     | 1.3     | 0.9     |
| $r_g$ (S)      | 0.02500              | 0.02563 | 0.02911 | 0.03514 | 0.04187 | 0.04904 | 0.05996 | 0.06847 |
| $r_g$ (L)      | 0.4000               | 0.4113  | 0.4777  | 0.5805  | 0.7061  | 0.8634  | 1.1690  | 1.4850  |
| $\sigma_g$ (S) | 2.239                | 2.239   | 2.239   | 2.239   | 2.239   | 2.239   | 2.239   | 2.239   |
| $\sigma_g$ (L) | 2.512                | 2.512   | 2.512   | 2.512   | 2.512   | 2.512   | 2.512   | 2.512   |

Table 4. Extinction coefficients ( $\text{km}^{-1}$ ) versus wavelength ( $\mu\text{m}$ ) for the urban aerosol model

| $\lambda$<br>( $\mu\text{m}$ )      | Relative Humidity(%) |         |         |         |         |         |         |         |
|-------------------------------------|----------------------|---------|---------|---------|---------|---------|---------|---------|
|                                     | 0                    | 50      | 70      | 80      | 90      | 95      | 98      | 99      |
| 0.35                                | 1.141                | 1.144   | 1.149   | 1.144   | 1.121   | 1.083   | 1.024   | 0.9800  |
| 0.40                                | 1.031                | 1.032   | 1.036   | 1.034   | 1.018   | 0.9941  | 0.9547  | 0.9254  |
| 0.45                                | 0.9334               | 0.9345  | 0.9358  | 0.9353  | 0.9267  | 0.9133  | 0.8900  | 0.8724  |
| 0.50                                | 0.8473               | 0.8481  | 0.8478  | 0.8489  | 0.8458  | 0.8403  | 0.8280  | 0.8212  |
| 0.55                                | 0.7711               | 0.7717  | 0.7714  | 0.7723  | 0.7714  | 0.7717  | 0.7694  | 0.7704  |
| 0.60                                | 0.7040               | 0.7045  | 0.7029  | 0.7046  | 0.7082  | 0.7112  | 0.7181  | 0.7233  |
| 0.65                                | 0.6453               | 0.6457  | 0.6441  | 0.6463  | 0.6519  | 0.6581  | 0.6707  | 0.6810  |
| 0.70                                | 0.5944               | 0.5946  | 0.5929  | 0.5951  | 0.6004  | 0.6089  | 0.6259  | 0.6398  |
| 0.75                                | 0.5473               | 0.5474  | 0.5459  | 0.5474  | 0.5545  | 0.5645  | 0.5847  | 0.6016  |
| 1.06                                | 0.3632               | 0.3551  | 0.3596  | 0.3571  | 0.3618  | 0.3737  | 0.3982  | 0.4237  |
| 3.00                                | 0.1244               | 0.1311  | 0.1651  | 0.2046  | 0.2317  | 0.2508  | 0.2727  | 0.2909  |
| 3.50                                | 0.1126               | 0.1130  | 0.1147  | 0.1136  | 0.1133  | 0.1168  | 0.1278  | 0.1433  |
| 4.00                                | 0.1042               | 0.1039  | 0.1040  | 0.10053 | 0.09799 | 0.09921 | 0.1069  | 0.1196  |
| 4.50                                | 0.09813              | 0.09782 | 0.09804 | 0.09489 | 0.09248 | 0.09359 | 0.1009  | 0.1130  |
| 5.00                                | 0.09165              | 0.09139 | 0.09138 | 0.08823 | 0.08601 | 0.08713 | 0.09420 | 0.1061  |
| 8.00                                | 0.06710              | 0.06670 | 0.06597 | 0.06451 | 0.06443 | 0.06737 | 0.07621 | 0.08904 |
| 8.50                                | 0.08252              | 0.08175 | 0.07797 | 0.07135 | 0.06749 | 0.06781 | 0.07483 | 0.08690 |
| 9.00                                | 0.09358              | 0.09427 | 0.09569 | 0.08812 | 0.07888 | 0.07437 | 0.07643 | 0.08641 |
| 9.50                                | 0.08207              | 0.08212 | 0.08108 | 0.07400 | 0.06752 | 0.06531 | 0.06965 | 0.08059 |
| 10.00                               | 0.07552              | 0.07544 | 0.07401 | 0.06764 | 0.06196 | 0.05818 | 0.06494 | 0.07559 |
| 10.50                               | 0.07069              | 0.07056 | 0.06899 | 0.06305 | 0.05807 | 0.05637 | 0.06722 | 0.07097 |
| 11.00                               | 0.06619              | 0.06616 | 0.06544 | 0.06122 | 0.05775 | 0.05719 | 0.06193 | 0.07144 |
| 11.50                               | 0.06310              | 0.06328 | 0.06388 | 0.06224 | 0.06110 | 0.06215 | 0.06790 | 0.07733 |
| 12.00                               | 0.06061              | 0.06114 | 0.06405 | 0.06644 | 0.06843 | 0.07007 | 0.07918 | 0.08958 |
| 14.00                               | 0.05348              | 0.05523 | 0.06538 | 0.07757 | 0.08652 | 0.09431 | 0.1058  | 0.1186  |
| 15.00                               | 0.05554              | 0.05754 | 0.06845 | 0.08050 | 0.08904 | 0.09641 | 0.1078  | 0.1207  |
| 18.00                               | 0.05115              | 0.05285 | 0.06236 | 0.07300 | 0.08085 | 0.08786 | 0.09962 | 0.1132  |
| 20.00                               | 0.04961              | 0.05102 | 0.05903 | 0.06741 | 0.07356 | 0.07978 | 0.09083 | 0.1042  |
| 25.00                               | 0.04139              | 0.04256 | 0.04903 | 0.05549 | 0.06048 | 0.06598 | 0.07666 | 0.09000 |
| 30.00                               | 0.03646              | 0.03737 | 0.04237 | 0.04726 | 0.05120 | 0.05611 | 0.06631 | 0.07954 |
| 35.00                               | 0.03348              | 0.03431 | 0.03874 | 0.04279 | 0.04604 | 0.05034 | 0.05984 | 0.07255 |
| 40.00                               | 0.03119              | 0.03206 | 0.03658 | 0.04075 | 0.04403 | 0.04822 | 0.05736 | 0.06971 |
| Number density ( $\text{cm}^{-3}$ ) | 87215                | 83364   | 64837   | 42781   | 27697   | 18219   | 10517   | 7287    |

Table 5. Mode radii ( $\mu\text{m}$ ), spread, and number densities ( $\text{cm}^{-3}$ ) as functions of relative humidity for the small (S) and large (L) modes of the AFGL rural haze aerosol model.

| Qty            | Relative Humidity(%) |         |         |         |         |         |         |         |
|----------------|----------------------|---------|---------|---------|---------|---------|---------|---------|
|                | 0                    | 50      | 70      | 80      | 90      | 95      | 98      | 99      |
| $N$ (S)        | 79076                | 76305   | 70804   | 51674   | 33895   | 27052   | 19290   | 14761   |
| $N$ (L)        | 9.9                  | 9.5     | 8.9     | 6.4     | 4.2     | 3.4     | 2.4     | 1.9     |
| $r_g$ (S)      | 0.02700              | 0.02748 | 0.02846 | 0.03274 | 0.03884 | 0.04238 | 0.04751 | 0.05215 |
| $r_g$ (L)      | 0.4300               | 0.4377  | 0.4571  | 0.5477  | 0.6462  | 0.7078  | 0.9728  | 1.1760  |
| $\sigma_g$ (S) | 2.239                | 2.239   | 2.239   | 2.239   | 2.239   | 2.239   | 2.239   | 2.239   |
| $\sigma_g$ (L) | 2.512                | 2.512   | 2.512   | 2.512   | 2.512   | 2.512   | 2.512   | 2.512   |

Table 6. Extinction coefficients ( $\text{km}^{-1}$ ) versus wavelength ( $\mu\text{m}$ ) for the rural aerosol model

| $\lambda$<br>( $\mu\text{m}$ )      | Relative Humidity(%) |         |         |         |         |         |         |         |
|-------------------------------------|----------------------|---------|---------|---------|---------|---------|---------|---------|
|                                     | 0                    | 50      | 70      | 80      | 90      | 95      | 98      | 99      |
| 0.35                                | 1.201                | 1.200   | 1.199   | 1.187   | 1.153   | 1.135   | 1.091   | 1.063   |
| 0.40                                | 1.071                | 1.071   | 1.069   | 1.062   | 1.039   | 1.027   | 0.9990  | 0.9819  |
| 0.45                                | 0.9571               | 0.9565  | 0.9548  | 0.9534  | 0.9398  | 0.9314  | 0.9153  | 0.9071  |
| 0.50                                | 0.8574               | 0.8572  | 0.8565  | 0.8569  | 0.8509  | 0.8468  | 0.8401  | 0.8376  |
| 0.55                                | 0.7711               | 0.7714  | 0.7711  | 0.7730  | 0.7700  | 0.7714  | 0.7703  | 0.7730  |
| 0.60                                | 0.6958               | 0.6959  | 0.6962  | 0.7009  | 0.7021  | 0.7040  | 0.7092  | 0.7158  |
| 0.65                                | 0.6305               | 0.6306  | 0.6317  | 0.6380  | 0.6419  | 0.6457  | 0.6553  | 0.6655  |
| 0.70                                | 0.5740               | 0.5743  | 0.5755  | 0.5830  | 0.5871  | 0.5922  | 0.6077  | 0.6204  |
| 0.75                                | 0.5216               | 0.5220  | 0.5235  | 0.5327  | 0.5374  | 0.5450  | 0.5631  | 0.5781  |
| 1.06                                | 0.3236               | 0.3235  | 0.3259  | 0.3341  | 0.3400  | 0.3473  | 0.3713  | 0.3936  |
| 3.00                                | 0.08639              | 0.09261 | 0.1069  | 0.1565  | 0.1957  | 0.2127  | 0.2711  | 0.2738  |
| 3.50                                | 0.08051              | 0.08100 | 0.08447 | 0.09481 | 0.09666 | 0.09921 | 0.1290  | 0.1480  |
| 4.00                                | 0.07271              | 0.07427 | 0.07694 | 0.08454 | 0.08379 | 0.08501 | 0.1140  | 0.1321  |
| 4.50                                | 0.07091              | 0.07096 | 0.07344 | 0.08045 | 0.07970 | 0.08070 | 0.1096  | 0.1277  |
| 5.00                                | 0.06524              | 0.06537 | 0.06929 | 0.07443 | 0.07384 | 0.1060  | 0.1278  | 0.1418  |
| 8.00                                | 0.03321              | 0.03382 | 0.03615 | 0.04611 | 0.05052 | 0.05324 | 0.08235 | 0.1018  |
| 8.50                                | 0.06738              | 0.06641 | 0.06620 | 0.06550 | 0.06093 | 0.06045 | 0.08427 | 0.1015  |
| 9.00                                | 0.09769              | 0.09736 | 0.09862 | 0.09676 | 0.08469 | 0.07981 | 0.09496 | 0.1074  |
| 9.50                                | 0.08006              | 0.07931 | 0.07954 | 0.07641 | 0.06736 | 0.06457 | 0.08152 | 0.09548 |
| 10.00                               | 0.07066              | 0.06982 | 0.06999 | 0.06711 | 0.05972 | 0.05765 | 0.07397 | 0.08749 |
| 10.50                               | 0.06362              | 0.06290 | 0.06293 | 0.06039 | 0.05439 | 0.05283 | 0.06768 | 0.08015 |
| 11.00                               | 0.05755              | 0.05697 | 0.05715 | 0.05583 | 0.05204 | 0.05148 | 0.06587 | 0.07790 |
| 11.50                               | 0.05311              | 0.05275 | 0.05330 | 0.05415 | 0.05326 | 0.05414 | 0.06959 | 0.08203 |
| 12.00                               | 0.04982              | 0.04979 | 0.05107 | 0.05560 | 0.05860 | 0.06090 | 0.07946 | 0.09342 |
| 14.00                               | 0.04109              | 0.04244 | 0.04645 | 0.06193 | 0.07334 | 0.07887 | 0.1049  | 0.1226  |
| 15.00                               | 0.04517              | 0.04684 | 0.05142 | 0.06780 | 0.07804 | 0.08297 | 0.1091  | 0.1269  |
| 18.00                               | 0.04798              | 0.04882 | 0.05214 | 0.06436 | 0.07189 | 0.07591 | 0.1028  | 0.1214  |
| 20.00                               | 0.04854              | 0.04918 | 0.05191 | 0.06168 | 0.06675 | 0.06980 | 0.09562 | 0.1138  |
| 25.00                               | 0.03996              | 0.04057 | 0.04289 | 0.05116 | 0.05500 | 0.05744 | 0.08165 | 0.09920 |
| 30.00                               | 0.03542              | 0.03586 | 0.03769 | 0.04416 | 0.04688 | 0.04882 | 0.07092 | 0.08751 |
| 35.00                               | 0.03422              | 0.03452 | 0.03602 | 0.04115 | 0.04292 | 0.04436 | 0.06406 | 0.07938 |
| 40.00                               | 0.03320              | 0.03352 | 0.03499 | 0.03985 | 0.04150 | 0.04286 | 0.06140 | 0.07583 |
| Number density ( $\text{cm}^{-3}$ ) | 79086                | 76315   | 70813   | 51680   | 33899   | 27055   | 19292   | 14763   |

Table 7. Liquid water content ( $\mu\text{g}/\text{m}^3$ ) as functions of relative humidity for small mode, large mode, and total content for rural, urban, and maritime aerosols.

| Aerosol Type | Relative Humidity(%) |       |       |       |        |        |        |        |
|--------------|----------------------|-------|-------|-------|--------|--------|--------|--------|
|              | 0                    | 50    | 70    | 80    | 90     | 95     | 98     | 99     |
| Maritime     |                      |       |       |       |        |        |        |        |
| Small        | 58.7                 | 56.8  | 49.9  | 38.0  | 44.3   | 41.4   | 36.4   | 32.6   |
| Large        | 301.7                | 338.7 | 454.4 | 860.5 | 1027.3 | 1313.0 | 1833.2 | 2400.9 |
| Total        | 360.3                | 395.5 | 504.3 | 898.5 | 1071.6 | 1354.4 | 1869.7 | 2433.5 |
| Urban        |                      |       |       |       |        |        |        |        |
| Small        | 106.2                | 109.4 | 124.6 | 144.7 | 158.4  | 167.5  | 176.7  | 182.3  |
| Large        | 133.0                | 137.9 | 168.3 | 201.3 | 234.8  | 282.1  | 395.8  | 561.7  |
| Total        | 239.2                | 247.3 | 292.9 | 346.0 | 393.3  | 449.6  | 572.5  | 744.0  |
| Rural        |                      |       |       |       |        |        |        |        |
| Small        | 121.3                | 123.4 | 127.2 | 141.3 | 154.8  | 160.5  | 161.2  | 163.2  |
| Large        | 150.0                | 151.8 | 162.0 | 200.4 | 216.0  | 229.8  | 421.1  | 588.9  |
| Total        | 271.3                | 275.3 | 289.2 | 341.7 | 370.8  | 390.3  | 582.3  | 752.1  |

## 2.3 Fog Models

The Shettle and Fenn (1979) data were also used for the heavy advection and radiation fog models. These models use the MG distribution, and their extinction coefficients are given in table 8 for wavelengths of 0.35 to 40.0  $\mu\text{m}$ . For heavy (advection) fog, the mode radius was 10.0  $\mu\text{m}$ , with a number density of 20 particles/cm<sup>3</sup>,  $\alpha$  was set to 3, and  $\gamma$  was set to 1; for radiation fog, the mode radius was 2.0  $\mu\text{m}$ , with a number density of 200 particles/cm<sup>3</sup>,  $\gamma$  was again set to 1, and  $\alpha$  was set to 6. The equivalent mass concentrations for these two distributions are in table 9 along with the rain and snow results from the following section. Other details may be found in Shettle and Fenn (1979).

## 2.4 Rain and Snow Models

Particle sizes of rain and snow generally are quite large compared to visible and infrared wavelengths, making Mie calculations to determine phase functions impractical. According to Hodkinson and Greenleaves (1963), when the airborne particles of an aerosol species are larger than a few wavelengths of the radiation being transmitted and a range of particle sizes or wavelengths exists, the combined single-scattering characteristics may be approximated by a combination of Fraunhofer diffraction and geometrical transmission and reflection. While studying light scattering by irregular particles larger than the wavelength (such as snow), Hodkinson (1963) found that, although the diffraction patterns of individual irregular particles vary greatly with shape, the resultant forward diffraction lobe for an ensemble of nonspherical particles with random orientations would be similar to an ensemble of spheres with cross-sectional areas equal to the particles' areas.

Table 8. Extinction coefficients ( $\text{km}^{-1}$ ) versus wavelength ( $\mu\text{m}$ ) for various fogs

| Wavelength<br>( $\mu\text{m}$ )           | Advection<br>Fog | Radiation<br>Fog |
|---|------------------|------------------|
| 0.35                                      | 28.52            | 8.404            |
| 0.40                                      | 28.60            | 8.478            |
| 0.45                                      | 28.63            | 8.533            |
| 0.50                                      | 28.69            | 8.580            |
| 0.55                                      | 28.75            | 8.614            |
| 0.60                                      | 28.81            | 8.690            |
| 0.65                                      | 28.84            | 8.714            |
| 0.70                                      | 28.89            | 8.799            |
| 0.75                                      | 28.94            | 8.840            |
| 1.06                                      | 29.20            | 9.108            |
| 3.00                                      | 30.14            | 9.608            |
| 3.50                                      | 30.79            | 12.739           |
| 4.00                                      | 31.12            | 11.925           |
| 4.50                                      | 31.40            | 10.292           |
| 5.00                                      | 31.70            | 9.049            |
| 8.00                                      | 33.78            | 3.992            |
| 8.50                                      | 34.30            | 3.400            |
| 9.00                                      | 34.84            | 2.884            |
| 9.50                                      | 35.27            | 2.453            |
| 10.00                                     | 35.25            | 2.093            |
| 10.50                                     | 33.57            | 1.919            |
| 11.00                                     | 30.36            | 2.081            |
| 11.50                                     | 28.24            | 2.498            |
| 12.00                                     | 28.09            | 3.073            |
| 14.00                                     | 31.17            | 4.743            |
| 15.00                                     | 32.02            | 4.965            |
| 18.00                                     | 33.82            | 4.822            |
| 20.00                                     | 34.63            | 4.199            |
| 25.00                                     | 35.80            | 2.989            |
| 30.00                                     | 36.44            | 2.160            |
| 35.00                                     | 35.72            | 1.765            |
| 40.00                                     | 34.62            | 1.673            |
| Number<br>density<br>( $\text{cm}^{-3}$ ) | 20.00            | 200.0            |

Table 9. Liquid water content ( $\mu\text{g}/\text{m}^3$ ) as a function of the type of precipitation.

| Precipitation Type             | Liquid Water Content ( $\mu\text{g}/\text{m}^3$ ) |
|--------------------------------|---|
| Advection Fog                  | 372300  |
| Radiation Fog                  | 15640   |
| Rain (Drizzle), 1 mm/hr        | 89000   |
| Rain (Widespread), 5 mm/hr     | 344000  |
| Rain (Thunderstorms), 10 mm/hr | 615700  |
| Snow                           | 68150   |

A special version of AGAUS for treating SNOW cases (AGSNOW) (Deepak et al. 1982) was developed to calculate the single-scattering characteristics of large spherical or irregular particles. AGSNOW consisted of a combination of Fraunhofer diffraction, geometrical reflection, and a parameterization (Pollack and Cuzzi 1980) for the refracted and internally reflected energy. Mie theory is used to compute the phase functions for particles with size parameters less than a user defined upper bound, and to compute extinction and scattering cross sections. The parameterization used for the refracted and internally reflected energy precludes the calculation of effects of rainbows and other such optical phenomena; thus, the phase functions at the affected angles are only approximate. Because the phase functions for typical rain and snow size distributions have sharp peaks in the forward direction, a set of angles concentrated in the forward direction must be used for these phase functions. Otherwise, difficulties arise in the phase function interpolation processes in various EOSAEL modules: a new set of angles is automatically read when the rain and snow phase functions are used.

Phase functions for rain were generated using the AGSNOW code for a MP particle size distribution with rain rates of 1, 5, and 10 mm/h, corresponding to rain types of drizzle, widespread, and thunderstorm, respectively, and to number densities of about 0.0019, 0.0027, and 0.0031 particles/cm<sup>3</sup>, respectively. The MP distribution yields somewhat larger particles at higher rain rates, causing the forward direction lobe of the phase function to be narrower and sharper. The phase functions given are considered to be reasonable for most rain conditions. The extinction coefficient for other rain rates may be calculated using the algorithm given in the EOSAEL XSCALE module (Fiegel 1994).

Snow phase functions were calculated using an MG particle size distribution that had been fit to a measured size distribution (Unpublished results taken from SNOW-ONE-A) as shown in figure 1. The MG model was chosen because it provides a realistic simulation of the relatively slow particle density decrease for  $r < r_c$ . The particle number density used was  $N = 40$  particles/m<sup>3</sup>, and the peak density particle diameter ( $D_c$ ) was set to  $D_c = 2r_c = 1.06$  mm, corresponding to a precipitation rate of roughly 4 mm/h, representing a light to moderate snow rate (e.g., Pruppacher and Klett 1980). Because snow particle size distributions may vary greatly for a given precipitation or snow accumulation rate, it is difficult to make generalizations about the scattering characteristics of a "typical" snow. Also, due to the use of the AGAUS Mie scattering code, snow scattering properties are being modeled using a spherical snowflake assumption. Winchester et al. (1983) note "Since the experimental studies have shown that the phase functions of snow crystals, with the possible exception of graupel, cannot be approximated using Mie theory computations for spheres with either equivalent area or equivalent volume." Thus, admittedly this is a poor substitute for an accurate snow model, but theoretical techniques characterizing non-spherical scatterers are currently inadequate to model snow at visible and infrared wavelengths on non-super computers. Yet extensions of measurements to arbitrary wavelength are impractical without some model.

Compounding these difficulties is the nature of the behavior of the refractive indices of ice. These are temperature and humidity, as well as wavelength, dependent. In conclusion, the phase function presented for snow can at best be considered an approximation to the actual phase function for snow, and at worst a simple placeholder for a future, more robust, representation of variable snow scattering characterization.

The extinction coefficients for other precipitation rates may be calculated using the algorithm given in XSCALE (Fiegel 1994). The extinction coefficients for the rain and snow distributions are presented in table 10.

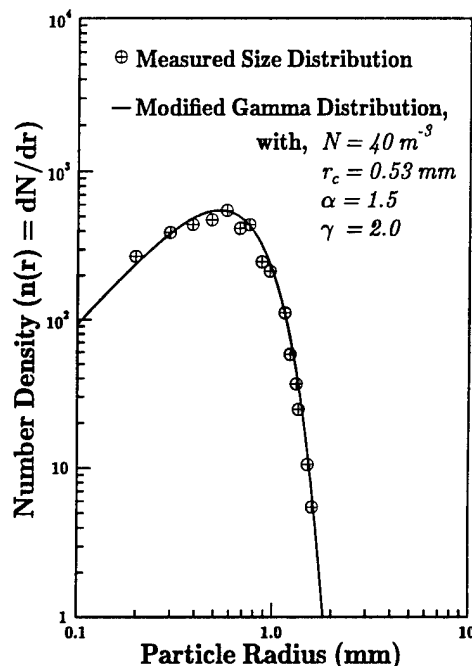


**Figure 1.** Measured/modeled snow distribution

## 2.5 Dust Aerosol Models

Soil-derived aerosols are an important component of the total atmospheric aerosol content in certain geographic locations. Reported results of size distribution measurements for these aerosols vary widely. However, the general consensus is that the dust aerosols follow a bimodal lognormal distribution. Empirical data (Patterson and Gillette 1977) fits this type of distribution well, and dust aerosols may be produced by a pulverization process in the soil. Epstein (1947) has shown that such processes result in lognormal

Table 10. Extinction coefficients ( $\text{km}^{-1}$ ) versus wavelength ( $\mu\text{m}$ ) for various natural aerosol models

| Wavelength<br>( $\mu\text{m}$ )        | Rain     |          |          | Snow     | Dust     |        |
|--|----------|----------|----------|----------|----------|--------|
|  | Light    | Moderate | Heavy    |          | Light    | Heavy  |
| 0.55                                   | 0.3664   | 1.009    | 1.561    | 0.1179   | 0.1018   | 4.319  |
| 1.06                                   | 0.3673   | 1.011    | 1.564    | 0.1180   | 0.05754  | 5.195  |
| 3.00                                   | 0.3697   | 1.017    | 1.572    | 0.1184   | 0.02799  | 2.605  |
| 3.50                                   | 0.3705   | 1.018    | 1.574    | 0.1186   | 0.02557  | 2.001  |
| 4.00                                   | 0.3711   | 1.020    | 1.576    | 0.1186   | 0.01907  | 1.576  |
| 4.50                                   | 0.3716   | 1.021    | 1.578    | 0.1187   | 0.01513  | 1.163  |
| 5.00                                   | 0.3721   | 1.022    | 1.579    | 0.1188   | 0.01276  | 0.9553 |
| 8.00                                   | 0.3747   | 1.028    | 1.588    | 0.1192   | 0.00675  | 0.6860 |
| 8.50                                   | 0.3751   | 1.029    | 1.589    | 0.1193   | 0.02951  | 4.695  |
| 9.00                                   | 0.3755   | 1.029    | 1.590    | 0.1193   | 0.04410  | 3.732  |
| 9.50                                   | 0.3758   | 1.030    | 1.591    | 0.1194   | 0.02062  | 2.592  |
| 10.00                                  | 0.3761   | 1.031    | 1.592    | 0.1194   | 0.01598  | 1.357  |
| 10.50                                  | 0.3760   | 1.031    | 1.592    | 0.1195   | 0.01235  | 0.9214 |
| 11.00                                  | 0.3754   | 1.030    | 1.590    | 0.1194   | 0.009668 | 0.7367 |
| 11.50                                  | 0.3745   | 1.028    | 1.588    | 0.1194   | 0.007398 | 0.6250 |
| 12.00                                  | 0.3743   | 1.028    | 1.588    | 0.1194   | 0.004920 | 0.5651 |
| Number density<br>( $\text{cm}^{-3}$ ) | 0.001951 | 0.002736 | 0.003165 | 0.000040 | 2480     | 1258   |

distributions. The bimodal distribution also provides a better fit, as empirical dust distributions appear to be characterized by more than one mode. Generally (Patterson and Gillette 1977), the accumulation or small mode appears to be a characteristic of dust aerosols under all conditions, while the coarse or large mode is more a function of the parent soil size distribution. The latter component usually appears only under conditions of moderate to heavy aerosol dust loading.

The parameters for light and heavy aerosol loading (table 11) were taken at various locations, predominantly in the southwestern United States. Analyses of the small particle mode showed (Jennings et al. 1978) that the constituents were primarily ammonium sulfate, carbon, calcite, sodium nitrate, quartz, and montmorillonite for both distributions. The particles contained in the large mode were seen to settle quickly, in both light and moderate cases, as the windspeed diminished. The accumulation mode was considered to be comprised of 80 percent quartz and 20 percent montmorillonite by mass for the heavy aerosol loading and 80 percent ammonium sulfate and 20 percent carbon by mass for the light aerosol loading case, to allow the distribution to be more representative of varying geographic locations (Gillespie and Lindberg 1992). The resulting distributions are representative of windblown dust, not vehicular or HE debris.

Table 11. Values of lognormal particle size distribution parameters (mode radius  $r_g$  and geometric standard deviation  $\sigma_g$ )

| Dust Type                                    | Light Loading    |        | Heavy Loading   |        |
|--|------------------|--------|-----------------|--------|
| Mode   | Small            | Large  | Small           | Large  |
| Species                                      | Ammonium Sulfate | Quartz | Montmorillonite | Quartz |
| Bulk Density<br>(g/cm <sup>3</sup> )         | 1.769            | 2.32   | 2.5             | 2.32   |
| Number Density<br>(cm <sup>-3</sup> )        | 1988             | 3.79   | 39.62           | 0.1128 |
| Mass loading<br>( $\mu\text{g}/\text{m}^3$ ) | 16               | 40     | 1000            | 10000  |
| $r_g$ ( $\mu\text{m}$ )                      | 0.05             | 0.5    | 0.5             | 15     |
| $\sigma_g$                                   | 2.0              | 2.0    | 2.25            | 1.6    |
| Species                                      | Carbon           |        | Quartz          |        |
| Bulk Density<br>(g/cm <sup>3</sup> )         | 1.8              |        | 2.32            |        |
| Number Density<br>(cm <sup>-3</sup> )        | 488.5            |        | 1218.6          |        |
| Mass loading<br>( $\mu\text{g}/\text{m}^3$ ) | 4                |        | 4000            |        |
| $r_g$ ( $\mu\text{m}$ )                      | 0.05             |        | 0.5             |        |
| $\sigma_g$                                   | 2.0              |        | 1.6             |        |

The refractive indices for quartz were interpolated from Weinman and Peterson (1969) for 0.55 and 1.06  $\mu\text{m}$ , from Jennings and Gillespie (1978) for 3.0 to 5.0  $\mu\text{m}$ , and from Spitzer and Kleinman (1961) for 8.0 to 12.0  $\mu\text{m}$ . The refractive indices for ammonium sulfate were interpolated from the work of Toon et al. (1976); the refractive indices of carbon were interpolated from the work of Gillespie and Goedecke (1989).

The refractive indices of montmorillonite at 0.55 and 1.06  $\mu\text{m}$  were interpolated from the work of Egan and Hilgeman (1979); for wavelengths greater than 4.5  $\mu\text{m}$ , values were interpolated from the work of Toon et al. (1977).

The errors introduced by the interpolation are probably small because of the close proximity of the wavelengths used here and tabulated in the aforementioned references. However, for the 3.0- to 4.5- $\mu\text{m}$  band, the refractive indices had to be interpolated between 2.6 and 5.0  $\mu\text{m}$ . Because montmorillonite is a clay material with water chemically bonded in its crystal lattice structure, the refractive indices and derived quantities should be used with extreme caution in this wavelength band (3.0 to 4.5  $\mu\text{m}$ ). Tables 12 and 13 present the refractive indices used for the various constituents.

The heavy loading dust type reflects very large mode radius constituents associated with high wind speeds. The light loading would be the case normally

Table 12. Real ( $n$ ) and imaginary ( $k$ ) indices of refraction for light dust constituents ammonium sulfate and carbon

| Wavelength<br>( $\mu\text{m}$ ) | Ammonium Sulfate |                      | Carbon |     |
|---------------------------------|------------------|----------------------|--------|-----|
|                                 | $n$              | $k$                  | $n$    | $k$ |
| 0.55                            | 1.53             | $1.0 \times 10^{-7}$ | 2.0    | 1.0 |
| 1.06                            | 1.51             | $2.1 \times 10^{-6}$ | 2.0    | 1.0 |
| 3.00                            | 1.36             | $8.9 \times 10^{-2}$ | 2.2    | 1.2 |
| 3.50                            | 1.62             | $1.4 \times 10^{-1}$ | 2.2    | 1.2 |
| 4.00                            | 1.55             | $1.7 \times 10^{-2}$ | 2.2    | 1.2 |
| 4.50                            | 1.50             | $7.9 \times 10^{-3}$ | 2.2    | 1.2 |
| 5.00                            | 1.46             | $7.0 \times 10^{-3}$ | 2.2    | 1.2 |
| 8.00                            | 1.31             | $8.0 \times 10^{-2}$ | 3.0    | 1.6 |
| 8.50                            | 0.90             | $2.7 \times 10^{-1}$ | 3.0    | 1.6 |
| 9.00                            | 0.99             | $1.7 \times 10^0$    | 3.0    | 1.6 |
| 9.50                            | 2.70             | $6.1 \times 10^{-1}$ | 3.0    | 1.6 |
| 10.00                           | 2.19             | $1.3 \times 10^{-1}$ | 3.0    | 1.6 |
| 10.50                           | 1.99             | $6.0 \times 10^{-2}$ | 3.0    | 1.6 |
| 11.00                           | 1.90             | $4.3 \times 10^{-2}$ | 3.0    | 1.6 |
| 11.50                           | 1.83             | $2.8 \times 10^{-2}$ | 3.0    | 1.6 |
| 12.00                           | 1.80             | $2.0 \times 10^{-2}$ | 3.0    | 1.6 |

Table 13. Real ( $n$ ) and imaginary ( $k$ ) indices of refraction for heavy dust constituents quartz and montmorillonite. Quartz results include ordinary and extraordinary indices.

| $\lambda$<br>( $\mu\text{m}$ ) | Quartz  |         |           |           | Montmorillonite |          |
|--------------------------------|---------|---------|-----------|-----------|-----------------|----------|
|                                | $n$     |         | $k$       |           | $n$             | $k$      |
|                                | Ordnry  | Extrord | Ordnry    | Extrord   |                 |          |
| 0.55                           | 1.546   | 1.555   | $10^{-7}$ | $10^{-7}$ | 1.524           | 0.000673 |
| 1.06                           | 1.534   | 1.543   | $10^{-7}$ | $10^{-7}$ | 1.519           | 0.00057  |
| 3.00                           | 1.500   | 1.500   | $10^{-6}$ | $10^{-6}$ | 1.483           | 0.00317  |
| 3.50                           | 1.485   | 1.485   | $10^{-5}$ | $10^{-6}$ | 1.463           | 0.00350  |
| 4.00                           | 1.472   | 1.476   | 0.00013   | 0.00014   | 1.442           | 0.00383  |
| 4.50                           | 1.426   | 1.432   | 0.00066   | 0.00073   | 1.421           | 0.00417  |
| 5.00                           | 1.412   | 1.419   | 0.00079   | 0.00091   | 1.400           | 0.00450  |
| 8.00                           | 0.42984 | 0.39076 | 0.13829   | 0.14379   | 1.035           | 0.125    |
| 8.50                           | 0.11260 | 0.08548 | 1.25062   | 1.21601   | 0.754           | 0.427    |
| 9.00                           | 0.17463 | 0.22905 | 2.59701   | 3.04158   | 0.923           | 0.869    |
| 9.50                           | 4.51517 | 3.90448 | 0.39770   | 0.23041   | 1.750           | 1.860    |
| 10.00                          | 2.66527 | 2.57228 | 0.05190   | 0.04402   | 2.590           | 0.625    |
| 10.50                          | 2.23766 | 2.20003 | 0.02452   | 0.02220   | 1.970           | 0.185    |
| 11.00                          | 2.01345 | 2.00007 | 0.01736   | 0.01588   | 1.845           | 0.245    |
| 11.50                          | 1.83358 | 1.84954 | 0.01875   | 0.01529   | 1.765           | 0.160    |
| 12.00                          | 1.56521 | 1.68256 | 0.04694   | 0.02369   | 1.693           | 0.128    |

considered. Mixing the heavy and light cases should simulate intermediate condition dust cases.

Table 13 provides information on both the ordinary and extraordinary indices of refraction for quartz. Because quartz is an optically positive uniaxial crystal (Born and Wolf, 1975) the scattering problem is divided into two parts. Two-thirds of the scattering material is treated using the ordinary indices of refraction. The remaining third of the material is treated using the extraordinary indices.

The HE dust model was generated using the empirical results of field tests (Pinnick et al. 1983) taken at Huntsville, Alabama; and Orogrande, New Mexico. The results were empirically fitted to a bimodal lognormal curve with the following parameters: for the small mode, particle concentration  $C = 15930 \mu\text{g}/\text{m}^3$ , number density  $N = 200\text{cm}^{-3}$ , geometric mean radius  $r_g = 0.5 \mu\text{m}$ , geometric standard deviation  $\sigma_g = 2.6$ , and particle bulk density  $\rho = 2.5\text{g}/\text{cm}^3$ ; for the large mode,  $C = 48680 \mu\text{g}/\text{m}^3$ ,  $N = 0.07\text{cm}^{-3}$ ,  $r_g = 22.5 \mu\text{m}$ ,  $\sigma_g = 1.87$ , and  $\rho = 2.5\text{g}/\text{cm}^3$ . The refractive indices were taken from the work of Ivlev and Popova (1973). The refractive indices are a synthetic spectra chosen because no consistent set of measurements covers the wavelength range in PFNDAT. A comparison of the synthesized spectrum with the measurements from Jennings et al. (1978) at the wavelengths available shows agreement. Table 14 shows that the values taken fall between the minimum and maximum values found in that reference. Table 15 lists the extinction coefficients for all smoke types along with the results for the HE dust type as functions of wavelength, as determined from runs of the AGAUS model.

Table 14. Derived real ( $n$ ) and imaginary ( $k$ ) indices of refraction for HE dust

| $\lambda (\mu\text{m})$ | $n$   | $k$    |
|-------------------------|-------|--------|
| 0.55                    | 1.65  | 0.005  |
| 1.06                    | 1.647 | 0.0051 |
| 3.00                    | 1.646 | 0.076  |
| 3.50                    | 1.655 | 0.020  |
| 4.00                    | 1.637 | 0.018  |
| 4.50                    | 1.620 | 0.018  |
| 5.00                    | 1.592 | 0.018  |
| 8.00                    | 1.269 | 0.178  |
| 8.50                    | 1.186 | 0.600  |
| 9.00                    | 1.650 | 1.240  |
| 9.50                    | 2.342 | 0.600  |
| 10.00                   | 2.140 | 0.126  |
| 10.50                   | 1.904 | 0.078  |
| 11.00                   | 1.751 | 0.143  |
| 11.50                   | 1.784 | 0.331  |
| 12.00                   | 1.756 | 0.230  |

Table 15. Extinction coefficients ( $\text{km}^{-1}$ ) versus wavelength ( $\mu\text{m}$ ) for various manmade aerosol models

| Wavelength<br>( $\mu\text{m}$ )              | HE Dust | White Phosphorus |        |        | Fog Oil | HC    |
|--|---------|------------------|--------|--------|---------|-------|
|  |         | 17% Rh           | 50% Rh | 90% Rh |         |       |
| 0.55   | 2.668   | 4191.            | 4282.  | 3957.  | 5367.   | 3227. |
| 1.06   | 2.806   | 1708.            | 1963.  | 2329.  | 3737.   | 2601. |
| 3.00   | 2.993   | 309.1            | 449.6  | 966.9  | 596.9   | 1141. |
| 3.50   | 3.049   | 414.8            | 421.5  | 342.1  | 641.4   | 383.6 |
| 4.00   | 3.022   | 280.4            | 287.2  | 208.6  | 297.7   | 187.3 |
| 4.50   | 2.985   | 255.3            | 258.5  | 180.5  | 208.2   | 143.8 |
| 5.00   | 2.918   | 179.0            | 180.8  | 127.4  | 148.9   | 110.6 |
| 8.00   | 1.944   | 548.2            | 519.6  | 231.7  | 38.61   | 56.0  |
| 8.50   | 2.399   | 421.3            | 421.7  | 201.3  | 31.81   | 53.5  |
| 9.00   | 3.022   | 444.0            | 430.7  | 204.3  | 25.31   | 49.6  |
| 9.50   | 2.944   | 516.2            | 471.0  | 248.4  | 22.42   | 49.5  |
| 10.00  | 2.892   | 405.5            | 423.2  | 236.2  | 19.34   | 57.4  |
| 10.50  | 2.713   | 361.5            | 385.0  | 234.0  | 17.27   | 67.7  |
| 11.00  | 2.500   | 248.9            | 286.5  | 226.5  | 14.20   | 84.5  |
| 11.50  | 2.515   | 136.3            | 157.1  | 168.8  | 14.92   | 108.7 |
| 12.00  | 2.432   | 117.4            | 138.7  | 182.6  | 12.49   | 141.8 |
| Number density<br>( $10^6 \text{ cm}^{-3}$ ) | 0.0002  | 5.667            | 4.566  | 2.239  | 8.261   | 1.399 |

## 2.6 Aerosol Smoke Models

The phase functions for inventory smokes can be calculated almost exactly because the particles are nearly spherical. Discrepancies between theory and measurement can be attributed to uncertainties in the particle size spectrum or complex refractive indices. Experiments (Jennings and Gillespie 1978) have shown that the particle size spectrum is closely approximated by a lognormal distribution. Reference to the mass loading or mass concentration ( $C$ ) of the particulate material (equation 4) rather than the number density is conventional in smoke applications. Since the bulk density ( $\rho$ ) for water is  $1 \text{ g/cm}^3$ ,  $\rho$  for a smoke is also numerically equal to the particulate specific gravity.

Table 16 lists the parameters considered representative of inventory smokes and includes the mass median diameter ( $MMD$ ) often used in the literature in place of  $r_g$ . The two are related as

$$\ln(MMD) = \ln 2r_g + 3 \ln^2 \sigma_g, \quad (22)$$

where  $r_g$  and  $\sigma_g$  are listed in table 16.

Table 16 shows that mass concentration  $C$  was arbitrarily set to  $10^6 \mu\text{g/m}^3$ . The magnitude of  $C$  has no effect on the phase function or the mass extinction coefficient  $\alpha_\epsilon$ , and only linearly scales the volume extinction coefficient  $\beta_\epsilon$ .

Table 16. Representative parameters for determining phase functions of inventory smokes at various relative humidities

| Aerosol Species:<br>Relative Humidity (%):      | White Phosphorus |        |        | Fog Oil | HC     |
|---|------------------|--------|--------|---------|--------|
|   | 17% Rh           | 50% Rh | 90% Rh |         |        |
| Geometric mean ( $\mu\text{m}$ ), $r_g$         | 0.241            | 0.269  | 0.365  | 0.190   | 0.422  |
| Width parameter, $\sigma_g$                     | 1.450            | 1.450  | 1.450  | 1.800   | 1.450  |
| Bulk density ( $\text{g}/\text{cm}^3$ ), $\rho$ | 1.617            | 1.443  | 1.178  | 0.890   | 1.220  |
| Mass loading ( $\mu\text{g}/\text{m}^3$ ), $C$  | $10^6$           | $10^6$ | $10^6$ | $10^6$  | $10^6$ |
| Mass median diameter, $MMD$                     | 0.729            | 0.814  | 1.104  | 0.575   | 1.338  |

Table 16 lists the fog oil particle spectrum parameters appropriate for fog oil dissemination by current military generators designed to produce particles most efficient for obscuration at the visible wavelengths (Carlon et al. 1977). Other experimental generators may produce larger particles. WP and HC have parameters listed for specific values of relative humidity. Hygroscopic growth has been modeled for these conditions by semiempirical relations (Frickel et al. 1979; Rubel 1978). Other evidence (Farmer 1980) shows that at high humidities (greater than 75 percent relative humidity) a bimodal particle size spectrum may be expected that would be most pronounced for WP smoke.

Tabulated real and imaginary refractive indices have also been provided. Reliable experimental measurements would be preferred, but such measurements are usually impossible (Weast and Astle 1980) because of the complex reaction products formed in producing smoke. Table 17 lists the utilized values for selected wavelengths from the visible through the infrared. Weast and Astle (1980) is the primary reference. They derived coefficients based on laboratory measurements performed on the major constituents — phosphoric acid,  $\text{H}_3\text{PO}_4$ , and zinc chloride,  $\text{ZnCl}_2$ , for WP and HC scatterers, respectively, at various humidity levels.

Fog oil smoke is not considered hygroscopic, so only a single data set is used. In the visible, the imaginary index for fog oil is so small as to be beyond instrumental sensitivity; it can be considered negligible for most applications. This small value for  $k$  leads to a single-scattering albedo of nearly unity, implying that extinction is entirely due to scattering.

Table 18 compares the average mass extinction coefficients  $\alpha_\epsilon$  as computed by AGAUS versus laboratory experimental results (Weast and Astle 1980; Frickel et al. 1979; Rubel 1978; Farmer 1980) for several spectral bands of interest. Since the measured results represent band averages, a typical cloud thickness was assumed ( $R = 0.01 \text{ km}$ ) and results were computed by averaging the computed transmission through  $1 \text{ g}/\text{m}^3$  density aerosols via,

$$\bar{k} = -\ln \left\{ \frac{\sum_i w_i \exp(-k_i R)}{\sum_i w_i} \right\} / R, \quad (23)$$

Table 17. Real ( $n$ ) and imaginary ( $k$ ) indices of refraction for the smoke aerosol models at indicated relative humidities

| $\lambda$ ( $\mu\text{m}$ ) | $\text{H}_3\text{PO}_4$ (WP) 17% RH |       | $\text{H}_3\text{PO}_4$ (WP) 50% RH |        | $\text{H}_3\text{PO}_4$ (WP) 90% RH |        |
|-----------------------------|-------------------------------------|-------|-------------------------------------|--------|-------------------------------------|--------|
|                             | $n$                                 | $k$   | $n$                                 | $k$    | $n$                                 | $k$    |
| 0.55                        | 1.438                               | 0.001 | 1.412                               | 0.0008 | 1.357                               | 0.0003 |
| 1.06                        | 1.414                               | 0.008 | 1.399                               | 0.0057 | 1.348                               | 0.0018 |
| 3.00                        | 1.278                               | 0.104 | 1.301                               | 0.133  | 1.350                               | 0.2290 |
| 3.50                        | 1.356                               | 0.178 | 1.363                               | 0.150  | 1.389                               | 0.0522 |
| 4.00                        | 1.338                               | 0.141 | 1.382                               | 0.118  | 1.360                               | 0.0393 |
| 4.50                        | 1.417                               | 0.150 | 1.403                               | 0.127  | 1.354                               | 0.0481 |
| 5.00                        | 1.399                               | 0.119 | 1.387                               | 0.101  | 1.344                               | 0.0395 |
| 8.00                        | 1.287                               | 0.622 | 1.288                               | 0.524  | 1.290                               | 0.184  |
| 8.50                        | 1.421                               | 0.557 | 1.383                               | 0.480  | 1.310                               | 0.172  |
| 9.00                        | 1.396                               | 0.615 | 1.374                               | 0.519  | 1.296                               | 0.186  |
| 9.50                        | 1.462                               | 0.807 | 1.510                               | 0.665  | 1.304                               | 0.242  |
| 10.00                       | 1.720                               | 0.827 | 1.636                               | 0.697  | 1.346                               | 0.248  |
| 10.50                       | 1.793                               | 0.826 | 1.691                               | 0.699  | 1.340                               | 0.259  |
| 11.00                       | 2.125                               | 0.768 | 1.962                               | 0.671  | 1.400                               | 0.272  |
| 11.50                       | 2.080                               | 0.404 | 1.920                               | 0.360  | 1.368                               | 0.209  |
| 12.00                       | 1.951                               | 0.329 | 1.810                               | 0.307  | 1.324                               | 0.232  |

| $\lambda$ ( $\mu\text{m}$ ) | Fog Oil, 50% RH |          | $\text{ZnCl}_2$ (HC), 85% RH |       |
|-----------------------------|-----------------|----------|------------------------------|-------|
|                             | $n$             | $k$      | $n$                          | $k$   |
| 0.55                        | 1.475           | 0.000002 | 1.390                        | 0.000 |
| 1.06                        | 1.474           | 0.000006 | 1.380                        | 0.000 |
| 3.00                        | 1.466           | 0.000337 | 1.480                        | 0.227 |
| 3.50                        | 1.518           | 0.0466   | 1.453                        | 0.021 |
| 4.00                        | 1.482           | 0.000701 | 1.405                        | 0.005 |
| 4.50                        | 1.479           | 0.000504 | 1.382                        | 0.016 |
| 5.00                        | 1.476           | 0.000357 | 1.376                        | 0.018 |
| 8.00                        | 1.485           | 0.00491  | 1.348                        | 0.037 |
| 8.50                        | 1.480           | 0.00514  | 1.336                        | 0.040 |
| 9.00                        | 1.480           | 0.00407  | 1.321                        | 0.041 |
| 9.50                        | 1.478           | 0.00504  | 1.300                        | 0.045 |
| 10.00                       | 1.479           | 0.00509  | 1.279                        | 0.057 |
| 10.50                       | 1.479           | 0.00557  | 1.253                        | 0.072 |
| 11.00                       | 1.479           | 0.00467  | 1.229                        | 0.095 |
| 11.50                       | 1.479           | 0.00714  | 1.204                        | 0.128 |
| 12.00                       | 1.478           | 0.00620  | 1.186                        | 0.174 |

where the  $w_i$  represent weight factors for each spectral band. A simple approach sets the weight factors in the first and last bands to 1/2, and the remaining weights to 1. This was the method used to produce the model results of table 18. This table shows that all the comparisons are reasonable. Disparities are no larger than those found among various experiments throughout the above cited literature. Comparison of results for WP in the 8 to 12- $\mu\text{m}$  region are sometimes

taken as evidence (Milham et al. 1977) that secondary reaction products are significant for WP smokes. Results for fog oil at visible wavelengths may be due to the use of a single wavelength for the modeled results. Results in the longwave IR band may reflect different assumptions regarding sources. Equation (23) assumes a flat source spectrum. The measurements would rely on the temperature of the background medium. It is probably significant that the experimental data were obtained by the vapor condensation method rather than by pyrotechnic dissemination. Disparities were noted before by Pinnick and Jennings (1980).

Table 18. Comparison of theoretical (from the AGAUS model) and experimentally measured (Expt) mass extinction coefficients ( $m^2/g$ ) at 50 percent relative humidity for various smoke aerosols

| $\lambda$ ( $\mu m$ ) | WP    |       | Fog Oil |       | HC    |       |
|-----------------------|-------|-------|---------|-------|-------|-------|
|                       | Model | Expt  | Model   | Expt  | Model | Exp   |
| visible*              | 4.282 | 3.940 | 5.367   | 7.730 | 3.227 | 4.579 |
| 1.06                  | 1.963 | 1.410 | 3.737   | 3.500 | 2.601 | 2.040 |
| 3-5                   | 0.284 | 0.290 | 0.262   | 0.270 | 0.193 | 0.190 |
| 8-12                  | 0.284 | 0.366 | 0.021   | 0.014 | 0.068 | 0.052 |

\*0.55  $\mu m$  for model; 0.4 to 0.7  $\mu m$  for experiment

Of further interest to the usage of phase functions for smoke aerosols are the single scattering albedos ( $\omega$ ) averaged over various wavebands. Table 19 lists the average single-scattering albedos for the inventory smokes in four spectral regions of interest. Due to the usage of updated fog oil imaginary refractive indices approximately an order of magnitude lower than those used in the EOSAEL87 version of PFNDAT, the fog oil single scattering albedos are considerably higher in the IR bands than previously reported. The significance of this updated finding is that scattering becomes more significant even at IR wavelengths.

Table 19. Average single-scattering albedo for the inventory smokes as calculated by AGAUS

| $\lambda$ ( $\mu m$ ) | WP    | Fog Oil | HC      |
|-----------------------|-------|---------|---------|
| 0.55                  | 0.995 | > 0.999 | > 0.999 |
| 1.06                  | 0.964 | > 0.999 | > 0.999 |
| 3-5                   | 0.155 | 0.916   | 0.745   |
| 8-12                  | 0.017 | 0.652   | 0.081   |

The phase function does not depend on number density, but the volume extinction coefficient does. Thus table 16 lists the parameter values used to compute the extinction coefficients for the various smokes. Because the

smoke density is a definite function of time, a method for reassessing the extinction coefficient at different times is necessary. This reassessment may be accomplished as follows: In the notation used here, the transmission  $T$  is,

$$T = \exp^{-\beta_\epsilon L} \quad (24)$$

$$= \exp^{-\alpha_\epsilon C L} \quad (25)$$

$$\beta_\epsilon = \alpha_\epsilon C \quad (26)$$

$$= N s, \quad (27)$$

where

- $L$  is the path length (cm),
- $\beta_\epsilon$  is the volume extinction coefficient ( $\text{cm}^{-1}$ ),
- $\alpha_\epsilon$  is the mass extinction coefficient ( $\text{cm}^2/\text{g}$ ), and
- $s$  is the extinction cross section per particle ( $\text{cm}^2$ ).

Thus the volume extinction coefficient  $\beta_\epsilon$  can be scaled as a function of time if  $N$  (or the quantity  $\alpha_\epsilon C$ ) is known as a function of time. In addition,  $L$  will vary with time according to statistical variations, elapsed time since the smoke event began, and the observer's geometry with respect to the cloud. The COMBIC module contained in EOSAEL provides mean estimates for the quantities  $T$  and  $L$  for specified LOS through various geometries of smoke clouds.

## 2.7 EOSAEL92 Improvements

The distinctions between the current version of PFNDAT (part of the 1992 release of EOSAEL (EOSAEL92)) and the 1987 release of PFNDAT (part of EOSAEL87, the EOSAEL version released in 1987) are significant. This version has expanded the visible band calculations to include results at 0.05- $\mu\text{m}$  resolution from 0.35 through 0.75  $\mu\text{m}$ . This version of the documentation also contains sufficient information for the user to duplicate the calculations made using the AGAUS model via a different Mie scattering routine. The version of AGAUS utilized was updated to include a continuing fraction expansion technique proposed by Lentz (1976). This approach allows for a more precise computation of forward scattering effects. The forward peaks of some of the larger aerosols (most notably rain and snow) have increased significantly, better reflecting the true forward scattering effects.

We have updated the index of smoke-aerosol refraction data used for WP and fog oil to reflect more recent data (Hoock and Sutherland 1993). The reported infrared imaginary indices of refraction for fog oil were adjusted (following remeasurement) from the values used in the original PFNDAT. Minor errors in the text were also corrected, as well as inconsistencies in notation used in the original document.

**This page left intentionally blank.**

## 3. USER'S GUIDE

### 3.1 Introduction

The aerosol phase function data files PFNDAT.nnn (where nnn varies from 1 to 57) are accessed by modules ASCAT and FCLOUD for a given aerosol distribution and wavelength. The selected phase function is renormalized by subroutine PFUNC for the MSCAT module (an EOSAEL Multiple SCATtering routine) and by subroutine PFN for the FCLOUD module so its normalization is compatible with the calling module. ASCAT requires no renormalization.

Computer code AGAUS and a geometrical optics version of code AGSNOW were used to construct the aerosol phase function data base. Table 20 lists the 38 different distributions contained in the database.

### 3.2 Usage

To use PFNDAT in one of the aforementioned codes requires the assignment of the FORTRAN unit number, IPHFUN, within the codes. This assignment depends on the specific location of the database within the user's computer system. The PFNDAT files are provided in two primary forms. In one, the individual scattering types are located in separate output files. In the other, the contents of the individual files are concatenated to produce a large master file.

If users wish to construct their own phase function(s) for use by one of the programs, this file must be formatted as explained in the structure section below. Program AGAUS, supplied as an ancillary code to EOSAEL, may be used to automatically construct a file compatible with EOSAEL usage. Instructions for the use of AGAUS are found as comments at the beginning of that code.

### 3.3 Structure

The phase function database comprises a series of ASCII files, one for each of the aerosol identifiers listed in table 20. The files are called PFNDAT.001 through PFNDAT.057. Each identifier nnn is associated with a file PFNDAT.nnn. Each file begins with 65 discrete angles between 0° and 180°; the number of angles is the current dimension size (65) of the pertinent arrays in the EOSAEL module cited above. The remainder of the file contains sets of phase function results at each wavelength. Each set is composed of a one-line preamble followed by the angular phase function data. The preamble is a record containing the number of angular data items (*NANG*, 65 in all cases), a phase function identifier

Table 20. Phase function data base for EOSAEL92

| Index   | Distribution Type         | % Rel. Hmdty. |
|---------|---------------------------|---------------|
| 1.      | Maritime                  | 0             |
| 2.      | Maritime                  | 50            |
| 3.      | Maritime                  | 70            |
| 4.      | Maritime                  | 80            |
| 5.      | Maritime                  | 90            |
| 6.      | Maritime                  | 95            |
| 7.      | Maritime                  | 98            |
| 8.      | Maritime                  | 99            |
| 9.      | Urban                     | 0             |
| 10.     | Urban                     | 50            |
| 11.     | Urban                     | 70            |
| 12.     | Urban                     | 80            |
| 13.     | Urban                     | 90            |
| 14.     | Urban                     | 95            |
| 15.     | Urban                     | 98            |
| 16.     | Urban                     | 99            |
| 17.     | Rural                     | 0             |
| 18.     | Rural                     | 50            |
| 19.     | Rural                     | 70            |
| 20.     | Rural                     | 80            |
| 21.     | Rural                     | 90            |
| 22.     | Rural                     | 95            |
| 23.     | Rural                     | 98            |
| 24.     | Rural                     | 99            |
| 25.     | Fog (heavy advection)     | NA            |
| 26.     | Fog (moderate radiation)  | NA            |
| 27.     | Rain (drizzle)            | NA            |
| 28.     | Rain (widespread)         | NA            |
| 29.     | Rain (thunderstorm)       | NA            |
| 30.     | Snow                      | NA            |
| 31.-49. | (Reserved for future use) |               |
| 50.     | Dust (light loading)      | NA            |
| 51.     | Dust (heavy loading)      | NA            |
| 52.     | High explosive (HE) dust  | NA            |
| 53.     | WP smoke                  | 17            |
| 54.     | WP smoke                  | 50            |
| 55.     | WP smoke                  | 90            |
| 56.     | Fog oil                   | 50            |
| 57.     | HC smoke                  | 85            |

(0 = user supplied), wavelength of this set (micrometers), the albedo for single scattering, and the extinction and scattering coefficients in inverse kilometers. Subsequent to the preamble are values of the phase function at each angle. For most scattering species there will be 32 such sets of angular data. For the smokes,

only 20 wavelength sets are provided, since data was unavailable at wavelengths beyond 12  $\mu\text{m}$ . Table 21 is a schematic example of the structure for PFNDAT.

The PFNDAT phase function data is formatted such that there is always one more data item than the number of angular results called for. The last value is always set to 999.99, which is used by the PFUNC routine to determine the end of the angular data. If a user-specified scattering species is used that has fewer than 65 angles, then a single additional value must be included in the file to indicate the end of each set of angular varying phase function data.

Subroutine PFUNC counts the number of angles, looking for a value of 999.99, and will compare this internally counted number with the value of  $NANG$ , the total number of input angles. Should the two numbers disagree, an error message is printed and execution is halted. The fog, rain, and snow distributions use a different set of angles that are included in subroutine PFUNC; the angles are automatically invoked by using the phase function identifier as a switch.

Table 21. Structure for Aerosol Phase Function Data File PFNDAT.nnn

| $\theta_1$                                  | $\theta_2$                               | ...                                 | $\theta_{11}$                               |
|---|--|-------------------------------------|---|
| $\vdots$                                    | $\ddots$                                 |                                     |   |
| $\theta_{56}$                               | ...                                      | $\theta_{65}$                       | 999.99                                      |
| <i>NANG</i>                                 | nnn                                      | $\lambda_1$                         | $\varpi$ $\beta_{ex}$ $\beta_s$             |
| $P(\theta_1, \lambda_1, \text{nnn})$        | $P(\theta_2, \lambda_1, \text{nnn})$     | ...                                 | $P(\theta_6, \lambda_1, \text{nnn})$        |
| $\vdots$                                    | $\ddots$                                 |                                     |   |
| $P(\theta_{61}, \lambda_1, \text{nnn})$     | $P(\theta_2, \lambda_1, \text{nnn})$     | ...                                 | $P(\theta_{65}, \lambda_1, \text{nnn})$     |
| <i>NANG</i>                                 | nnn                                      | $\lambda_2$                         | $\varpi$ $\beta_{ex}$ $\beta_s$             |
| $P(\theta_1, \lambda_2, \text{nnn})$        | $P(\theta_2, \lambda_2, \text{nnn})$     | ...                                 | $P(\theta_6, \lambda_2, \text{nnn})$        |
| $\vdots$                                    | $\ddots$                                 |                                     |   |
| $P(\theta_{61}, \lambda_2, \text{nnn})$     | $P(\theta_2, \lambda_2, \text{nnn})$     | ...                                 | $P(\theta_{65}, \lambda_2, \text{nnn})$     |
| $\vdots$                                    | $\vdots$                                 | $\vdots$ $\vdots$ $\vdots$ $\vdots$ | $\vdots$                                    |
| <i>NANG</i>                                 | nnn                                      | $\lambda_{max}$                     | $\varpi$ $\beta_{ex}$ $\beta_s$             |
| $P(\theta_1, \lambda_{max}, \text{nnn})$    | $P(\theta_2, \lambda_{max}, \text{nnn})$ | ...                                 | $P(\theta_6, \lambda_{max}, \text{nnn})$    |
| $\vdots$                                    | $\ddots$                                 |                                     |   |
| $P(\theta_{61}, \lambda_{max}, \text{nnn})$ | $P(\theta_2, \lambda_{max}, \text{nnn})$ | ...                                 | $P(\theta_{65}, \lambda_{max}, \text{nnn})$ |

$\theta_i$  = discrete angles (degrees)

*NANG* = number of discrete angles

nnn = phase function identifier from table 20

$\lambda$  = wavelength (micrometers)

$\varpi$  = albedo for single scattering

$\beta_{ex}$  = extinction coefficient ( $\text{km}^{-1}$ )

$\beta_s$  = scattering coefficient ( $\text{km}^{-1}$ )

$P(\theta_i, \lambda_l, \text{nnn})$  = the value of the phase function at angle  $i$ , wavelength  $\ell$ , and aerosol type identifier nnn

## REFERENCES

- Born, M., and E. Wolf, *Principles of Optics, 5th Edition*, Pergamon Press, Oxford, UK, 1975.
- Carlon, H. R., et al., "Infrared Extinction Spectra of Some Cannon Liquid Aerosols," *Applied Optics*, **1b**, p. 1598-1605, 1977.
- Deepak, A., Y. K. Behl, and E. J. Burlbaw, *Modification of the AGAUS Code to Include Scattering by Snow*, STC Technical Report 2004, Science and Technology Corporation, 1982.
- Duncan, L. D., et al., *The Electro-Optical Systems Atmosphere Effects Library, Volume I, Technical Documentation*, ASL-TR-0047, U.S. Army Atmospheric Sciences Laboratory, White Sands Missile Range, NM, 1979.
- Duncan, L. D., editor, *EOSAEL 80, Volume I, Technical Documentation*, ASL-TR-0072, U.S. Army Atmospheric Sciences Laboratory, White Sands Missile Range, NM, 1981.
- Egan, W. G., and T. W. Hilgeman, *Optical Properties of Inhomogeneous Materials*, Academic Press, New York, 1979.
- Epstein, B., "The Mathematical Description of Certain Breakage Mechanisms Leading to the Logarithmic-Normal Distribution," *Journal of the Franklin Institute*, **244**, p. 471-477, 1947.
- Farmer, W. M., "An Evaluation of Data Obtained During the H3S Test," *Proceedings of Smoke Symposium IV*, p. 49-86, Adelphi, MD, 1980.
- Fiegel, R. P., *Natural Aerosol Extinction Module XSCALE92 User's Guide*, ARL-TR-273, U.S. Army Research Laboratory, White Sands Missile Range, NM, 1994.
- Frickel, R. H., G. O. Rubel, and E. W. Stuebing, "Relative Humidity Dependence of the Infrared Extinction by Aerosol Clouds of Phosphoric Acid, UNCLASSIFIED," *Proceedings of Smoke Symposium III (U), CONFIDENTIAL*, PM Smoke/Obscurants, Aberdeen Proving Ground, MD, 1979.
- Gillespie, J. B., and G. Goedecke, "Refractive Indices of Powdered Materials Using Attenuated Total Reflectance Spectroscopy," *Applied Optics*, **28**, p. 3985-3992, 1989.
- Gillespie, J. B., and J. D. Lindberg, "Seasonal and Geographic Variations in Imaginary Refractive Index of Atmospheric Particular Matter." *Applied Optics*, **31**, p. 2107-2112, 1992.

- Gradshteyn, I. S., and I. M. Ryzhik, *Table of Integrals, Series, and Products*, Academic Press, Orlando, FL, 1980.
- Hodkinson, J. R., and L. Greenleaves, "Computations of Light Scattering and Extinction by Spheres According to Diffraction and Geometrical Optics," *Journal of the Optical Society of America*, **53**, p. 577-588, 1963.
- Hodkinson, J. R., "Light Scattering and Extinction by Irregular Particles Larger than the Wavelength," in *Electromagnetic Scattering*, M. Kerker, ed., Macmillan, New York, 1963.
- Hoock, D. W., and R. A. Sutherland, "Obscuration Countermeasures," chapter 6 of *The IR & EO Systems Handbook, Volume 7, Countermeasure Systems*, D. Pollock, ed., ERIM and SPIE Press, Ann Arbor, MI, 1993.
- Ivlev, L. S., and S. I. Popova, "The Complex Refractive Indices of Substances in the Atmosphere-Aerosol Dispersed Phase," *Atmospheric and Oceanic Physics*, **9**, p. 587-591, 1973.
- Jennings, S. G., and J. B. Gillespie, *Mie Theory Sensitivity Studies - The Effects of Aerosol Complex Refractive Index and Size Distribution Variations on Extinction and Absorption Coefficients*, ASL-TR-0003, U.S. Army Atmospheric Sciences Laboratory, White Sands Missile Range, NM, 1978.
- Jennings, S. G., R. G. Pinnick, and H. J. Auvermann, "Effects of Particulate Complex Refractive Index and Particle Size Distribution Variations on Atmospheric Extinction and Absorption for Visible Through Middle IR Wavelengths," *Applied Optics*, **17**, p. 3922-3928, 1978.
- Lentz, W. J., "Generating Bessel Functions in Mie Scattering Calculations Using Continued Fractions," *Applied Optics*, **15**, p. 668-671, 1976.
- Marshall, J. S., and W. M. Palmer, "The Distribution of Raindrops with Size," *Journal of Meteorology*, **5**, p. 165-166, 1948.
- Milham, M. E., et al., *New Findings on the Nature of WP/RP Smokes*, ARCSL-TR-77067, Chemical Systems Laboratory, Aberdeen Proving Ground, MD, 1977.
- Miller, A., *Mie Code AGAUS 82*, ASL-CR-83-0100-3, U.S. Army Atmospheric Sciences Laboratory, White Sands Missile Range, NM, 1983.
- Patterson, E. M., and D. A. Gillette, "Commonalities in Measured Size Distributions for Aerosols Having a Soil-Derived Component," *Journal of Geophysics Research*, **82**, p. 2074-2082, 1977.
- Pinnick, R. G., and S. G. Jennings, *Relationships Between Radiative Properties and Mass Content of Phosphoric Acid, HC, Petroleum Oil, and Sulfuric Acid Military Smokes*, ASL-TR-0052, U.S. Army Atmospheric Sciences Laboratory, White Sands Missile Range, NM, 1980.
- Pinnick, R. G., G. Fernandez, and B. D. Hinds, "Explosion Dust Particle Size Measurements," *Applied Optics*, **22**, p. 95-102, 1983.

- Pollack, J. B., and J. N. Cuzzi, "Scattering by Nonspherical Particles of Size Comparable to a Wavelength: A New Semi-empirical Theory and Its Application to Tropospheric Aerosols," *Journal of the Atmospheric Sciences*, **37**, p. 868-881, 1980.
- Pruppacher, H. R., and J. D. Klett, *Microphysics of Clouds and Precipitation*, D. Reidel Publishing, Boston, MA, 1980.
- Rubel, G. O., *Predicting the Droplet Size and Yield Factors of a Phosphorus Smoke as a Function of Droplet Composition and Ambient Relative Humidity Under Tactical Conditions*, ARCSL-TR-78057, Chemical Systems Laboratory, Aberdeen Proving Ground, MD, 1978.
- Shettle E. P., and R. W. Fenn, *Models for the Aerosols of the Lower Atmosphere and the Effects of Humidity Variations on Their Optical Properties*, AFGL-TR-79-0214, Air Force Geophysics Laboratory, Hanscom Air Force Base, MA, 1979.
- Shirkey, R. C., R. A. Sutherland, and M. A. Seagraves, *EOSAEL 87, Volume 26, Aerosol Phase Function Data Base PFNDAT*, ASL-TR-0221-26, U.S. Army Atmospheric Sciences Laboratory, White Sands Missile Range, NM, 1987.
- Spitzer, W. G., and D. A. Kleinman, "Infrared Lattice Bands of Quartz," *Physical Review*, **121**, p. 1324-1335, 1961.
- Toon, O. B., J. B. Pollack, and B. N. Khare, "Optical Constants of Several Atmospheric Aerosol Species, Ammonium Sulphate, Aluminum Oxide and Sodium Chloride," *Journal of Geophysics Research*, **81**, p. 5733-5748, 1976.
- Toon, O. B., J. B. Pollack, and C. Sagan, "Physical Properties of the Particles Composing the Martian Dust Storm of 1971-1972," *Icarus*, **30**, p. 663-696, 1977.
- R. C. Weast and M. J. Astle, eds., *CRC Handbook of Chemistry and Physics, 61st Edition*, CRC Press, Boca Raton, FL, 1980-1981.
- Weinman J. A., and J. T. Peterson, "Optical Properties of Quartz Dust Particles at Infrared Wavelengths," *Journal of Geophysics Research*, **74**, p. 6947-6952, 1969.
- Winchester, L. W., Jr., N. K. Hanson, and J. E. Jackovich, "Phase Function Measurements of Snow Crystals," *Proceedings of Snow Symposium III*, Cold Regions Research & Engineering Laboratory, Hanover, NH, 1983.

**This page left intentionally blank.**

## ACRONYMS and ABBREVIATIONS

|          |   |
|----------|---|
| ASL      | - The U.S. Army Atmospheric Sciences Laboratory           |
| AFGL     | - The Air Force Geophysics Laboratory                     |
| ARL      | - The U.S. Army Research Laboratory                       |
| AGAUS    | - August Miller's Mie Scattering Code                     |
| AGSNOW   | - A special version of AGAUS for treating SNOW cases      |
| ASCAT    | - An Approximate multiple Scattering model within EOSAEL  |
| EOSAEL   | - The Electro-Optical Systems Atmospheric Effects Library |
| EOSAEL92 | - The 1992 Release of EOSAEL                              |
| FCLOUD   | - A Finite Cloud Transmission model within EOSAEL         |
| HC       | - Hexachloroethane smoke munition                         |
| HE       | - High Explosive artillery munition                       |
| LOS      | - Line of Sight   |
| MSCAT    | - A Multiple Scattering model within EOSAEL               |
| WP       | - White Phosphorus smoke munition                         |

**This page left intentionally blank.**

## Appendix A INDICES OF REFRACTION

The refractive index information for the various haze aerosol constituents is included in this appendix for consistency and completeness. The rural aerosol is composed of small and large rural aerosol components. The urban aerosol is composed of small and large urban aerosol components. The maritime aerosol is composed of the small rural and oceanic aerosol components. Care is needed in composing the correct constituent components of each aerosol. The aerosol extinction coefficient information listed in the main text is produced by using the specific particle size distribution information contained in the tables in the main text and the index of refraction information contained in this appendix as input to the AGAUS model in a Mie scattering calculation.

Table A-1. Index of refraction as a function of relative humidity (0-80 %) for small urban aerosols

| $\lambda$<br>( $\mu\text{m}$ ) | Relative Humidity(%) |        |       |        |       |        |       |        |
|--------------------------------|----------------------|--------|-------|--------|-------|--------|-------|--------|
|                                | 0                    |        | 50    |        | 70    |        | 80    |        |
|                                | $n$                  | $k$    | $n$   | $k$    | $n$   | $k$    | $n$   | $k$    |
| 0.3371                         | 1.574                | 0.0987 | 1.558 | 0.0917 | 1.490 | 0.0625 | 1.427 | 0.0356 |
| 0.4000                         | 1.574                | 0.0967 | 1.557 | 0.0898 | 1.488 | 0.0612 | 1.424 | 0.0348 |
| 0.4880                         | 1.574                | 0.0947 | 1.557 | 0.0880 | 1.486 | 0.0600 | 1.421 | 0.0341 |
| 0.5145                         | 1.574                | 0.0947 | 1.557 | 0.0880 | 1.486 | 0.0600 | 1.420 | 0.0341 |
| 0.5500                         | 1.574                | 0.0933 | 1.557 | 0.0866 | 1.486 | 0.0591 | 1.420 | 0.0336 |
| 0.6328                         | 1.574                | 0.0913 | 1.557 | 0.0848 | 1.485 | 0.0578 | 1.419 | 0.0329 |
| 0.6943                         | 1.574                | 0.0918 | 1.557 | 0.0853 | 1.485 | 0.0581 | 1.419 | 0.0331 |
| 0.8600                         | 1.566                | 0.0946 | 1.549 | 0.0879 | 1.479 | 0.0599 | 1.414 | 0.0341 |
| 1.0600                         | 1.566                | 0.0994 | 1.549 | 0.0823 | 1.478 | 0.0630 | 1.412 | 0.0358 |
| 3.0000                         | 1.442                | 0.123  | 1.437 | 0.134  | 1.416 | 0.178  | 1.396 | 0.218  |
| 3.5000                         | 1.495                | 0.117  | 1.488 | 0.110  | 1.460 | 0.0778 | 1.434 | 0.0483 |
| 4.0000                         | 1.501                | 0.122  | 1.490 | 0.113  | 1.446 | 0.0787 | 1.405 | 0.0468 |
| 4.5000                         | 1.508                | 0.129  | 1.495 | 0.120  | 1.443 | 0.0864 | 1.395 | 0.0549 |
| 5.0000                         | 1.506                | 0.131  | 1.493 | 0.122  | 1.440 | 0.0872 | 1.390 | 0.0550 |
| 7.9000                         | 1.372                | 0.180  | 1.366 | 0.170  | 1.343 | 0.126  | 1.322 | 0.0865 |
| 8.2000                         | 1.263                | 0.210  | 1.264 | 0.197  | 1.271 | 0.146  | 1.278 | 0.0980 |
| 8.5000                         | 1.470                | 0.280  | 1.456 | 0.263  | 1.400 | 0.191  | 1.347 | 0.124  |
| 9.0000                         | 2.276                | 0.381  | 2.203 | 0.356  | 1.904 | 0.256  | 1.627 | 0.163  |
| 9.5000                         | 1.945                | 0.270  | 1.895 | 0.254  | 1.688 | 0.188  | 1.496 | 0.126  |
| 10.0000                        | 1.881                | 0.233  | 1.834 | 0.220  | 1.638 | 0.166  | 1.457 | 0.117  |
| 10.5910                        | 1.818                | 0.214  | 1.773 | 0.204  | 1.584 | 0.160  | 1.409 | 0.120  |
| 11.0000                        | 1.798                | 0.199  | 1.752 | 0.192  | 1.561 | 0.162  | 1.385 | 0.134  |
| 11.5000                        | 1.765                | 0.198  | 1.719 | 0.194  | 1.530 | 0.178  | 1.356 | 0.162  |
| 12.5000                        | 1.724                | 0.201  | 1.681 | 0.205  | 1.503 | 0.222  | 1.339 | 0.238  |
| 14.0000                        | 1.700                | 0.216  | 1.665 | 0.227  | 1.520 | 0.273  | 1.387 | 0.315  |
| 15.0000                        | 1.638                | 0.294  | 1.612 | 0.302  | 1.503 | 0.334  | 1.403 | 0.363  |
| 18.0000                        | 1.982                | 0.293  | 1.942 | 0.303  | 1.777 | 0.342  | 1.624 | 0.378  |
| 20.0000                        | 2.080                | 0.346  | 2.037 | 0.349  | 1.860 | 0.363  | 1.696 | 0.376  |
| 25.0000                        | 2.028                | 0.392  | 1.992 | 0.390  | 1.845 | 0.379  | 1.710 | 0.369  |
| 30.0000                        | 1.965                | 0.455  | 1.936 | 0.446  | 1.813 | 0.408  | 1.700 | 0.374  |
| 35.0000                        | 2.057                | 0.538  | 2.020 | 0.524  | 1.865 | 0.464  | 1.721 | 0.409  |
| 40.0000                        | 2.084                | 0.624  | 2.043 | 0.607  | 1.876 | 0.536  | 1.722 | 0.471  |

Table A-2. Index of refraction as a function of relative humidity (90-99 %) for small urban aerosols

| $\lambda$<br>( $\mu\text{m}$ ) | Relative Humidity(%) |        |       |        |       |         |       |         |
|--------------------------------|----------------------|--------|-------|--------|-------|---------|-------|---------|
|                                | 90                   |        | 95    |        | 98    |         | 99    |         |
|                                | $n$                  | $k$    | $n$   | $k$    | $n$   | $k$     | $n$   | $k$     |
| 0.3371                         | 1.394                | 0.0210 | 1.375 | 0.0131 | 1.362 | 0.00716 | 1.356 | 0.00480 |
| 0.4000                         | 1.389                | 0.0206 | 1.370 | 0.0128 | 1.356 | 0.00701 | 1.350 | 0.00471 |
| 0.4880                         | 1.386                | 0.0202 | 1.367 | 0.0125 | 1.352 | 0.00687 | 1.347 | 0.00461 |
| 0.5145                         | 1.385                | 0.0202 | 1.366 | 0.0125 | 1.351 | 0.00687 | 1.346 | 0.00461 |
| 0.5500                         | 1.384                | 0.0199 | 1.365 | 0.0124 | 1.350 | 0.00676 | 1.345 | 0.00454 |
| 0.6328                         | 1.384                | 0.0194 | 1.364 | 0.0121 | 1.350 | 0.00662 | 1.344 | 0.00444 |
| 0.6943                         | 1.383                | 0.0196 | 1.363 | 0.0122 | 1.349 | 0.00666 | 1.343 | 0.00447 |
| 0.8600                         | 1.379                | 0.0201 | 1.360 | 0.0125 | 1.346 | 0.00686 | 1.341 | 0.00461 |
| 1.0600                         | 1.377                | 0.0212 | 1.358 | 0.0132 | 1.343 | 0.00721 | 1.338 | 0.00484 |
| 3.0000                         | 1.386                | 0.240  | 1.380 | 0.252  | 1.376 | 0.261   | 1.374 | 0.265   |
| 3.5000                         | 1.420                | 0.0324 | 1.413 | 0.0237 | 1.407 | 0.0172  | 1.405 | 0.0147  |
| 4.0000                         | 1.383                | 0.0295 | 1.371 | 0.0201 | 1.362 | 0.0131  | 1.358 | 0.0103  |
| 4.5000                         | 1.369                | 0.0379 | 1.355 | 0.0286 | 1.345 | 0.0218  | 1.341 | 0.0190  |
| 5.0000                         | 1.364                | 0.0376 | 1.349 | 0.0281 | 1.338 | 0.0210  | 1.334 | 0.0182  |
| 7.9000                         | 1.311                | 0.0650 | 1.304 | 0.0533 | 1.300 | 0.0445  | 1.298 | 0.0410  |
| 8.2000                         | 1.281                | 0.0723 | 1.283 | 0.0582 | 1.284 | 0.0478  | 1.285 | 0.0436  |
| 8.5000                         | 1.319                | 0.0885 | 1.303 | 0.0689 | 1.292 | 0.0543  | 1.287 | 0.0485  |
| 9.0000                         | 1.478                | 1.12   | 1.396 | 0.0851 | 1.335 | 0.0646  | 1.311 | 0.0565  |
| 9.5000                         | 1.392                | 0.0925 | 1.336 | 0.0743 | 1.294 | 0.0607  | 1.277 | 0.0554  |
| 10.0000                        | 1.359                | 0.0896 | 1.306 | 0.0750 | 1.266 | 0.0640  | 1.250 | 0.0597  |
| 10.5910                        | 1.315                | 0.0986 | 1.264 | 0.0868 | 1.225 | 0.0780  | 1.210 | 0.0745  |
| 11.0000                        | 1.290                | 0.119  | 1.238 | 0.110  | 1.200 | 0.104   | 1.184 | 0.102   |
| 11.5000                        | 1.262                | 0.154  | 1.211 | 0.149  | 1.172 | 0.146   | 1.157 | 0.145   |
| 12.5000                        | 1.251                | 0.247  | 1.203 | 0.251  | 1.167 | 0.255   | 1.152 | 0.256   |
| 14.0000                        | 1.314                | 0.337  | 1.275 | 0.350  | 1.246 | 0.359   | 1.234 | 0.363   |
| 15.0000                        | 1.348                | 0.379  | 1.319 | 0.388  | 1.297 | 0.394   | 1.288 | 0.397   |
| 18.0000                        | 1.542                | 0.398  | 1.497 | 0.408  | 1.464 | 0.416   | 1.450 | 0.420   |
| 20.0000                        | 1.608                | 0.383  | 1.560 | 0.387  | 1.524 | 0.390   | 1.509 | 0.391   |
| 25.0000                        | 1.637                | 0.364  | 1.597 | 0.361  | 1.567 | 0.359   | 1.555 | 0.358   |
| 30.0000                        | 1.639                | 0.355  | 1.606 | 0.345  | 1.581 | 0.337   | 1.571 | 0.334   |
| 35.0000                        | 1.644                | 0.379  | 1.602 | 0.363  | 1.570 | 0.351   | 1.558 | 0.346   |
| 40.0000                        | 1.639                | 0.436  | 1.594 | 0.417  | 1.560 | 0.402   | 1.546 | 0.397   |

Table A-3. Index of refraction as a function of relative humidity (0-80 %) for large urban aerosols

| $\lambda$<br>( $\mu\text{m}$ ) | Relative Humidity(%) |        |       |        |       |        |       |        |
|--------------------------------|----------------------|--------|-------|--------|-------|--------|-------|--------|
|                                | 0                    |        | 50    |        | 70    |        | 80    |        |
|                                | $n$                  | $k$    | $n$   | $k$    | $n$   | $k$    | $n$   | $k$    |
| 0.3371                         | 1.574                | 0.0987 | 1.556 | 0.0908 | 1.479 | 0.0580 | 1.428 | 0.0323 |
| 0.4000                         | 1.574                | 0.0967 | 1.555 | 0.0890 | 1.477 | 0.0568 | 1.416 | 0.0316 |
| 0.4880                         | 1.574                | 0.0947 | 1.555 | 0.0871 | 1.475 | 0.0556 | 1.413 | 0.0310 |
| 0.5145                         | 1.574                | 0.0947 | 1.555 | 0.0871 | 1.475 | 0.0556 | 1.413 | 0.0310 |
| 0.5500                         | 1.574                | 0.0933 | 1.555 | 0.0858 | 1.474 | 0.0548 | 1.412 | 0.0305 |
| 0.6328                         | 1.574                | 0.0913 | 1.555 | 0.0840 | 1.474 | 0.0536 | 1.411 | 0.0299 |
| 0.6943                         | 1.574                | 0.0918 | 1.555 | 0.0845 | 1.474 | 0.0539 | 1.411 | 0.0300 |
| 0.8600                         | 1.566                | 0.0946 | 1.547 | 0.0871 | 1.468 | 0.0556 | 1.407 | 0.0310 |
| 1.0600                         | 1.566                | 0.0994 | 1.547 | 0.0815 | 1.467 | 0.0584 | 1.405 | 0.0325 |
| 3.0000                         | 1.442                | 0.123  | 1.436 | 0.135  | 1.412 | 0.185  | 1.394 | 0.223  |
| 3.5000                         | 1.495                | 0.117  | 1.488 | 0.109  | 1.456 | 0.0728 | 1.431 | 0.0448 |
| 4.0000                         | 1.501                | 0.122  | 1.489 | 0.112  | 1.439 | 0.0733 | 1.400 | 0.0429 |
| 4.5000                         | 1.508                | 0.129  | 1.494 | 0.119  | 1.435 | 0.0811 | 1.390 | 0.0511 |
| 5.0000                         | 1.506                | 0.131  | 1.492 | 0.121  | 1.431 | 0.0818 | 1.384 | 0.0511 |
| 7.9000                         | 1.372                | 0.180  | 1.366 | 0.168  | 1.340 | 0.120  | 1.320 | 0.0817 |
| 8.2000                         | 1.263                | 0.210  | 1.265 | 0.196  | 1.272 | 0.134  | 1.278 | 0.0922 |
| 8.5000                         | 1.470                | 0.280  | 1.455 | 0.261  | 1.391 | 0.180  | 1.341 | 0.116  |
| 9.0000                         | 2.276                | 0.381  | 2.194 | 0.354  | 1.857 | 0.240  | 1.594 | 0.151  |
| 9.5000                         | 1.945                | 0.270  | 1.889 | 0.252  | 1.655 | 0.177  | 1.473 | 0.118  |
| 10.0000                        | 1.881                | 0.233  | 1.828 | 0.219  | 1.607 | 0.158  | 1.435 | 0.111  |
| 10.5910                        | 1.818                | 0.214  | 1.767 | 0.202  | 1.554 | 0.153  | 1.388 | 0.115  |
| 11.0000                        | 1.798                | 0.199  | 1.746 | 0.191  | 1.532 | 0.157  | 1.364 | 0.130  |
| 11.5000                        | 1.765                | 0.198  | 1.714 | 0.194  | 1.501 | 0.175  | 1.335 | 0.160  |
| 12.5000                        | 1.724                | 0.201  | 1.676 | 0.206  | 1.476 | 0.225  | 1.320 | 0.240  |
| 14.0000                        | 1.700                | 0.216  | 1.661 | 0.229  | 1.498 | 0.280  | 1.370 | 0.320  |
| 15.0000                        | 1.638                | 0.294  | 1.609 | 0.303  | 1.486 | 0.339  | 1.390 | 0.367  |
| 18.0000                        | 1.982                | 0.293  | 1.938 | 0.304  | 1.751 | 0.348  | 1.606 | 0.383  |
| 20.0000                        | 2.080                | 0.346  | 2.032 | 0.350  | 1.832 | 0.365  | 1.676 | 0.378  |
| 25.0000                        | 2.028                | 0.392  | 1.988 | 0.389  | 1.823 | 0.377  | 1.693 | 0.368  |
| 30.0000                        | 1.965                | 0.455  | 1.932 | 0.445  | 1.794 | 0.402  | 1.687 | 0.369  |
| 35.0000                        | 2.057                | 0.538  | 2.015 | 0.522  | 1.840 | 0.455  | 1.704 | 0.402  |
| 40.0000                        | 2.084                | 0.624  | 2.038 | 0.605  | 1.850 | 0.525  | 1.704 | 0.463  |

Table A-4. Index of refraction as a function of relative humidity (90-99 %) for large urban aerosols

| $\lambda$<br>( $\mu\text{m}$ ) | Relative Humidity(%) |        |       |         |       |         |       |         |
|--------------------------------|----------------------|--------|-------|---------|-------|---------|-------|---------|
|                                | 90                   |        | 95    |         | 98    |         | 99    |         |
|                                | $n$                  | $k$    | $n$   | $k$     | $n$   | $k$     | $n$   | $k$     |
| 0.3371                         | 1.387                | 0.0179 | 1.368 | 0.00982 | 1.354 | 0.00395 | 1.349 | 0.00193 |
| 0.4000                         | 1.382                | 0.0176 | 1.362 | 0.00962 | 1.348 | 0.00387 | 1.344 | 0.00189 |
| 0.4880                         | 1.378                | 0.0172 | 1.359 | 0.00942 | 1.345 | 0.00379 | 1.340 | 0.00185 |
| 0.5145                         | 1.378                | 0.0172 | 1.358 | 0.00942 | 1.344 | 0.00379 | 1.339 | 0.00185 |
| 0.5500                         | 1.377                | 0.0170 | 1.357 | 0.00928 | 1.343 | 0.00374 | 1.338 | 0.00182 |
| 0.6328                         | 1.376                | 0.0166 | 1.356 | 0.00908 | 1.342 | 0.00366 | 1.337 | 0.00178 |
| 0.6943                         | 1.375                | 0.0167 | 1.355 | 0.00913 | 1.341 | 0.00368 | 1.336 | 0.00179 |
| 0.8600                         | 1.372                | 0.0172 | 1.353 | 0.00941 | 1.338 | 0.00379 | 1.334 | 0.00185 |
| 1.0600                         | 1.370                | 0.0181 | 1.350 | 0.00989 | 1.336 | 0.00399 | 1.331 | 0.00194 |
| 3.0000                         | 1.384                | 0.245  | 1.378 | 0.257   | 1.374 | 0.266   | 1.372 | 0.269   |
| 3.5000                         | 1.417                | 0.0290 | 1.409 | 0.0201  | 1.404 | 0.0137  | 1.402 | 0.0115  |
| 4.0000                         | 1.378                | 0.0259 | 1.366 | 0.0162  | 1.357 | 0.00929 | 1.354 | 0.00688 |
| 4.5000                         | 1.364                | 0.0344 | 1.350 | 0.0249  | 1.339 | 0.0180  | 1.335 | 0.0156  |
| 5.0000                         | 1.358                | 0.0339 | 1.343 | 0.0241  | 1.332 | 0.0171  | 1.329 | 0.0147  |
| 7.9000                         | 1.308                | 0.0605 | 1.302 | 0.0484  | 1.297 | 0.0398  | 1.296 | 0.0368  |
| 8.2000                         | 1.282                | 0.0669 | 1.284 | 0.0525  | 1.285 | 0.0421  | 1.286 | 0.0385  |
| 8.5000                         | 1.313                | 0.0809 | 1.297 | 0.0608  | 1.286 | 0.0464  | 1.282 | 0.0414  |
| 9.0000                         | 1.446                | 0.102  | 1.363 | 0.0738  | 1.303 | 0.0536  | 1.282 | 0.0466  |
| 9.5000                         | 1.371                | 0.0855 | 1.313 | 0.0668  | 1.271 | 0.0534  | 1.257 | 0.0488  |
| 10.0000                        | 1.339                | 0.0840 | 1.264 | 0.0689  | 1.245 | 0.0581  | 1.231 | 0.0544  |
| 10.5910                        | 1.295                | 0.0941 | 1.243 | 0.0820  | 1.265 | 0.0733  | 1.191 | 0.0703  |
| 11.0000                        | 1.270                | 0.115  | 1.217 | 0.107   | 1.179 | 0.101   | 1.166 | 0.0988  |
| 11.5000                        | 1.242                | 0.152  | 1.190 | 0.148   | 1.152 | 0.144   | 1.138 | 0.143   |
| 12.5000                        | 1.232                | 0.249  | 1.133 | 0.253   | 1.147 | 0.257   | 1.135 | 0.258   |
| 14.0000                        | 1.299                | 0.342  | 1.259 | 0.355   | 1.230 | 0.364   | 1.220 | 0.367   |
| 15.0000                        | 1.337                | 0.382  | 1.307 | 0.391   | 1.285 | 0.398   | 1.277 | 0.400   |
| 18.0000                        | 1.525                | 0.402  | 1.475 | 0.413   | 1.445 | 0.421   | 1.434 | 0.423   |
| 20.0000                        | 1.589                | 0.384  | 1.540 | 0.388   | 1.504 | 0.391   | 1.492 | 0.392   |
| 25.0000                        | 1.621                | 0.363  | 1.580 | 0.360   | 1.551 | 0.357   | 1.541 | 0.357   |
| 30.0000                        | 1.626                | 0.351  | 1.592 | 0.341   | 1.568 | 0.333   | 1.559 | 0.336   |
| 35.0000                        | 1.627                | 0.373  | 1.584 | 0.356   | 1.553 | 0.344   | 1.542 | 0.348   |
| 40.0000                        | 1.622                | 0.428  | 1.575 | 0.409   | 1.542 | 0.395   | 1.530 | 0.398   |

Table A-5. Index of refraction as a function of relative humidity (0-80 %) for small rural aerosols

| $\lambda$<br>( $\mu\text{m}$ ) | Relative Humidity(%) |         |       |         |       |         |       |         |
|--------------------------------|----------------------|---------|-------|---------|-------|---------|-------|---------|
|                                | 0                    |         | 50    |         | 70    |         | 80    |         |
|                                | $n$                  | $k$     | $n$   | $k$     | $n$   | $k$     | $n$   | $k$     |
| 0.3371                         | 1.530                | 0.00590 | 1.520 | 0.00560 | 1.503 | 0.00504 | 1.449 | 0.00331 |
| 0.4000                         | 1.530                | 0.00590 | 1.520 | 0.00560 | 1.502 | 0.00504 | 1.446 | 0.00331 |
| 0.4880                         | 1.530                | 0.00590 | 1.520 | 0.00560 | 1.501 | 0.00504 | 1.444 | 0.00331 |
| 0.5145                         | 1.530                | 0.00590 | 1.520 | 0.00560 | 1.501 | 0.00504 | 1.444 | 0.00331 |
| 0.5500                         | 1.530                | 0.00660 | 1.520 | 0.00626 | 1.501 | 0.00563 | 1.443 | 0.00370 |
| 0.6328                         | 1.530                | 0.00660 | 1.520 | 0.00626 | 1.501 | 0.00563 | 1.443 | 0.00370 |
| 0.6943                         | 1.530                | 0.00730 | 1.520 | 0.00692 | 1.501 | 0.00623 | 1.443 | 0.00409 |
| 0.8600                         | 1.520                | 0.0108  | 1.510 | 0.0102  | 1.492 | 0.00922 | 1.436 | 0.00606 |
| 1.0600                         | 1.520                | 0.0143  | 1.510 | 0.0136  | 1.492 | 0.0122  | 1.435 | 0.00802 |
| 3.0000                         | 1.342                | 0.0190  | 1.343 | 0.0320  | 1.346 | 0.0560  | 1.355 | 0.130   |
| 3.5000                         | 1.399                | 0.00680 | 1.399 | 0.00693 | 1.399 | 0.00718 | 1.399 | 0.00794 |
| 4.0000                         | 1.397                | 0.00710 | 1.394 | 0.00697 | 1.390 | 0.00673 | 1.377 | 0.00600 |
| 4.5000                         | 1.400                | 0.0133  | 1.397 | 0.0133  | 1.390 | 0.0133  | 1.370 | 0.0133  |
| 5.0000                         | 1.390                | 0.0132  | 1.387 | 0.0132  | 1.380 | 0.0131  | 1.361 | 0.0128  |
| 7.9000                         | 1.185                | 0.0575  | 1.191 | 0.0563  | 1.201 | 0.0540  | 1.233 | 0.0471  |
| 8.2000                         | 1.046                | 0.0922  | 1.058 | 0.0893  | 1.081 | 0.0839  | 1.151 | 0.0671  |
| 8.5000                         | 1.300                | 0.178   | 1.299 | 0.170   | 1.297 | 0.157   | 1.290 | 0.116   |
| 9.0000                         | 2.302                | 0.301   | 2.249 | 0.288   | 2.150 | 0.263   | 1.845 | 0.186   |
| 9.5000                         | 1.884                | 0.161   | 1.851 | 0.155   | 1.790 | 0.144   | 1.602 | 0.110   |
| 10.0000                        | 1.799                | 0.112   | 1.769 | 0.108   | 1.714 | 0.103   | 1.544 | 0.0849  |
| 10.5910                        | 1.718                | 0.0850  | 1.690 | 0.0841  | 1.639 | 0.0824  | 1.481 | 0.0773  |
| 11.0000                        | 1.690                | 0.0665  | 1.662 | 0.0681  | 1.611 | 0.0709  | 1.454 | 0.0798  |
| 11.5000                        | 1.646                | 0.0629  | 1.619 | 0.0670  | 1.570 | 0.0745  | 1.418 | 0.0976  |
| 12.5000                        | 1.587                | 0.0641  | 1.563 | 0.0741  | 1.519 | 0.0926  | 1.383 | 0.150   |
| 14.0000                        | 1.548                | 0.0766  | 1.531 | 0.0917  | 1.499 | 0.120   | 1.400 | 0.205   |
| 15.0000                        | 1.465                | 0.170   | 1.455 | 0.182   | 1.436 | 0.204   | 1.379 | 0.272   |
| 18.0000                        | 1.878                | 0.161   | 1.855 | 0.174   | 1.811 | 0.199   | 1.678 | 0.277   |
| 20.0000                        | 1.988                | 0.220   | 1.962 | 0.229   | 1.914 | 0.245   | 1.765 | 0.296   |
| 25.0000                        | 1.907                | 0.268   | 1.888 | 0.273   | 1.852 | 0.281   | 1.742 | 0.307   |
| 30.0000                        | 1.814                | 0.336   | 1.800 | 0.336   | 1.776 | 0.335   | 1.698 | 0.332   |
| 35.0000                        | 1.914                | 0.430   | 1.894 | 0.425   | 1.858 | 0.416   | 1.746 | 0.389   |
| 40.0000                        | 1.932                | 0.530   | 1.911 | 0.523   | 1.872 | 0.509   | 1.751 | 0.466   |

Table A-6. Index of refraction as a function of relative humidity (90-99 %) for small rural aerosols

| $\lambda$<br>( $\mu\text{m}$ ) | Relative Humidity(%) |         |       |         |       |         |       |          |
|--------------------------------|----------------------|---------|-------|---------|-------|---------|-------|----------|
|                                | 90                   |         | 95    |         | 98    |         | 99    |          |
|                                | $n$                  | $k$     | $n$   | $k$     | $n$   | $k$     | $n$   | $k$      |
| 0.3371                         | 1.407                | 0.00198 | 1.393 | 0.00153 | 1.379 | 0.00108 | 1.371 | 0.000819 |
| 0.4000                         | 1.403                | 0.00198 | 1.388 | 0.00153 | 1.374 | 0.00108 | 1.366 | 0.000819 |
| 0.4880                         | 1.401                | 0.00198 | 1.385 | 0.00153 | 1.371 | 0.00108 | 1.362 | 0.000819 |
| 0.5145                         | 1.400                | 0.00198 | 1.385 | 0.00153 | 1.370 | 0.00108 | 1.361 | 0.000819 |
| 0.5500                         | 1.399                | 0.00222 | 1.384 | 0.00171 | 1.369 | 0.00121 | 1.360 | 0.000916 |
| 0.6328                         | 1.399                | 0.00222 | 1.383 | 0.00171 | 1.368 | 0.00121 | 1.359 | 0.000916 |
| 0.6943                         | 1.398                | 0.00245 | 1.382 | 0.00189 | 1.368 | 0.00134 | 1.359 | 0.00101  |
| 0.8600                         | 1.393                | 0.00363 | 1.378 | 0.00279 | 1.364 | 0.00198 | 1.356 | 0.00150  |
| 1.0600                         | 1.391                | 0.00481 | 1.376 | 0.00370 | 1.362 | 0.00263 | 1.353 | 0.00199  |
| 3.0000                         | 1.361                | 0.187   | 1.364 | 0.207   | 1.366 | 0.266   | 1.367 | 0.237    |
| 3.5000                         | 1.400                | 0.00853 | 1.400 | 0.00873 | 1.400 | 0.00892 | 1.400 | 0.00904  |
| 4.0000                         | 1.366                | 0.00544 | 1.363 | 0.00525 | 1.359 | 0.00506 | 1.357 | 0.00495  |
| 4.5000                         | 1.355                | 0.0134  | 1.350 | 0.0134  | 1.344 | 0.0134  | 1.341 | 0.0134   |
| 5.0000                         | 1.347                | 0.0127  | 1.342 | 0.0126  | 1.337 | 0.0125  | 1.344 | 0.0125   |
| 7.9000                         | 1.257                | 0.0418  | 1.266 | 0.0400  | 1.274 | 0.0382  | 1.279 | 0.0372   |
| 8.2000                         | 1.205                | 0.0543  | 1.224 | 0.0499  | 1.242 | 0.0456  | 1.253 | 0.0430   |
| 8.5000                         | 1.285                | 0.0840  | 1.284 | 0.0731  | 1.282 | 0.0625  | 1.281 | 0.0562   |
| 9.0000                         | 1.611                | 0.128   | 1.531 | 0.107   | 1.453 | 0.0878  | 1.406 | 0.0761   |
| 9.5000                         | 1.458                | 0.0834  | 1.409 | 0.0744  | 1.361 | 0.0657  | 1.332 | 0.0605   |
| 10.0000                        | 1.413                | 0.0712  | 1.368 | 0.0665  | 1.325 | 0.0620  | 1.299 | 0.0592   |
| 10.5910                        | 1.360                | 0.0733  | 1.318 | 0.0720  | 1.278 | 0.0706  | 1.254 | 0.0699   |
| 11.0000                        | 1.333                | 0.0866  | 1.292 | 0.0890  | 1.252 | 0.0912  | 1.228 | 0.0926   |
| 11.5000                        | 1.301                | 0.115   | 1.260 | 0.122   | 1.221 | 0.127   | 1.198 | 0.131    |
| 12.5000                        | 1.279                | 0.194   | 1.243 | 0.209   | 1.208 | 0.223   | 1.187 | 0.232    |
| 14.0000                        | 1.324                | 0.271   | 1.297 | 0.294   | 1.272 | 0.316   | 1.257 | 0.329    |
| 15.0000                        | 1.336                | 0.324   | 1.320 | 0.342   | 1.306 | 0.359   | 1.297 | 0.370    |
| 18.0000                        | 1.576                | 0.337   | 1.541 | 0.357   | 1.507 | 0.377   | 1.486 | 0.389    |
| 20.0000                        | 1.651                | 0.335   | 1.611 | 0.348   | 1.573 | 0.361   | 1.550 | 0.369    |
| 25.0000                        | 1.657                | 0.326   | 1.628 | 0.333   | 1.600 | 0.340   | 1.583 | 0.344    |
| 30.0000                        | 1.639                | 0.331   | 1.619 | 0.330   | 1.599 | 0.329   | 1.587 | 0.329    |
| 35.0000                        | 1.660                | 0.368   | 1.631 | 0.360   | 1.602 | 0.353   | 1.585 | 0.349    |
| 40.0000                        | 1.658                | 0.434   | 1.626 | 0.422   | 1.595 | 0.412   | 1.576 | 0.405    |

Table A-7. Index of refraction as a function of relative humidity (0-80 %) for large rural aerosols

| $\lambda$<br>( $\mu\text{m}$ ) | Relative Humidity(%) |         |       |         |       |         |       |         |
|--------------------------------|----------------------|---------|-------|---------|-------|---------|-------|---------|
|                                | 0                    |         | 50    |         | 70    |         | 80    |         |
|                                | $n$                  | $k$     | $n$   | $k$     | $n$   | $k$     | $n$   | $k$     |
| 0.3371                         | 1.53                 | 0.00590 | 1.520 | 0.00559 | 1.499 | 0.00491 | 1.435 | 0.00286 |
| 0.4000                         | 1.53                 | 0.00590 | 1.520 | 0.00559 | 1.498 | 0.00491 | 1.431 | 0.00286 |
| 0.4880                         | 1.53                 | 0.00590 | 1.520 | 0.00559 | 1.497 | 0.00491 | 1.429 | 0.00286 |
| 0.5145                         | 1.53                 | 0.00590 | 1.520 | 0.00559 | 1.497 | 0.00491 | 1.429 | 0.00286 |
| 0.5500                         | 1.53                 | 0.00660 | 1.520 | 0.00626 | 1.497 | 0.00549 | 1.428 | 0.00319 |
| 0.6328                         | 1.53                 | 0.00660 | 1.520 | 0.00626 | 1.497 | 0.00549 | 1.428 | 0.00319 |
| 0.6943                         | 1.53                 | 0.00730 | 1.520 | 0.00692 | 1.497 | 0.00608 | 1.427 | 0.00353 |
| 0.8600                         | 1.52                 | 0.0108  | 1.510 | 0.0102  | 1.488 | 0.00899 | 1.421 | 0.00523 |
| 1.0600                         | 1.52                 | 0.0143  | 1.510 | 0.0136  | 1.487 | 0.0119  | 1.420 | 0.00692 |
| 3.0000                         | 1.342                | 0.0190  | 1.344 | 0.0321  | 1.347 | 0.0614  | 1.357 | 0.150   |
| 3.5000                         | 1.399                | 0.00680 | 1.399 | 0.00693 | 1.399 | 0.00724 | 1.400 | 0.00814 |
| 4.0000                         | 1.379                | 0.00710 | 1.394 | 0.00697 | 1.389 | 0.00668 | 1.373 | 0.00581 |
| 4.5000                         | 1.40                 | 0.0133  | 1.396 | 0.0133  | 1.389 | 0.0133  | 1.365 | 0.0134  |
| 5.0000                         | 1.39                 | 0.0132  | 1.387 | 0.0132  | 1.397 | 0.0131  | 1.356 | 0.0128  |
| 7.9000                         | 1.185                | 0.0575  | 1.191 | 0.0563  | 1.203 | 0.0535  | 1.241 | 0.0453  |
| 8.2000                         | 1.046                | 0.0922  | 1.058 | 0.0892  | 1.086 | 0.0826  | 1.170 | 0.0627  |
| 8.5000                         | 1.30                 | 0.178   | 1.299 | 0.170   | 1.296 | 0.154   | 1.289 | 0.105   |
| 9.0000                         | 2.302                | 0.301   | 2.248 | 0.287   | 2.128 | 0.257   | 1.765 | 0.166   |
| 9.5000                         | 1.884                | 0.161   | 1.851 | 0.155   | 1.777 | 0.141   | 1.553 | 0.101   |
| 10.0000                        | 1.799                | 0.112   | 1.769 | 0.108   | 1.702 | 0.101   | 1.499 | 0.0802  |
| 10.5910                        | 1.718                | 0.0850  | 1.690 | 0.0841  | 1.628 | 0.0821  | 1.440 | 0.0759  |
| 11.0000                        | 1.69                 | 0.0665  | 1.662 | 0.0681  | 1.600 | 0.0716  | 1.413 | 0.0821  |
| 11.5000                        | 1.646                | 0.0629  | 1.619 | 0.0670  | 1.559 | 0.0762  | 1.378 | 0.104   |
| 12.5000                        | 1.587                | 0.0641  | 1.563 | 0.0742  | 1.509 | 0.0968  | 1.348 | 0.165   |
| 14.0000                        | 1.548                | 0.0766  | 1.531 | 0.0918  | 1.491 | 0.126   | 1.374 | 0.228   |
| 15.0000                        | 1.465                | 0.170   | 1.455 | 0.182   | 1.432 | 0.209   | 1.364 | 0.290   |
| 18.0000                        | 1.878                | 0.161   | 1.854 | 0.174   | 1.802 | 0.205   | 1.643 | 0.298   |
| 20.0000                        | 1.988                | 0.220   | 1.962 | 0.228   | 1.903 | 0.249   | 1.726 | 0.309   |
| 25.0000                        | 1.907                | 0.268   | 1.888 | 0.273   | 1.844 | 0.283   | 1.713 | 0.313   |
| 30.0000                        | 1.814                | 0.336   | 1.800 | 0.336   | 1.770 | 0.335   | 1.678 | 0.332   |
| 35.0000                        | 1.914                | 0.430   | 1.894 | 0.425   | 1.850 | 0.414   | 1.717 | 0.381   |
| 40.0000                        | 1.932                | 0.530   | 1.911 | 0.522   | 1.863 | 0.506   | 1.719 | 0.455   |

Table A-8. Index of refraction as a function of relative humidity (90-99 %) for large rural aerosols

| $\lambda$<br>( $\mu\text{m}$ ) | Relative Humidity(%) |          |          |          |          |          |          |          |
|--------------------------------|----------------------|----------|----------|----------|----------|----------|----------|----------|
|                                | 90                   |          | 95       |          | 98       |          | 99       |          |
|                                | <i>n</i>             | <i>k</i> | <i>n</i> | <i>k</i> | <i>n</i> | <i>k</i> | <i>n</i> | <i>k</i> |
| 0.3371                         | 1.40                 | 0.00174  | 1.386    | 0.00132  | 1.361    | 0.000509 | 1.354    | 0.000289 |
| 0.4000                         | 1.395                | 0.00174  | 1.382    | 0.00132  | 1.355    | 0.000509 | 1.348    | 0.000289 |
| 0.4880                         | 1.392                | 0.00174  | 1.379    | 0.00132  | 1.352    | 0.000509 | 1.345    | 0.000289 |
| 0.5145                         | 1.392                | 0.00174  | 1.378    | 0.00132  | 1.351    | 0.000509 | 1.344    | 0.000289 |
| 0.5500                         | 1.391                | 0.00194  | 1.377    | 0.00148  | 1.350    | 0.000570 | 1.343    | 0.000323 |
| 0.6328                         | 1.39                 | 0.00194  | 1.376    | 0.00148  | 1.349    | 0.000570 | 1.342    | 0.000323 |
| 0.6943                         | 1.39                 | 0.00215  | 1.376    | 0.00164  | 1.348    | 0.000630 | 1.341    | 0.000357 |
| 0.8600                         | 1.385                | 0.00318  | 1.372    | 0.00242  | 1.345    | 0.000933 | 1.338    | 0.000529 |
| 1.0600                         | 1.383                | 0.00422  | 1.369    | 0.00321  | 1.343    | 0.100    | 1.335    | 0.000240 |
| 3.0000                         | 1.362                | 0.197    | 1.364    | 0.215    | 1.368    | 0.250    | 1.370    | 0.260    |
| 3.5000                         | 1.40                 | 0.00863  | 1.400    | 0.00882  | 1.400    | 0.00918  | 1.400    | 0.00927  |
| 4.0000                         | 1.364                | 0.00534  | 1.361    | 0.00516  | 1.355    | 0.00482  | 1.353    | 0.00472  |
| 4.5000                         | 1.352                | 0.0134   | 1.347    | 0.0134   | 1.338    | 0.0134   | 1.335    | 0.0134   |
| 5.0000                         | 1.344                | 0.0126   | 1.340    | 0.0126   | 1.331    | 0.0126   | 1.328    | 0.0125   |
| 7.9000                         | 1.262                | 0.0409   | 1.270    | 0.0392   | 1.285    | 0.0359   | 1.289    | 0.0351   |
| 8.2000                         | 1.215                | 0.0519   | 1.232    | 0.0479   | 1.265    | 0.0400   | 1.274    | 0.0379   |
| 8.5000                         | 1.284                | 0.0781   | 1.283    | 0.0682   | 1.280    | 0.0488   | 1.279    | 0.0435   |
| 9.0000                         | 1.568                | 0.117    | 1.495    | 0.0984   | 1.352    | 0.0624   | 1.313    | 0.0527   |
| 9.5000                         | 1.432                | 0.0786   | 1.387    | 0.0704   | 1.298    | 0.0544   | 1.274    | 0.0500   |
| 10.0000                        | 1.389                | 0.0687   | 1.348    | 0.0644   | 1.268    | 0.0561   | 1.246    | 0.0538   |
| 10.5910                        | 1.338                | 0.0726   | 1.300    | 0.0714   | 1.226    | 0.0689   | 1.205    | 0.0683   |
| 11.0000                        | 1.311                | 0.0879   | 1.273    | 0.0900   | 1.199    | 0.0942   | 1.179    | 0.0953   |
| 11.5000                        | 1.279                | 0.119    | 1.243    | 0.124    | 1.171    | 0.135    | 1.151    | 0.138    |
| 12.5000                        | 1.26                 | 0.202    | 1.227    | 0.215    | 1.163    | 0.242    | 1.146    | 0.249    |
| 14.0000                        | 1.31                 | 0.284    | 1.286    | 0.304    | 1.239    | 0.345    | 1.227    | 0.356    |
| 15.0000                        | 1.327                | 0.334    | 1.314    | 0.350    | 1.287    | 0.382    | 1.280    | 0.391    |
| 18.0000                        | 1.557                | 0.348    | 1.525    | 0.366    | 1.462    | 0.403    | 1.445    | 0.413    |
| 20.0000                        | 1.63                 | 0.342    | 1.594    | 0.354    | 1.524    | 0.378    | 1.505    | 0.385    |
| 25.0000                        | 1.642                | 0.330    | 1.615    | 0.336    | 1.563    | 0.348    | 1.549    | 0.352    |
| 30.0000                        | 1.628                | 0.330    | 1.610    | 0.330    | 1.574    | 0.329    | 1.564    | 0.328    |
| 35.0000                        | 1.645                | 0.364    | 1.618    | 0.357    | 1.565    | 0.344    | 1.551    | 0.341    |
| 40.0000                        | 1.641                | 0.428    | 1.612    | 0.418    | 1.555    | 0.398    | 1.539    | 0.392    |

Table A-9. Index of refraction as a function of relative humidity (0-80 %) for oceanic aerosols

| $\lambda$<br>( $\mu\text{m}$ ) | Relative Humidity(%) |                       |       |                       |       |                       |       |                       |
|--------------------------------|----------------------|-----------------------|-------|-----------------------|-------|-----------------------|-------|-----------------------|
|                                | 0                    |                       | 50    |                       | 70    |                       | 80    |                       |
|                                | $n$                  | $k$                   | $n$   | $k$                   | $n$   | $k$                   | $n$   | $k$                   |
| 0.3371                         | 1.510                | $4.00 \times 10^{-7}$ | 1.480 | $3.29 \times 10^{-7}$ | 1.425 | $1.97 \times 10^{-7}$ | 1.366 | $5.83 \times 10^{-8}$ |
| 0.4000                         | 1.500                | $3.00 \times 10^{-8}$ | 1.471 | $2.49 \times 10^{-8}$ | 1.417 | $1.54 \times 10^{-8}$ | 1.359 | $5.44 \times 10^{-9}$ |
| 0.4880                         | 1.500                | $2.00 \times 10^{-8}$ | 1.470 | $1.65 \times 10^{-8}$ | 1.415 | $1.01 \times 10^{-8}$ | 1.356 | $3.39 \times 10^{-9}$ |
| 0.5145                         | 1.500                | $1.00 \times 10^{-8}$ | 1.470 | $8.40 \times 10^{-9}$ | 1.414 | $5.43 \times 10^{-9}$ | 1.355 | $2.30 \times 10^{-9}$ |
| 0.5500                         | 1.500                | $1.00 \times 10^{-8}$ | 1.470 | $8.54 \times 10^{-9}$ | 1.413 | $5.83 \times 10^{-9}$ | 1.354 | $2.98 \times 10^{-9}$ |
| 0.6328                         | 1.490                | $2.00 \times 10^{-8}$ | 1.461 | $1.90 \times 10^{-8}$ | 1.408 | $1.72 \times 10^{-8}$ | 1.352 | $1.53 \times 10^{-8}$ |
| 0.6943                         | 1.490                | $1.00 \times 10^{-7}$ | 1.461 | $8.74 \times 10^{-8}$ | 1.408 | $6.40 \times 10^{-8}$ | 1.351 | $3.94 \times 10^{-8}$ |
| 0.8600                         | 1.480                | $3.00 \times 10^{-6}$ | 1.453 | $2.52 \times 10^{-6}$ | 1.402 | $1.62 \times 10^{-6}$ | 1.348 | $6.69 \times 10^{-7}$ |
| 1.0600                         | 1.470                | $2.00 \times 10^{-4}$ | 1.444 | $1.64 \times 10^{-4}$ | 1.395 | $9.85 \times 10^{-5}$ | 1.344 | $2.91 \times 10^{-5}$ |
| 3.0000                         | 1.610                | $1.00 \times 10^{-2}$ | 1.567 | $5.76 \times 10^{-2}$ | 1.486 | $1.46 \times 10^{-1}$ | 1.401 | $2.39 \times 10^{-1}$ |
| 3.5000                         | 1.480                | $1.60 \times 10^{-3}$ | 1.465 | $3.02 \times 10^{-3}$ | 1.439 | $5.64 \times 10^{-3}$ | 1.410 | $8.41 \times 10^{-3}$ |
| 4.0000                         | 1.480                | $1.40 \times 10^{-3}$ | 1.457 | $1.98 \times 10^{-3}$ | 1.413 | $3.06 \times 10^{-3}$ | 1.367 | $4.19 \times 10^{-3}$ |
| 4.5000                         | 1.490                | $1.40 \times 10^{-3}$ | 1.461 | $3.58 \times 10^{-3}$ | 1.408 | $7.62 \times 10^{-3}$ | 1.352 | $1.19 \times 10^{-2}$ |
| 5.0000                         | 1.470                | $2.50 \times 10^{-3}$ | 1.444 | $4.30 \times 10^{-3}$ | 1.395 | $7.63 \times 10^{-3}$ | 1.343 | $1.11 \times 10^{-2}$ |
| 7.9000                         | 1.400                | $1.30 \times 10^{-2}$ | 1.381 | $1.68 \times 10^{-2}$ | 1.345 | $2.38 \times 10^{-2}$ | 1.307 | $3.12 \times 10^{-2}$ |
| 8.2000                         | 1.420                | $2.00 \times 10^{-2}$ | 1.396 | $2.27 \times 10^{-2}$ | 1.351 | $2.78 \times 10^{-2}$ | 1.303 | $3.32 \times 10^{-2}$ |
| 8.5000                         | 1.480                | $2.60 \times 10^{-2}$ | 1.443 | $2.79 \times 10^{-2}$ | 1.375 | $3.15 \times 10^{-2}$ | 1.304 | $3.53 \times 10^{-2}$ |
| 9.0000                         | 1.650                | $2.80 \times 10^{-2}$ | 1.580 | $3.02 \times 10^{-2}$ | 1.449 | $3.42 \times 10^{-2}$ | 1.311 | $3.84 \times 10^{-2}$ |
| 9.5000                         | 1.580                | $1.80 \times 10^{-2}$ | 1.519 | $2.28 \times 10^{-2}$ | 1.405 | $3.17 \times 10^{-2}$ | 1.286 | $4.10 \times 10^{-2}$ |
| 10.0000                        | 1.548                | $1.50 \times 10^{-2}$ | 1.482 | $2.15 \times 10^{-2}$ | 1.373 | $3.35 \times 10^{-2}$ | 1.259 | $4.62 \times 10^{-2}$ |
| 10.5910                        | 1.500                | $1.40 \times 10^{-2}$ | 1.442 | $2.37 \times 10^{-2}$ | 1.334 | $4.17 \times 10^{-2}$ | 1.220 | $6.06 \times 10^{-2}$ |
| 11.0000                        | 1.480                | $1.40 \times 10^{-2}$ | 1.421 | $2.90 \times 10^{-2}$ | 1.311 | $5.69 \times 10^{-2}$ | 1.195 | $8.63 \times 10^{-2}$ |
| 11.5000                        | 1.480                | $1.40 \times 10^{-2}$ | 1.416 | $3.72 \times 10^{-2}$ | 1.297 | $8.03 \times 10^{-2}$ | 1.171 | $1.26 \times 10^{-1}$ |
| 12.5000                        | 1.420                | $1.60 \times 10^{-2}$ | 1.366 | $6.01 \times 10^{-2}$ | 1.266 | $1.42 \times 10^{-1}$ | 1.161 | $2.28 \times 10^{-1}$ |
| 14.0000                        | 1.410                | $2.30 \times 10^{-2}$ | 1.374 | $8.60 \times 10^{-2}$ | 1.306 | $2.03 \times 10^{-1}$ | 1.235 | $3.26 \times 10^{-1}$ |
| 15.0000                        | 1.450                | $3.50 \times 10^{-2}$ | 1.417 | $1.02 \times 10^{-1}$ | 1.357 | $2.25 \times 10^{-1}$ | 1.293 | $3.55 \times 10^{-1}$ |
| 18.0000                        | 1.780                | $1.30 \times 10^{-1}$ | 1.715 | $1.84 \times 10^{-1}$ | 1.595 | $2.83 \times 10^{-1}$ | 1.468 | $3.88 \times 10^{-1}$ |
| 20.0000                        | 1.760                | $1.52 \times 10^{-1}$ | 1.709 | $1.96 \times 10^{-1}$ | 1.615 | $2.77 \times 10^{-1}$ | 1.516 | $3.62 \times 10^{-1}$ |
| 25.0000                        | 1.760                | $2.05 \times 10^{-1}$ | 1.718 | $2.32 \times 10^{-1}$ | 1.641 | $2.83 \times 10^{-1}$ | 1.560 | $3.37 \times 10^{-1}$ |
| 30.0000                        | 1.770                | $3.00 \times 10^{-1}$ | 1.730 | $3.05 \times 10^{-1}$ | 1.657 | $3.15 \times 10^{-1}$ | 1.579 | $3.24 \times 10^{-1}$ |
| 35.0000                        | 1.760                | $5.00 \times 10^{-1}$ | 1.719 | $4.70 \times 10^{-1}$ | 1.642 | $4.15 \times 10^{-1}$ | 1.561 | $3.57 \times 10^{-1}$ |
| 40.0000                        | 1.740                | 1.00                  | 1.700 | $8.88 \times 10^{-1}$ | 1.626 | $6.81 \times 10^{-1}$ | 1.547 | $4.63 \times 10^{-1}$ |

Table A-10. Index of refraction as a function of relative humidity (90-99 %) for oceanic aerosols

| $\lambda$<br>( $\mu\text{m}$ ) | Relative Humidity(%) |                       |       |                       |       |                       |       |                       |
|--------------------------------|----------------------|-----------------------|-------|-----------------------|-------|-----------------------|-------|-----------------------|
|                                | 90                   |                       | 95    |                       | 98    |                       | 99    |                       |
|                                | $n$                  | $k$                   | $n$   | $k$                   | $n$   | $k$                   | $n$   | $k$                   |
| 0.3371                         | 1.357                | $3.76 \times 10^{-8}$ | 1.352 | $2.49 \times 10^{-8}$ | 1.348 | $1.58 \times 10^{-8}$ | 1.347 | $1.22 \times 10^{-8}$ |
| 0.4000                         | 1.351                | $3.96 \times 10^{-9}$ | 1.346 | $3.04 \times 10^{-9}$ | 1.342 | $2.39 \times 10^{-9}$ | 1.341 | $2.13 \times 10^{-9}$ |
| 0.4880                         | 1.347                | $2.39 \times 10^{-9}$ | 1.342 | $1.77 \times 10^{-9}$ | 1.338 | $1.33 \times 10^{-9}$ | 1.337 | $1.15 \times 10^{-9}$ |
| 0.5145                         | 1.346                | $1.83 \times 10^{-9}$ | 1.341 | $1.54 \times 10^{-9}$ | 1.337 | $1.34 \times 10^{-9}$ | 1.336 | $1.26 \times 10^{-9}$ |
| 0.5500                         | 1.345                | $2.56 \times 10^{-9}$ | 1.340 | $2.30 \times 10^{-9}$ | 1.336 | $2.11 \times 10^{-9}$ | 1.335 | $2.04 \times 10^{-9}$ |
| 0.6328                         | 1.344                | $1.50 \times 10^{-8}$ | 1.339 | $1.49 \times 10^{-8}$ | 1.335 | $1.47 \times 10^{-8}$ | 1.334 | $1.47 \times 10^{-8}$ |
| 0.6943                         | 1.343                | $3.57 \times 10^{-8}$ | 1.338 | $3.34 \times 10^{-8}$ | 1.334 | $3.18 \times 10^{-8}$ | 1.333 | $3.12 \times 10^{-8}$ |
| 0.8600                         | 1.340                | $5.28 \times 10^{-7}$ | 1.335 | $4.41 \times 10^{-7}$ | 1.332 | $3.79 \times 10^{-7}$ | 1.330 | $3.55 \times 10^{-7}$ |
| 1.0600                         | 1.337                | $1.88 \times 10^{-5}$ | 1.332 | $1.24 \times 10^{-5}$ | 1.329 | $7.85 \times 10^{-6}$ | 1.327 | $6.08 \times 10^{-6}$ |
| 3.0000                         | 1.389                | $2.52 \times 10^{-1}$ | 1.381 | $2.61 \times 10^{-1}$ | 1.375 | $2.67 \times 10^{-1}$ | 1.373 | $2.69 \times 10^{-1}$ |
| 3.5000                         | 1.406                | $8.82 \times 10^{-3}$ | 1.403 | $9.07 \times 10^{-3}$ | 1.401 | $9.25 \times 10^{-3}$ | 1.401 | $9.32 \times 10^{-3}$ |
| 4.0000                         | 1.361                | $4.36 \times 10^{-3}$ | 1.356 | $4.47 \times 10^{-3}$ | 1.353 | $4.54 \times 10^{-3}$ | 1.352 | $4.57 \times 10^{-3}$ |
| 4.5000                         | 1.344                | $1.25 \times 10^{-2}$ | 1.339 | $1.29 \times 10^{-2}$ | 1.335 | $1.32 \times 10^{-2}$ | 1.334 | $1.33 \times 10^{-2}$ |
| 5.0000                         | 1.336                | $1.17 \times 10^{-2}$ | 1.331 | $1.20 \times 10^{-2}$ | 1.328 | $1.22 \times 10^{-2}$ | 1.326 | $1.23 \times 10^{-2}$ |
| 7.9000                         | 1.302                | $3.23 \times 10^{-2}$ | 1.298 | $3.30 \times 10^{-2}$ | 1.296 | $3.35 \times 10^{-2}$ | 1.295 | $3.37 \times 10^{-2}$ |
| 8.2000                         | 1.296                | $3.40 \times 10^{-2}$ | 1.292 | $3.45 \times 10^{-2}$ | 1.289 | $3.48 \times 10^{-2}$ | 1.287 | $3.50 \times 10^{-2}$ |
| 8.5000                         | 1.293                | $3.59 \times 10^{-2}$ | 1.286 | $3.62 \times 10^{-2}$ | 1.282 | $3.65 \times 10^{-2}$ | 1.280 | $3.65 \times 10^{-2}$ |
| 9.0000                         | 1.291                | $3.90 \times 10^{-2}$ | 1.278 | $3.94 \times 10^{-2}$ | 1.269 | $3.97 \times 10^{-2}$ | 1.266 | $3.98 \times 10^{-2}$ |
| 9.5000                         | 1.268                | $4.24 \times 10^{-2}$ | 1.257 | $4.32 \times 10^{-2}$ | 1.249 | $4.39 \times 10^{-2}$ | 1.246 | $4.41 \times 10^{-2}$ |
| 10.0000                        | 1.242                | $4.81 \times 10^{-2}$ | 1.231 | $4.93 \times 10^{-2}$ | 1.224 | $5.01 \times 10^{-2}$ | 1.221 | $5.05 \times 10^{-2}$ |
| 10.5910                        | 1.203                | $6.34 \times 10^{-2}$ | 1.192 | $6.52 \times 10^{-2}$ | 1.185 | $6.64 \times 10^{-2}$ | 1.182 | $6.69 \times 10^{-2}$ |
| 11.0000                        | 1.177                | $9.06 \times 10^{-2}$ | 1.167 | $9.33 \times 10^{-2}$ | 1.159 | $9.52 \times 10^{-2}$ | 1.156 | $9.60 \times 10^{-2}$ |
| 11.5000                        | 1.152                | $1.32 \times 10^{-1}$ | 1.141 | $1.37 \times 10^{-1}$ | 1.133 | $1.40 \times 10^{-1}$ | 1.129 | $1.41 \times 10^{-1}$ |
| 12.5000                        | 1.145                | $2.41 \times 10^{-1}$ | 1.135 | $2.49 \times 10^{-1}$ | 1.129 | $2.54 \times 10^{-1}$ | 1.126 | $2.57 \times 10^{-1}$ |
| 14.0000                        | 1.225                | $3.44 \times 10^{-1}$ | 1.218 | $3.55 \times 10^{-1}$ | 1.214 | $3.63 \times 10^{-1}$ | 1.212 | $3.67 \times 10^{-1}$ |
| 15.0000                        | 1.283                | $3.75 \times 10^{-1}$ | 1.278 | $3.87 \times 10^{-1}$ | 1.273 | $3.95 \times 10^{-1}$ | 1.272 | $3.98 \times 10^{-1}$ |
| 18.0000                        | 1.450                | $4.04 \times 10^{-1}$ | 1.438 | $4.14 \times 10^{-1}$ | 1.430 | $4.20 \times 10^{-1}$ | 1.426 | $4.23 \times 10^{-1}$ |
| 20.0000                        | 1.501                | $3.75 \times 10^{-1}$ | 1.492 | $3.83 \times 10^{-1}$ | 1.485 | $3.88 \times 10^{-1}$ | 1.483 | $3.91 \times 10^{-1}$ |
| 25.0000                        | 1.548                | $3.45 \times 10^{-1}$ | 1.541 | $3.50 \times 10^{-1}$ | 1.535 | $3.53 \times 10^{-1}$ | 1.533 | $3.55 \times 10^{-1}$ |
| 30.0000                        | 1.567                | $3.26 \times 10^{-1}$ | 1.560 | $3.27 \times 10^{-1}$ | 1.555 | $3.27 \times 10^{-1}$ | 1.553 | $3.28 \times 10^{-1}$ |
| 35.0000                        | 1.549                | $3.48 \times 10^{-1}$ | 1.542 | $3.43 \times 10^{-1}$ | 1.536 | $3.39 \times 10^{-1}$ | 1.534 | $3.38 \times 10^{-1}$ |
| 40.0000                        | 1.535                | $4.31 \times 10^{-1}$ | 1.528 | $4.11 \times 10^{-1}$ | 1.523 | $3.97 \times 10^{-1}$ | 1.521 | $3.91 \times 10^{-1}$ |

**This page left intentionally blank.**

## Appendix B GRAPHS

The following pages contain three-dimensional plots of the Phase FuNction DATabase (PFNDAT) phase functions (on the ordinate axis) versus angle and wavelength. PFNDAT cases 1 to 30 have been evaluated at 32 different wavelengths from 0.35 to 40  $\mu\text{m}$  and the remainder of the cases at 16 different wavelengths ranging from 0.55 to 12  $\mu\text{m}$ . The wavelength scale used in the plots (the y dimension) is log-based as is the vertical scale (the z dimension) that represents the phase function value. In a majority of the plots the variation of the zero peak phase function value is linear with wavelength. This is due to the direct relationship between the amount of forward scatter and the particle size parameter. The plots are created using exactly the wavelength and angle information contained in the database. Thus, where the plot lines are sparse, so are the computed data.

Maritime Aerosol, 0% Rh EOSAEL 01

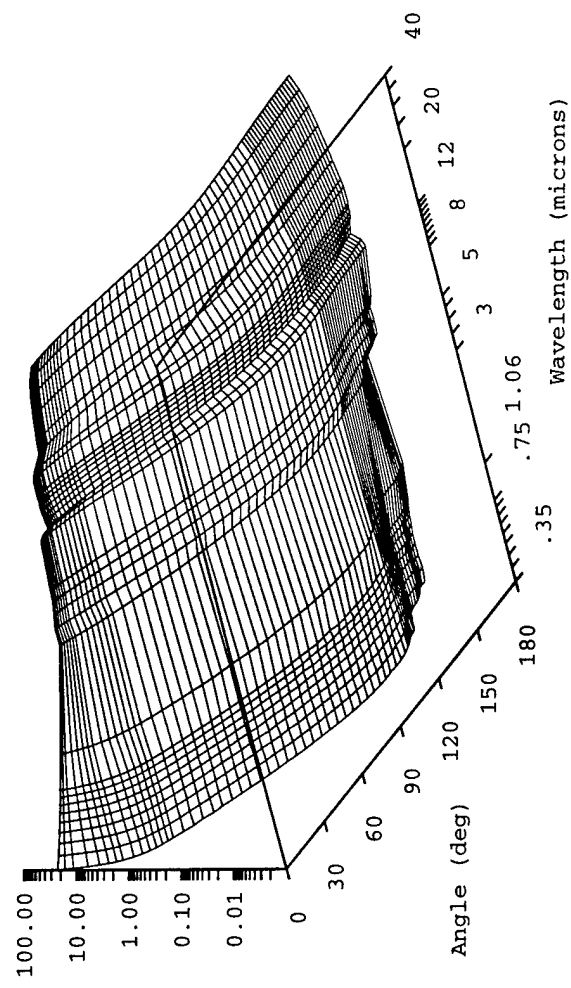


**Figure B-1.** Maritime aerosol, 0 percent relative humidity.

Maritime Aerosol, 50% Rh EOSAEL 02

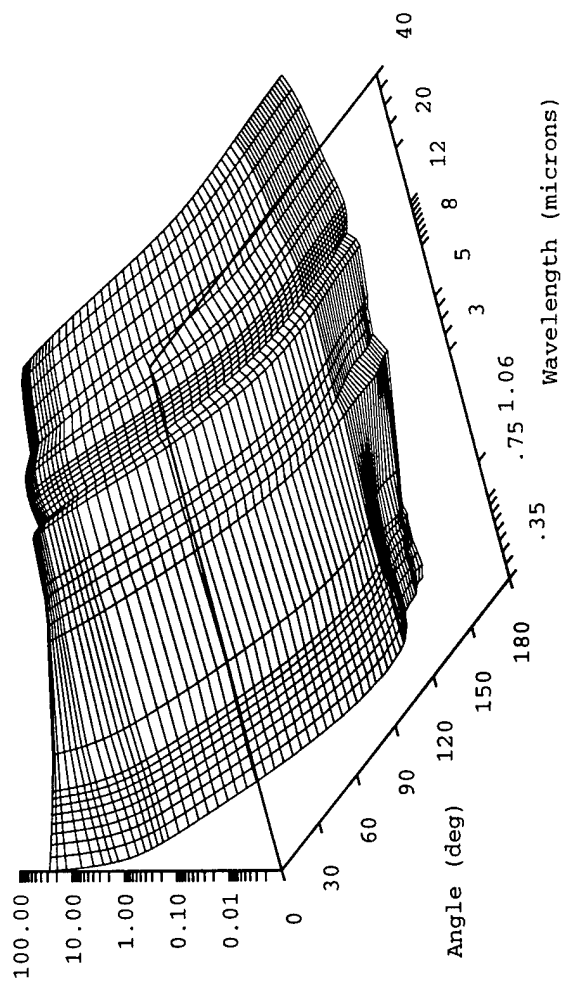


**Figure B-2.** Maritime aerosol, 50 percent relative humidity.

Maritime Aerosol, 70% Rh EOSAEL 03

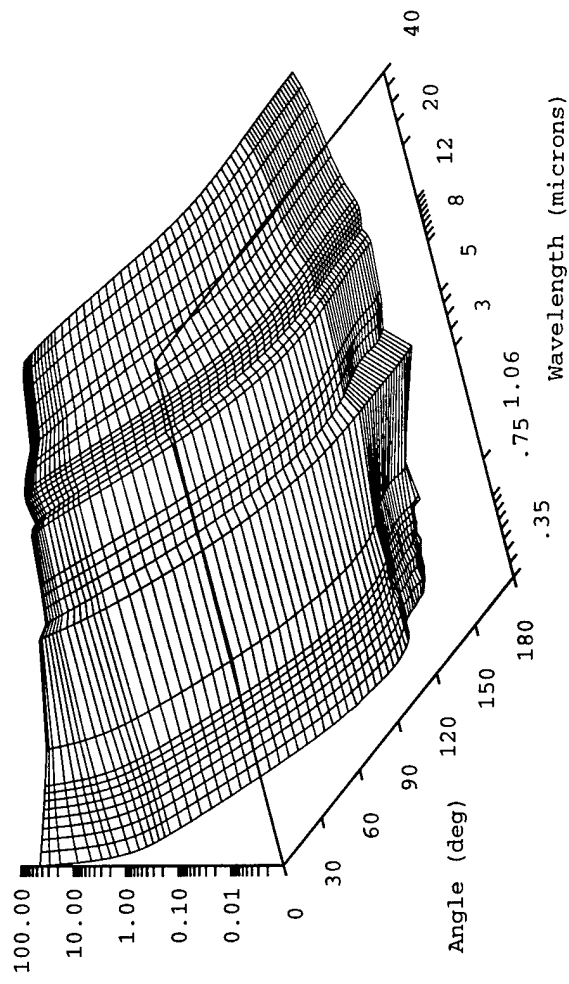


**Figure B-3.** Maritime aerosol, 70 percent relative humidity.

Maritime Aerosol, 80% Rh EOSAEL 04

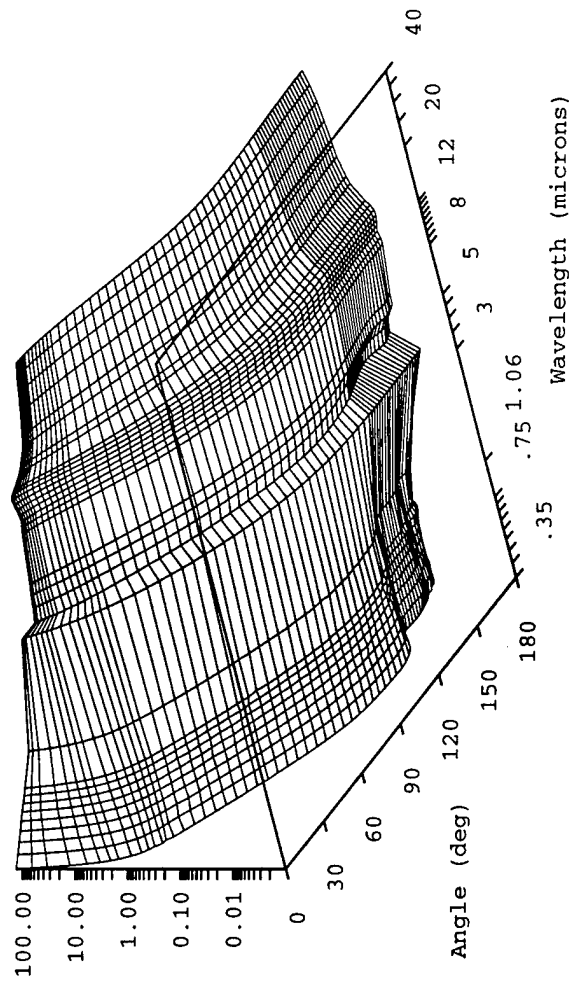


**Figure B-4.** Maritime aerosol, 80 percent relative humidity.

Maritime Aerosol, 90% Rh EOSAEL 05

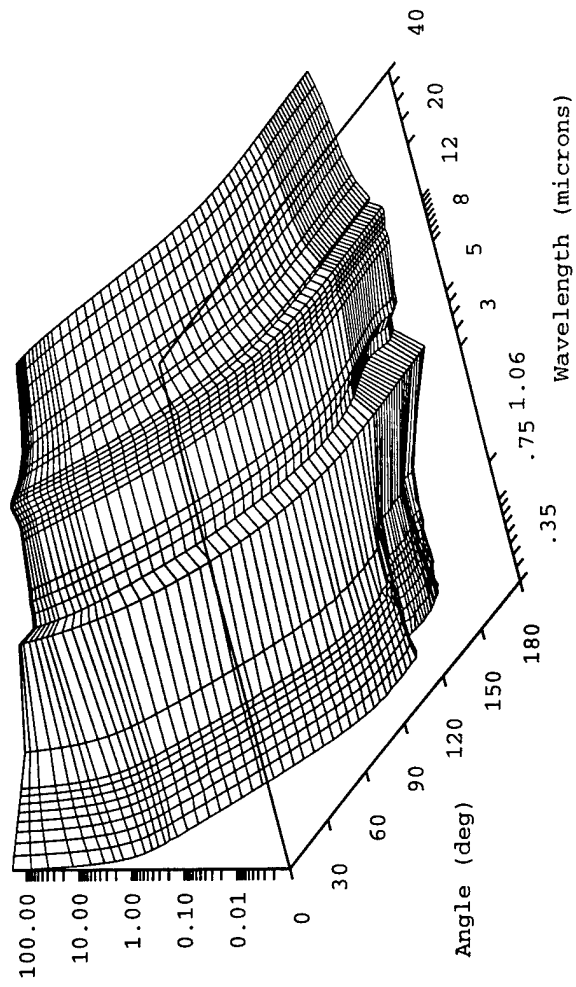


**Figure B-5.** Maritime aerosol, 90 percent relative humidity.

Maritime Aerosol, 95% Rh EOSAEL 06

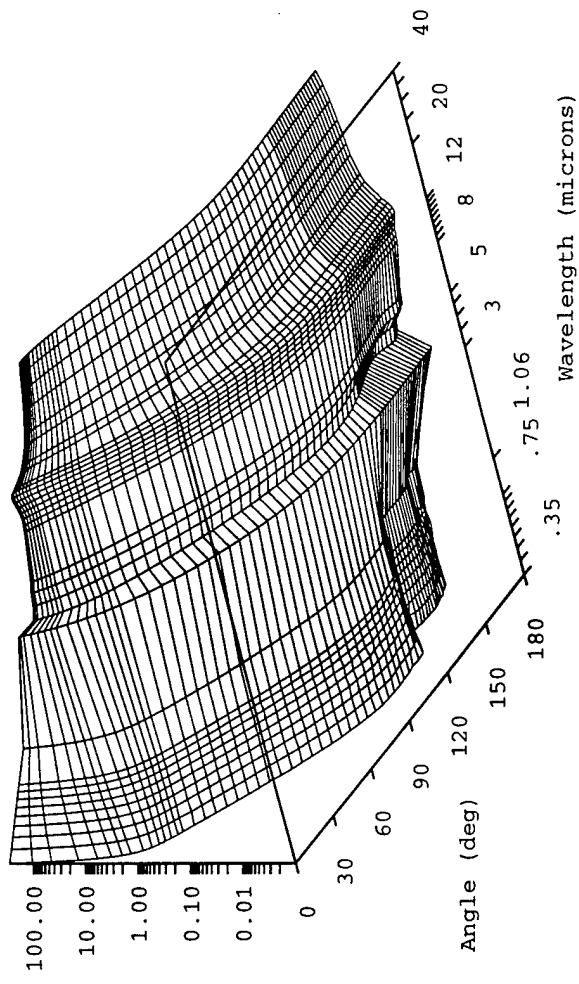


**Figure B-6.** Maritime aerosol, 95 percent relative humidity.

Maritime Aerosol, 98% Rh EOSAEL 07

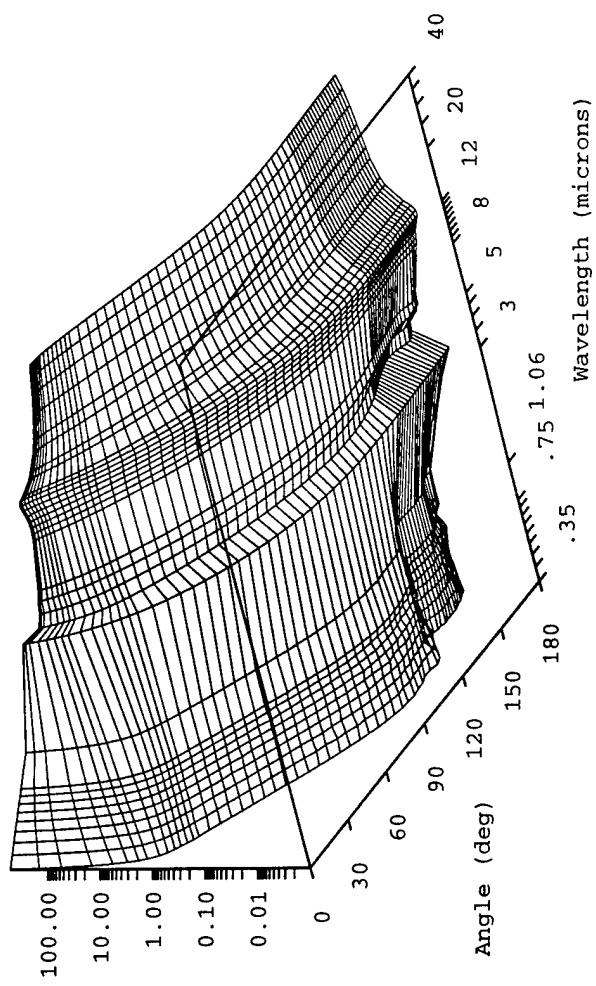


**Figure B-7.** Maritime aerosol, 98 percent relative humidity.

Maritime Aerosol, 99% Rh EOSAEL 08

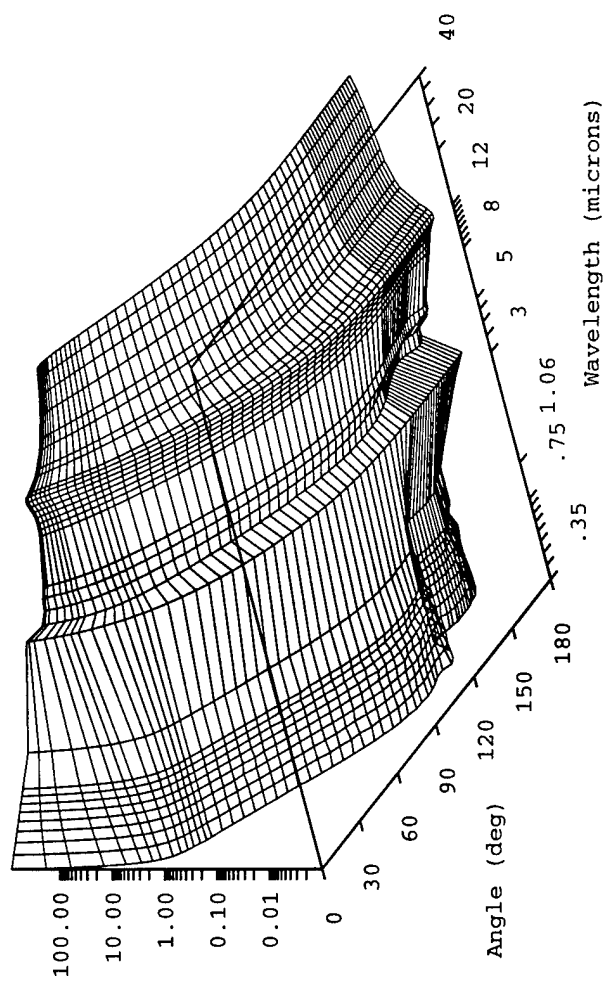


**Figure B-8.** Maritime aerosol, 99 percent relative humidity.

Urban Aerosol, 0% Rh    EC8AEL 09

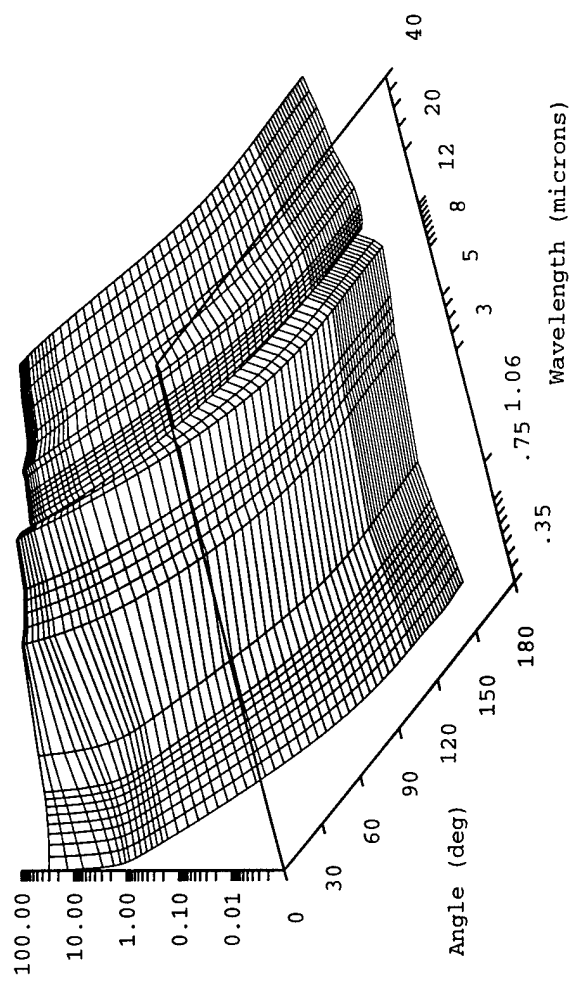


**Figure B-9.** Urban aerosol, 0 percent relative humidity.

Urban Aerosol, 50% Rh EOSAEL 10

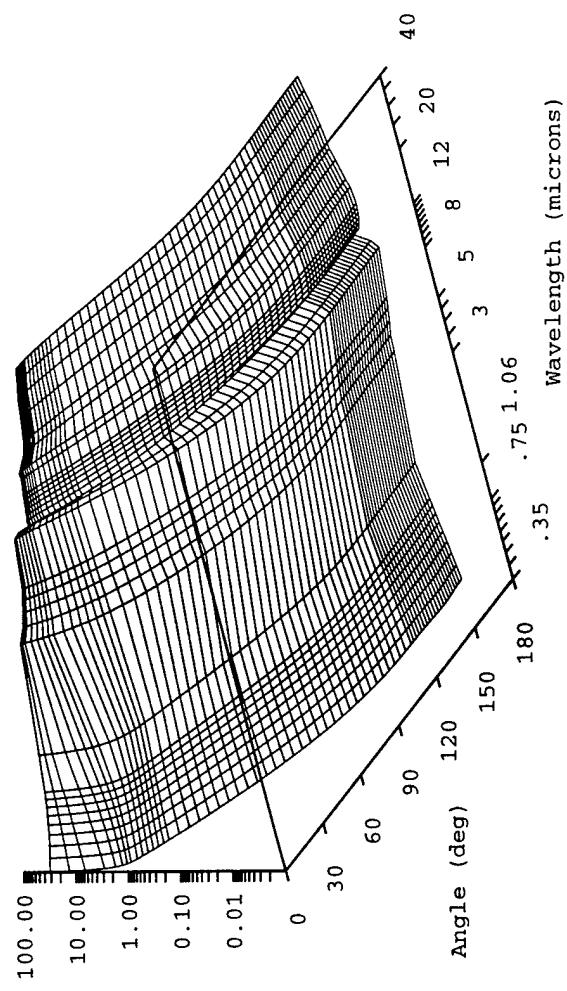


**Figure B-10.** Urban aerosol, 50 percent relative humidity.

Urban Aerosol, 70% Rh EOSAEL 11

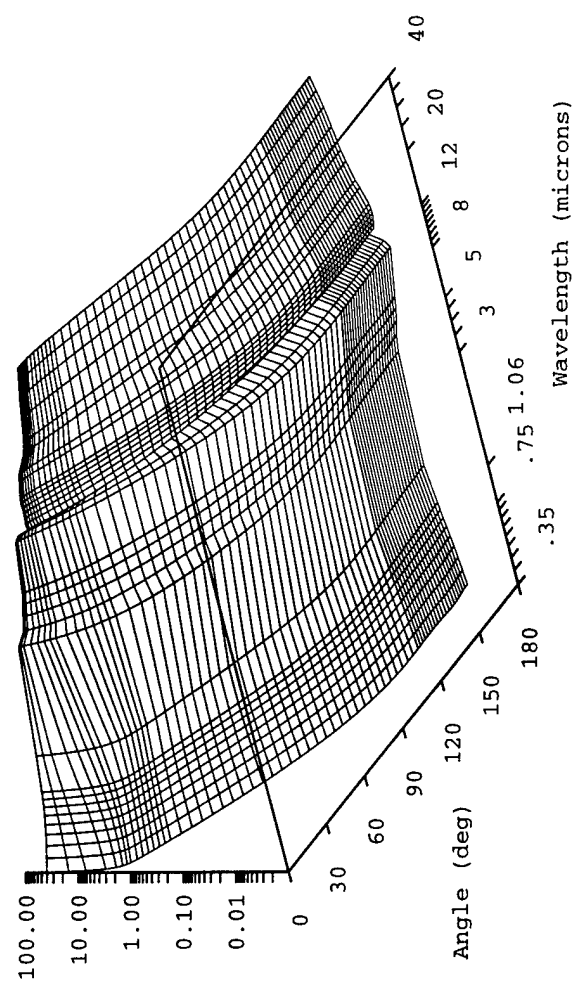


**Figure B-11.** Urban aerosol, 70 percent relative humidity.

Urban Aerosol, 80% Rh EOSAEL 12

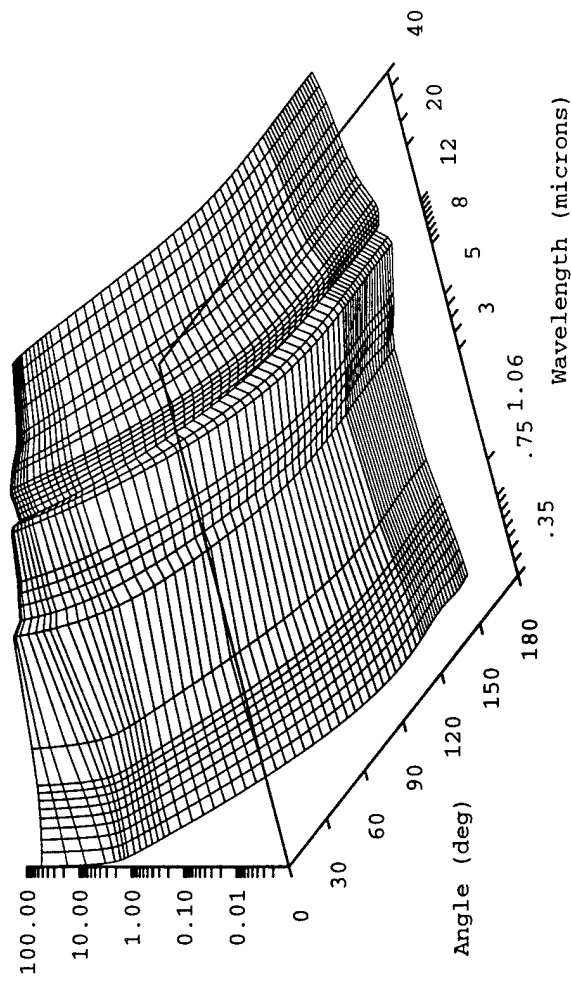


**Figure B-12.** Urban aerosol, 80 percent relative humidity.

Urban Aerosol, 90% Rh EOSAEL 13

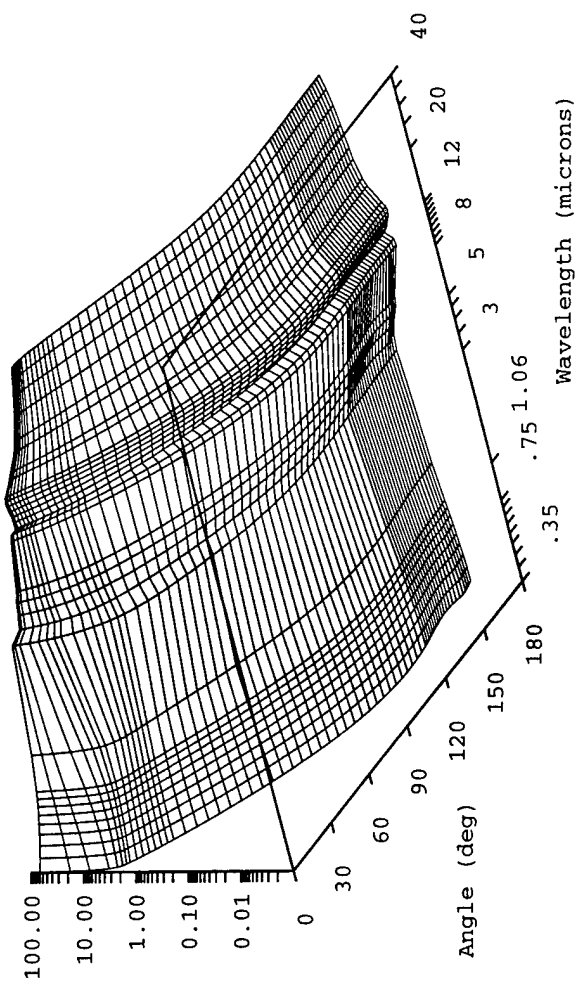


**Figure B-13.** Urban aerosol, 90 percent relative humidity.

Urban Aerosol, 95% Rh EOSAEL 14

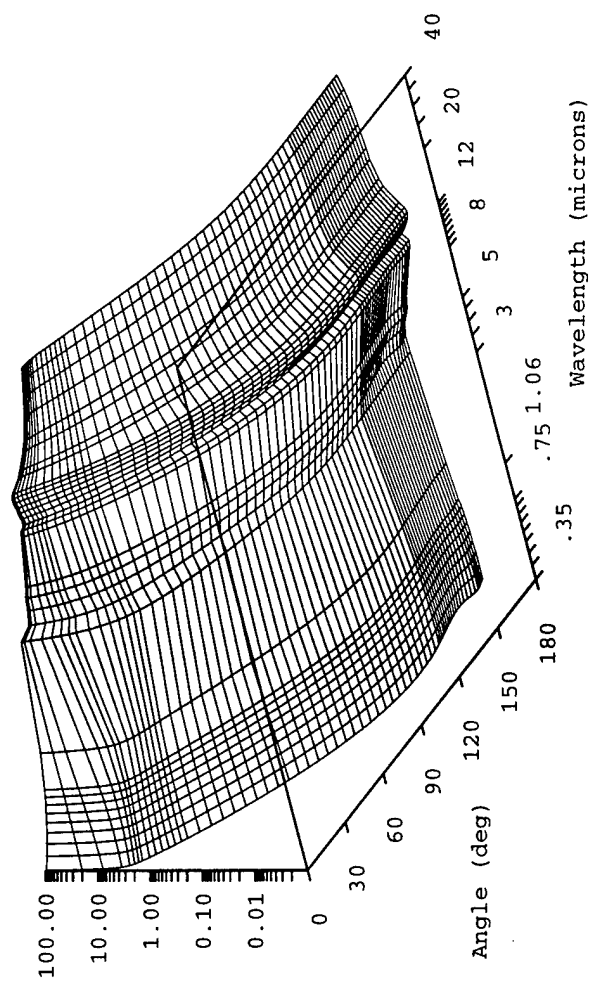


**Figure B-14.** Urban aerosol, 95 percent relative humidity.

Urban Aerosol, 98% Rh EOSAEL 15

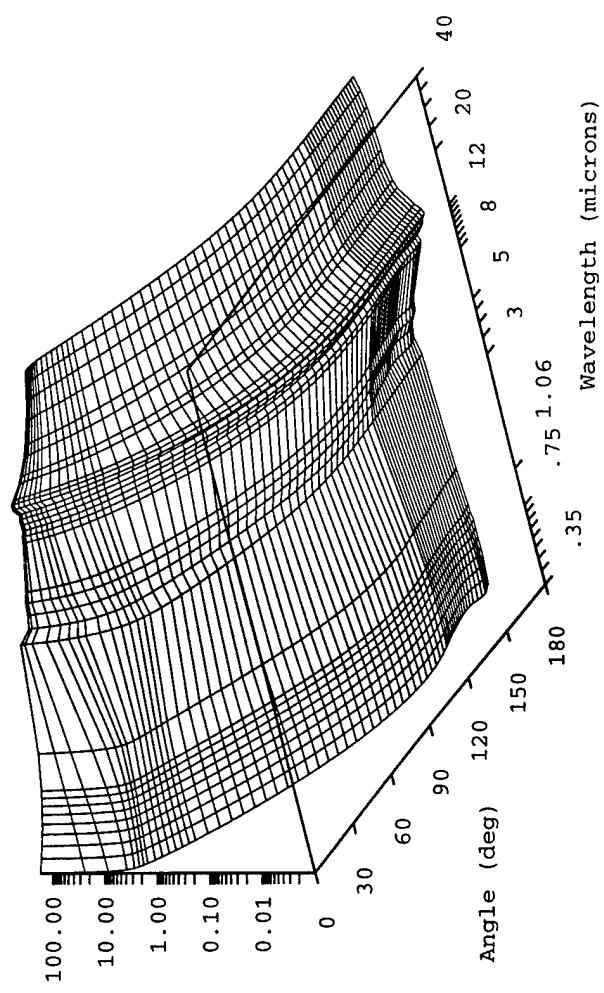


**Figure B-15.** Urban aerosol, 98 percent relative humidity.

Urban Aerosol, 99% Rh EOSAEL 16

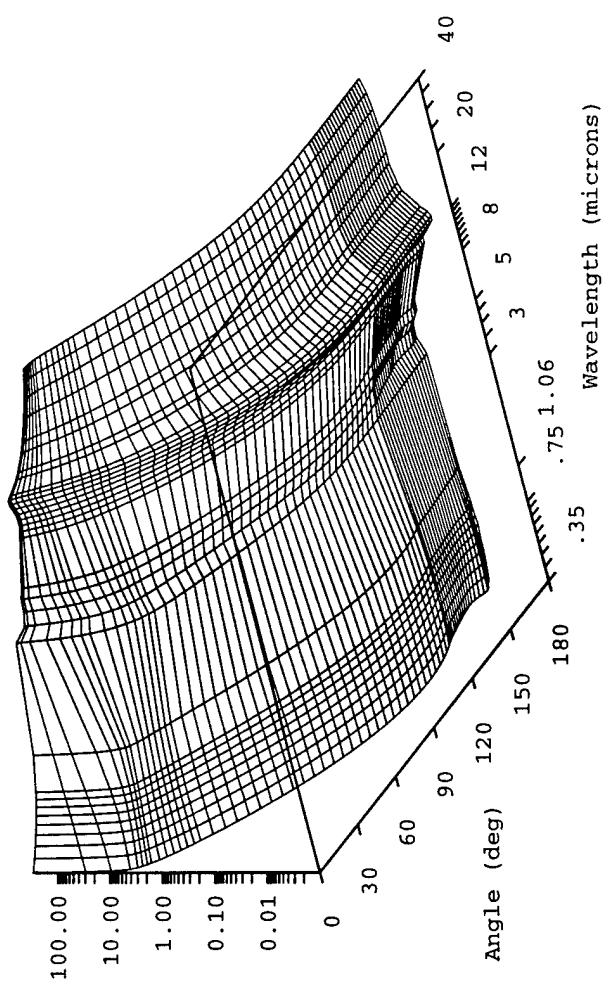


**Figure B-16.** Urban aerosol, 99 percent relative humidity.

Rural Aerosol, 0% Rh EOSAEL 17

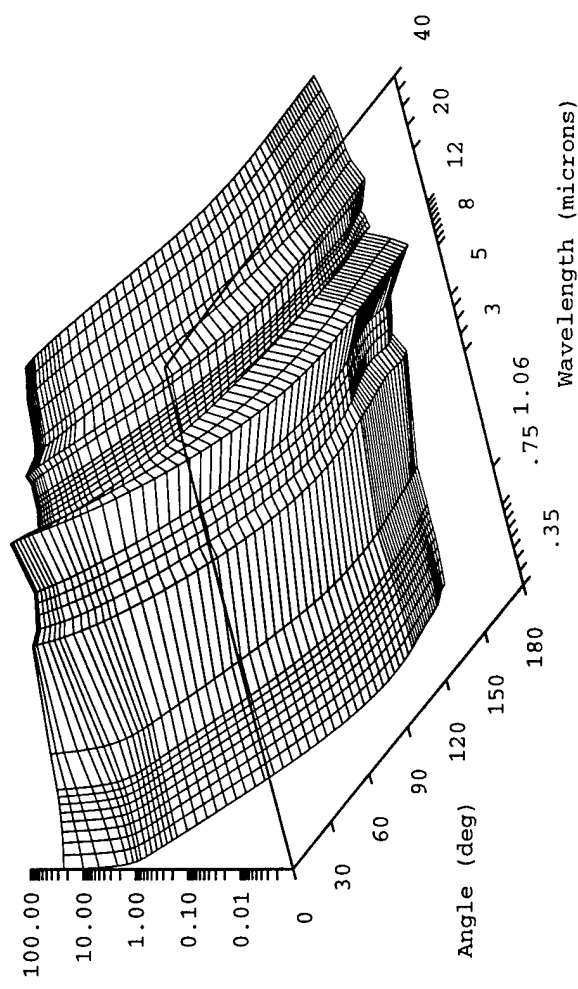


**Figure B-17.** Rural aerosol, 0 percent relative humidity.

Rural Aerosol, 50% Rh EOSAEL 18

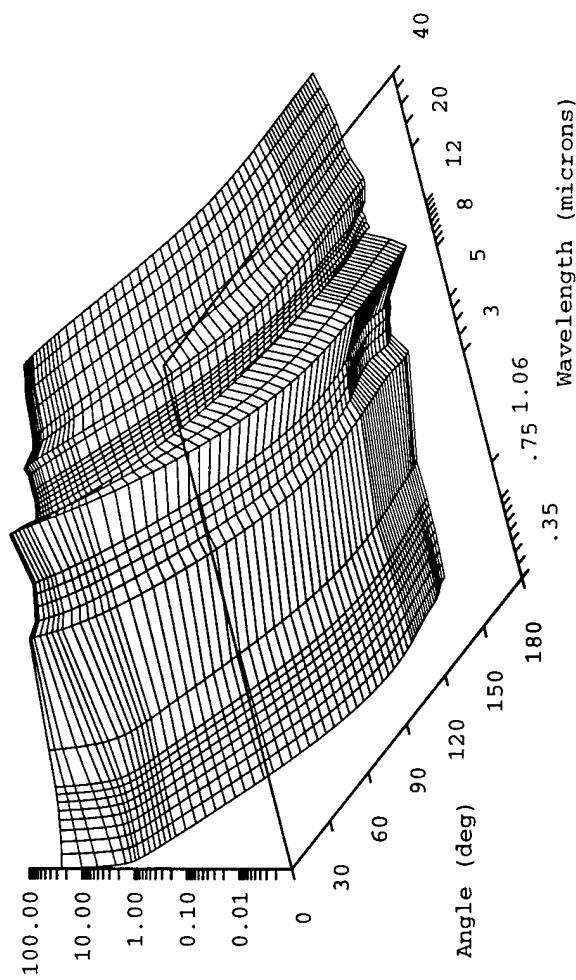


**Figure B-18.** Rural aerosol, 50 percent relative humidity.

Rural Aerosol, 70% Rh EOSAEL '19

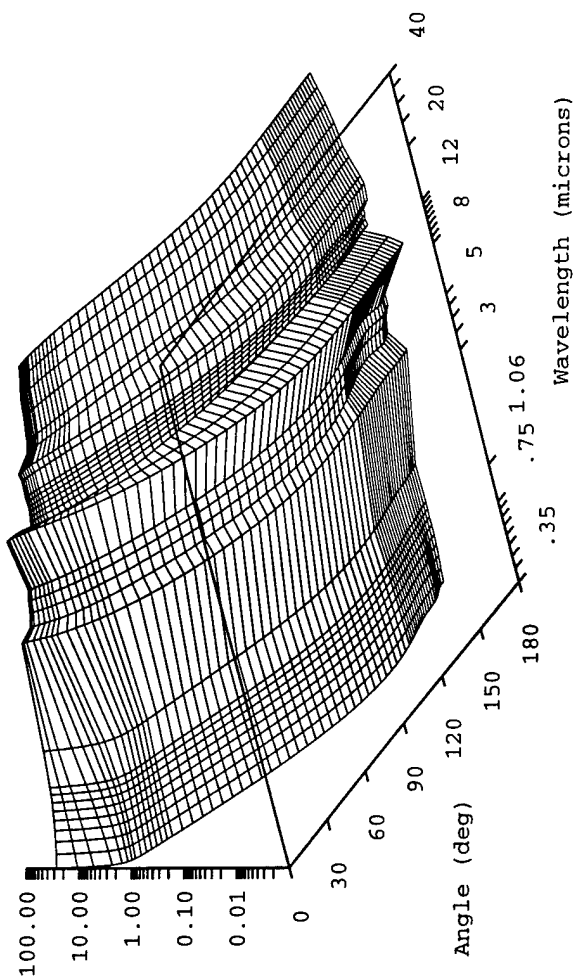


**Figure B-19.** Rural aerosol, 70 percent relative humidity.

Rural Aerosol, 80% Rh    EOSSAEL 20

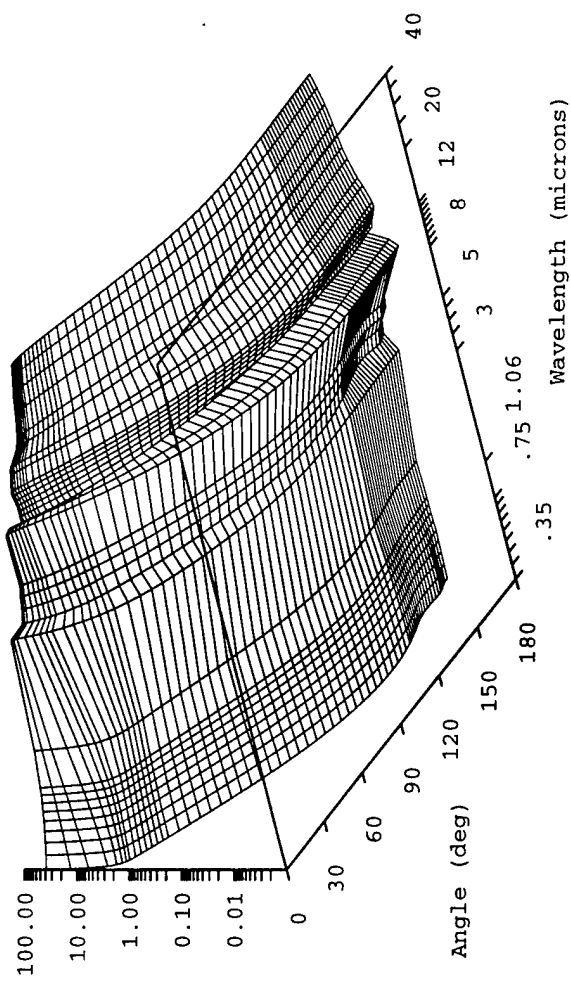


**Figure B-20.** Rural aerosol, 80 percent relative humidity.

Rural Aerosol, 90% Rh EOSAEL 21

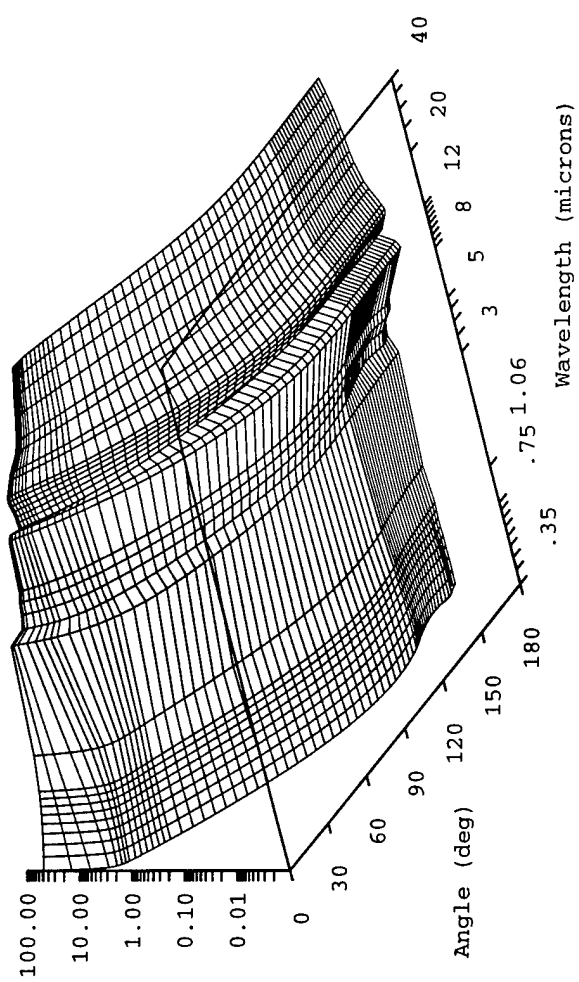


**Figure B-21.** Rural aerosol, 90 percent relative humidity.

Rural Aerosol, 95% Rh EOSAEL 22

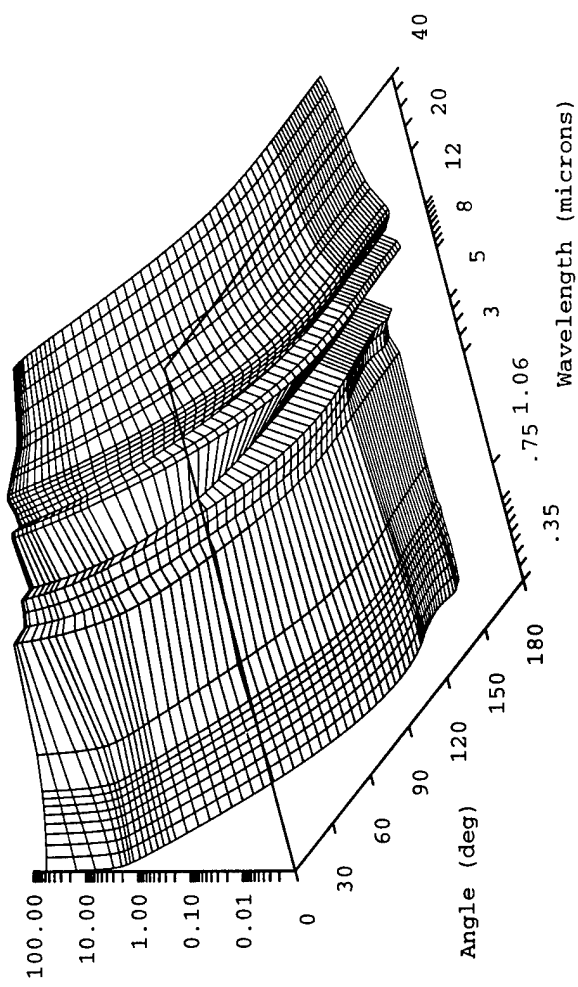


**Figure B-22.** Rural aerosol, 95 percent relative humidity.

Rural Aerosol, 98% Rh EOSAEL 23

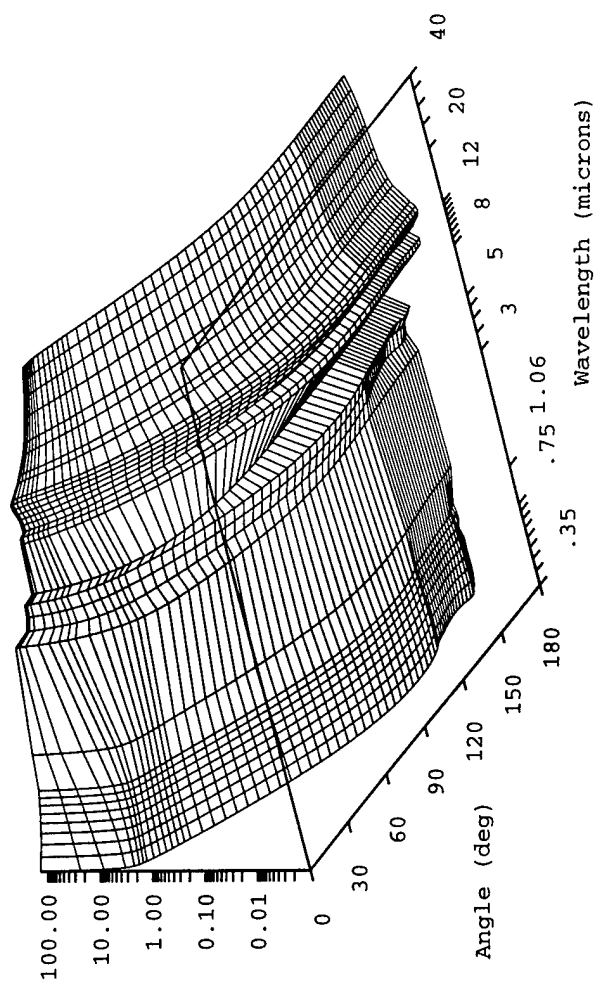


**Figure B-23.** Rural aerosol, 98 percent relative humidity.

Rural Aerosol, 99% Rh EOSAEL 24

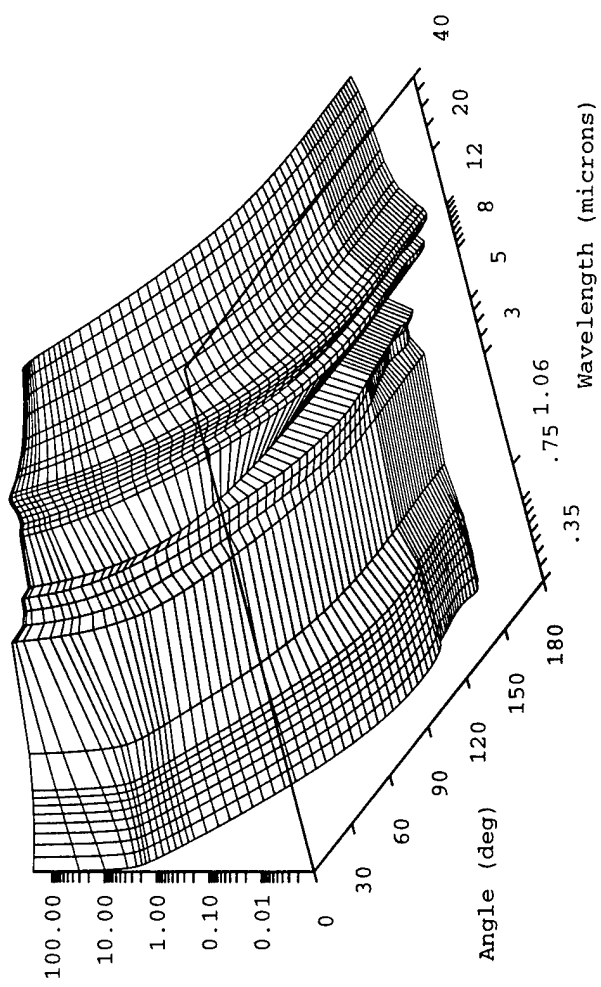


**Figure B-24.** Rural aerosol, 99 percent relative humidity.

Advection Fog EOSAEL 25

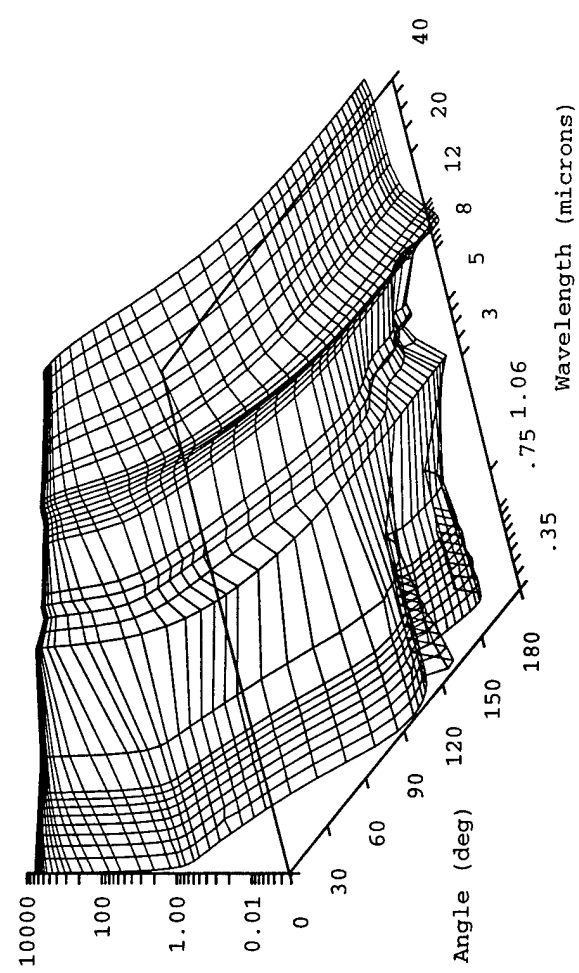


**Figure B-25.** Fog (heavy advection).

Radiation Fog EOSAEU 26

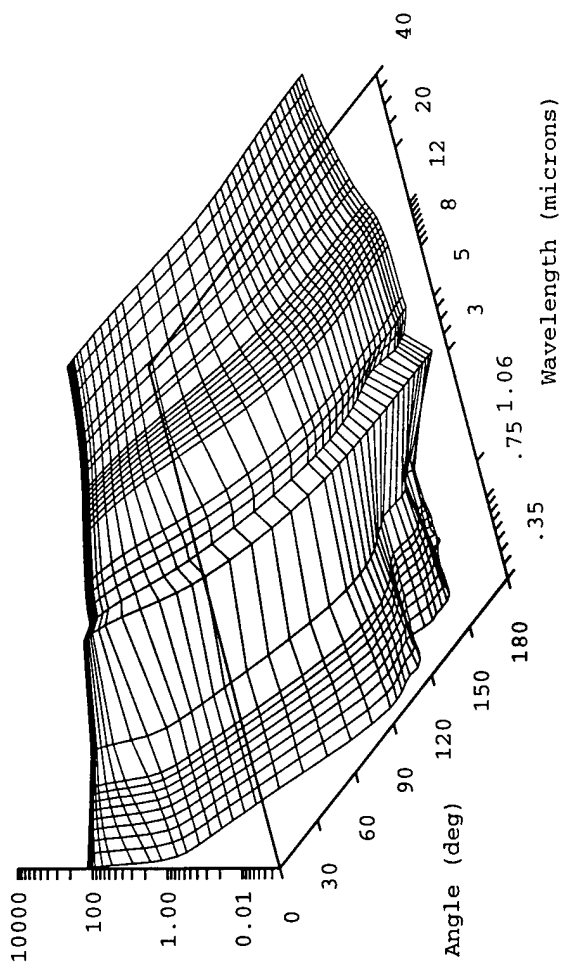


**Figure B-26.** Fog (moderate radiation).

Drizzle, 1mm/hr EOSAEL 27

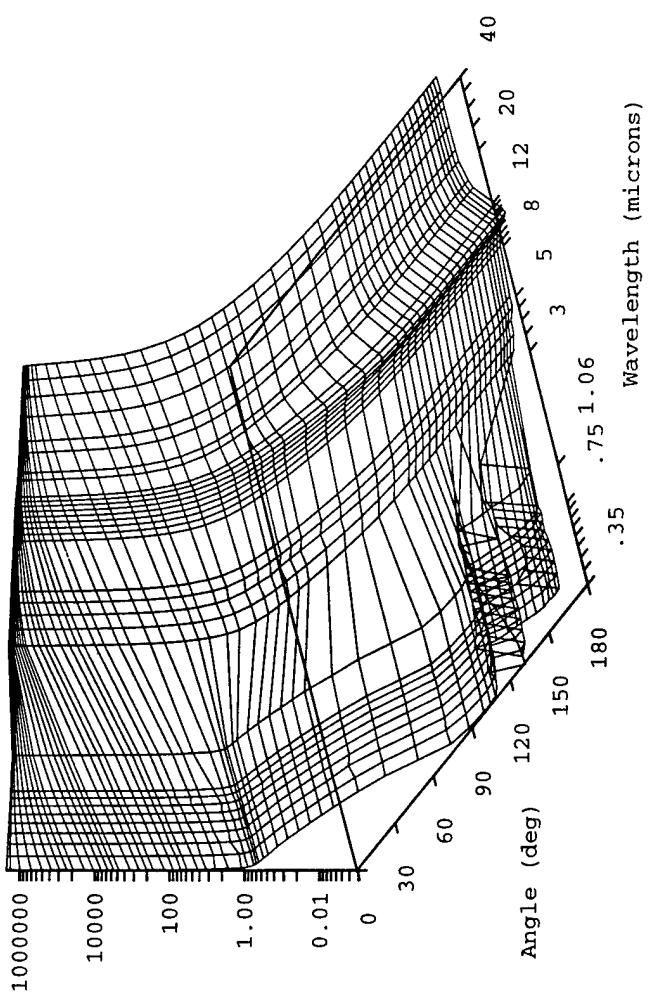


**Figure B-27.** Rain (drizzle).

Widespread Rain, 5mm/hr EOSAEL 28

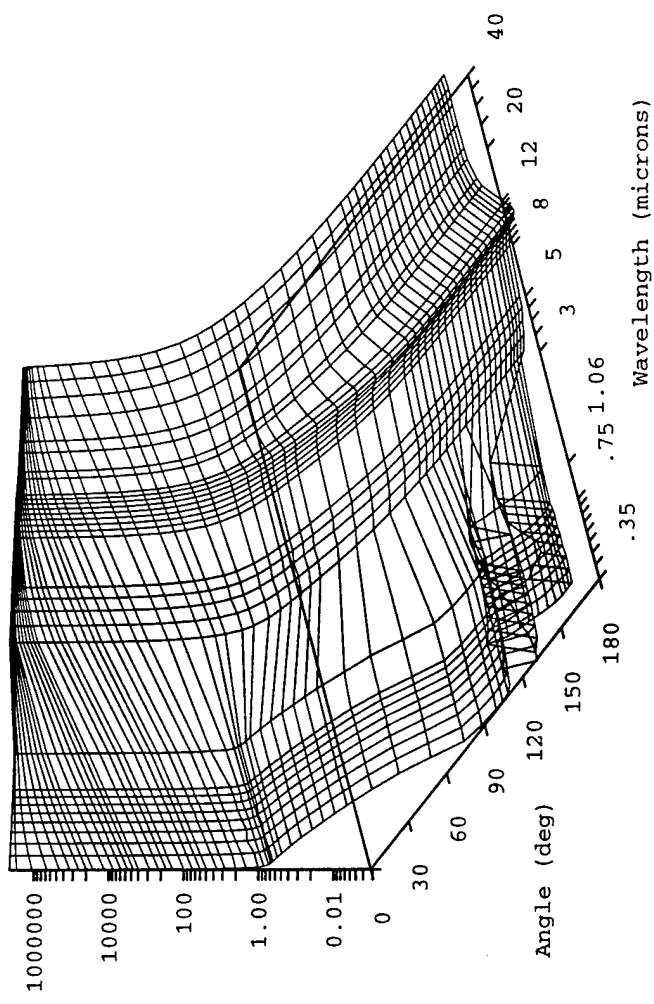


**Figure B-28.** Rain (widespread).

Thunder Storm, 1.0mm/hr EOSAEL 2.9

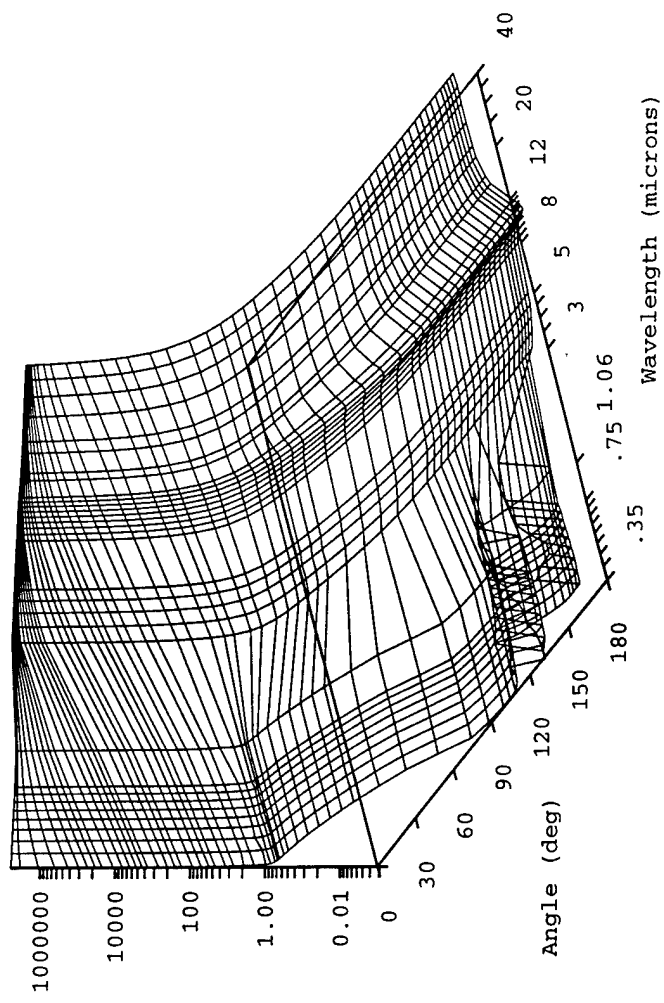


**Figure B-29.** Rain (thunderstorm).

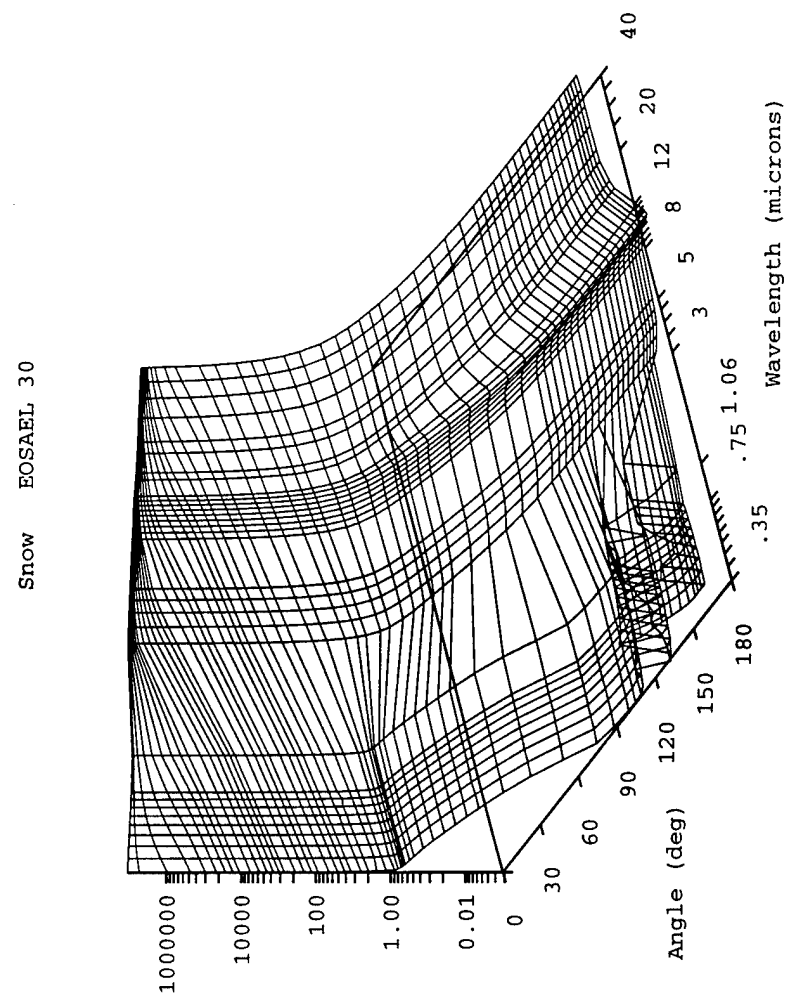


**Figure B-30.** Snow.

Light Loading Dust EOSAEL 50

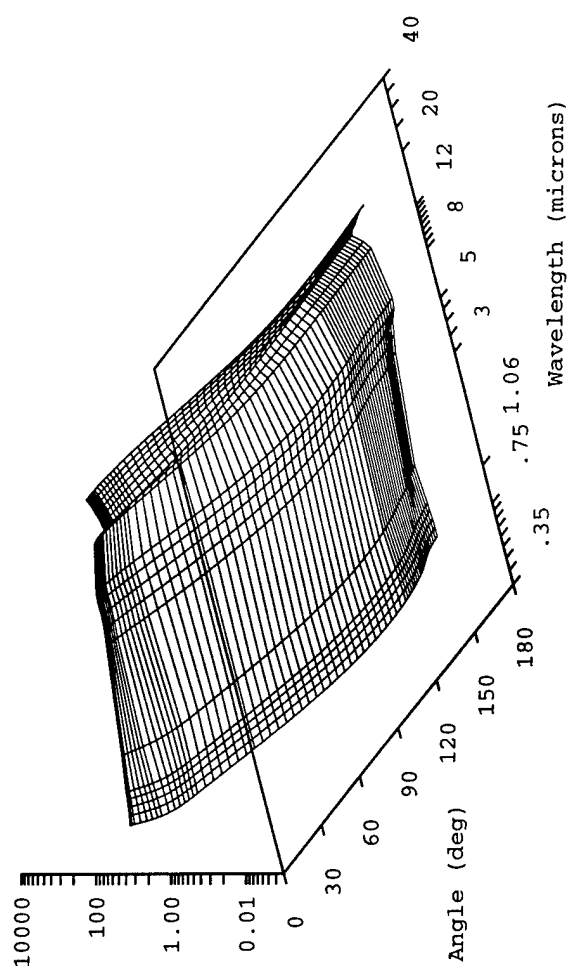


**Figure B-31.** Dust (light aerosol loading).

Heavy Loading Dust      EOSAEL 51

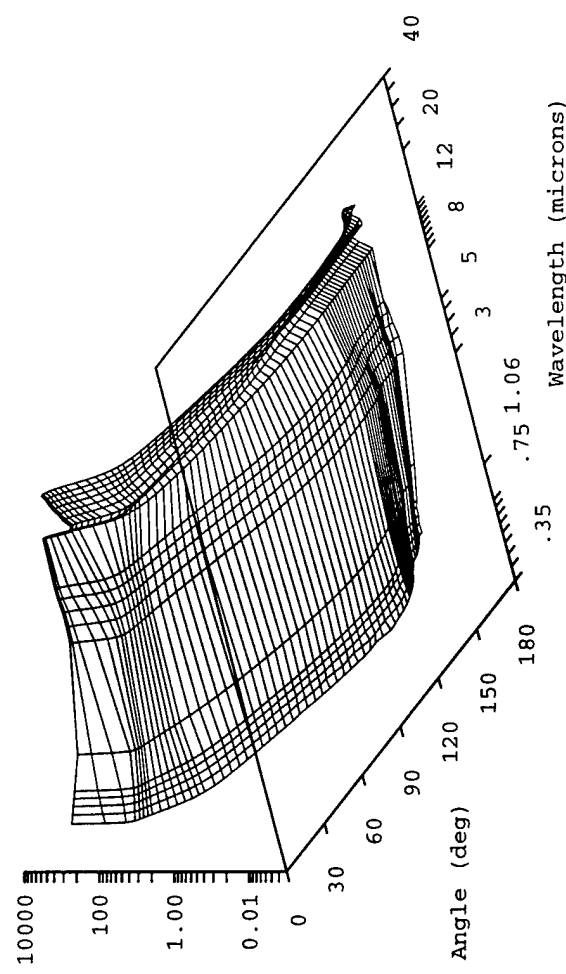


**Figure B-32.** Dust (heavy aerosol loading).

High Explosive Dust EOSAEL 52

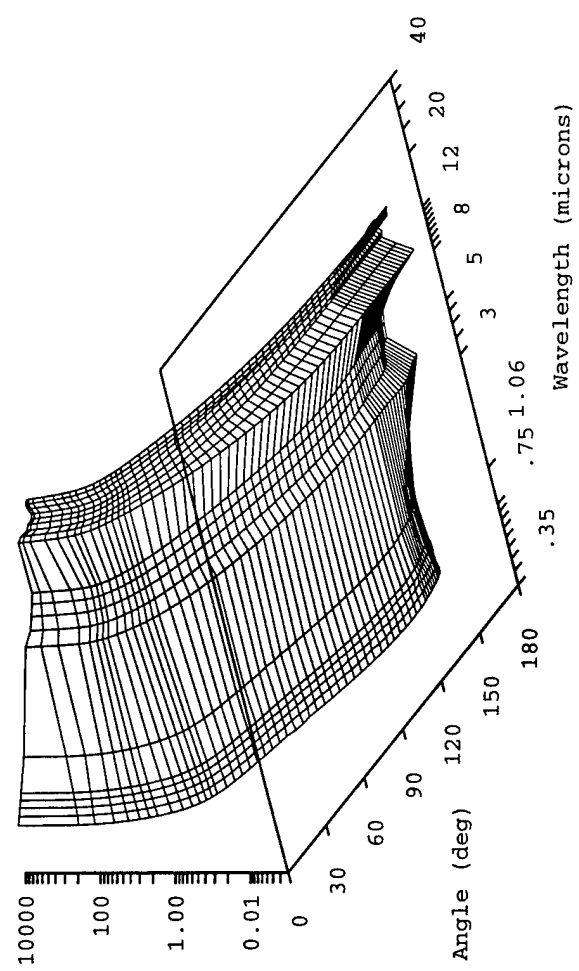


**Figure B-33.** Dust (high explosive (HE)).

White Phosphorus, 17% Rh    EOSAEL 53

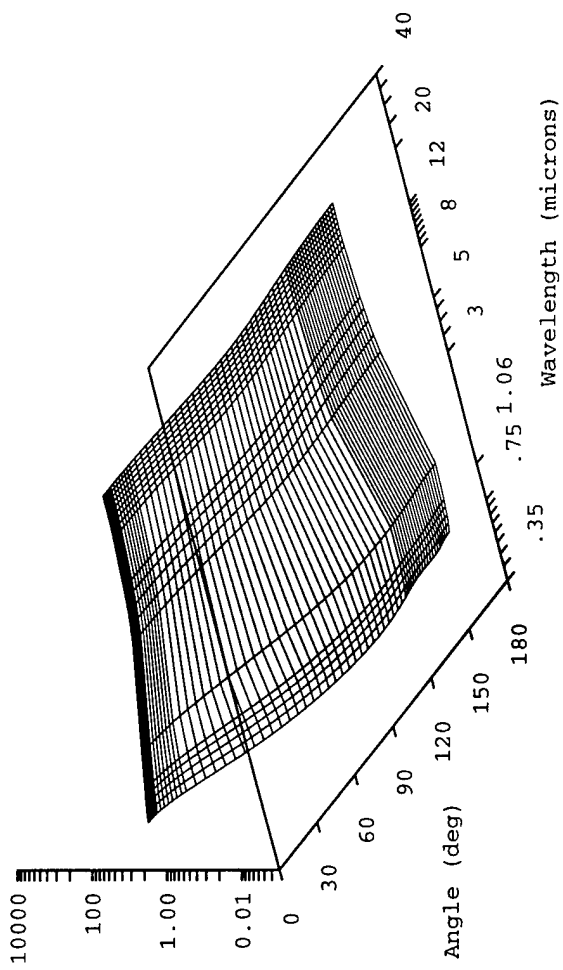


**Figure B-34.** Smoke (white phosphorous), 17 percent relative humidity.

White Phosphorus, 50% Rh EOSAEL 54

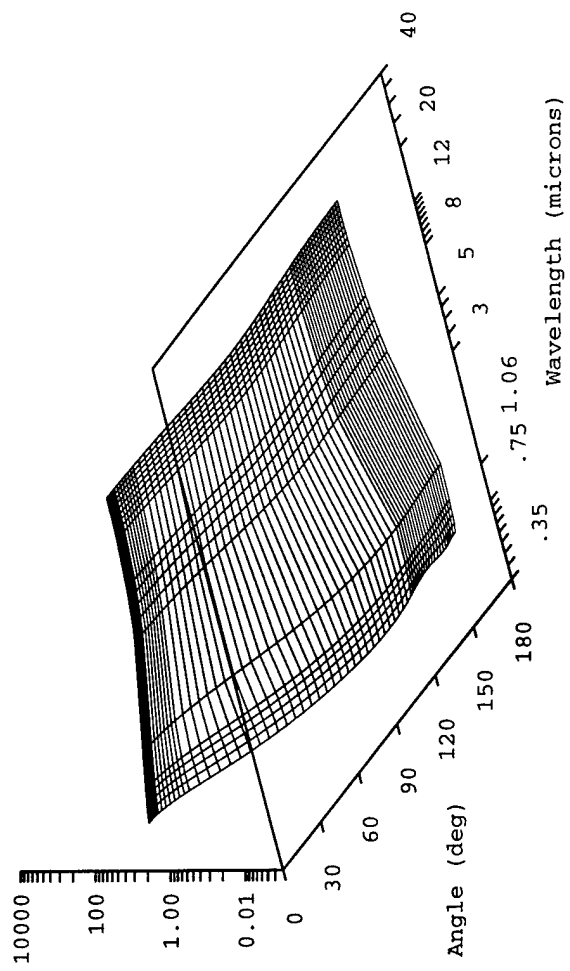


**Figure B-35.** Smoke (white phosphorous), 50 percent relative humidity.

White Phosphorus, 90% Rh EOSAEL 55

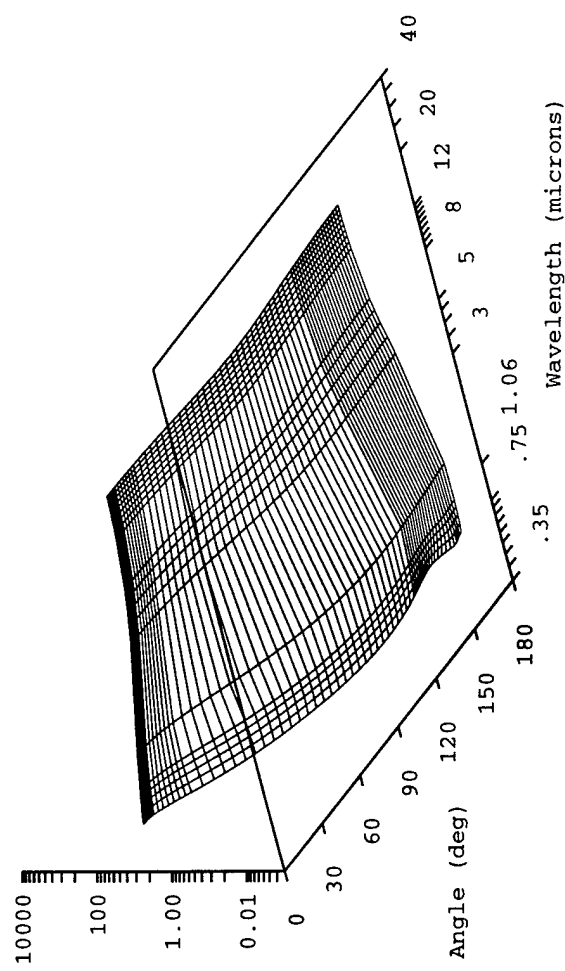


**Figure B-36.** Smoke (white phosphorous), 90 percent relative humidity.

Fog Oil Smoke, 50% Rh EOSAEL 56

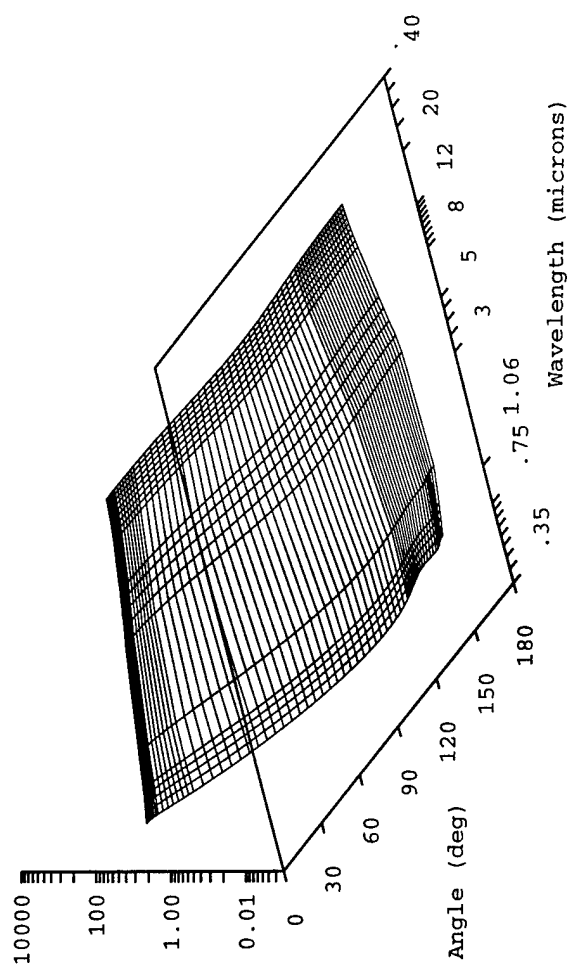


**Figure B-37.** Smoke (fog oil), 50 percent relative humidity.

HC Smoke, 85% Rh EOSAEL 57

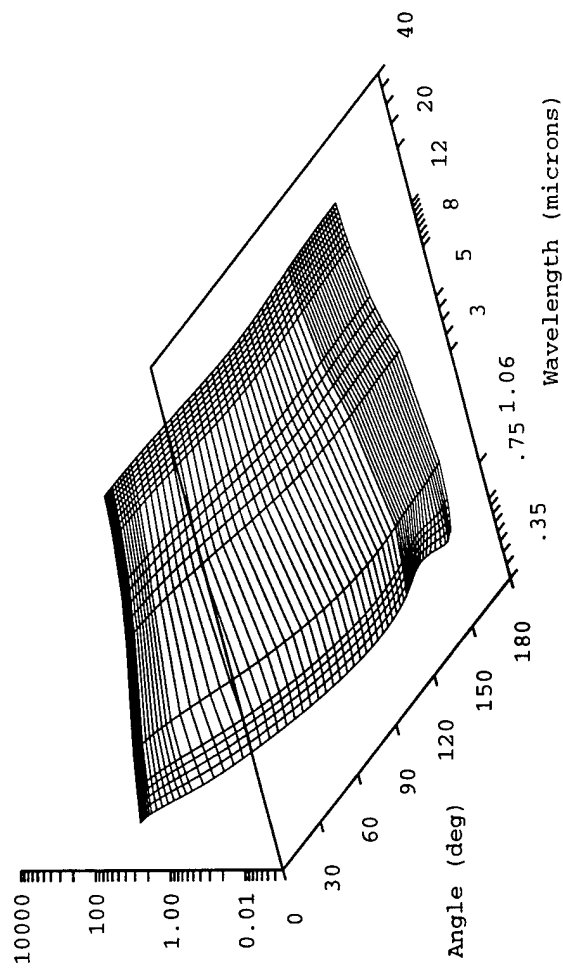


**Figure B-38.** Smoke (hexachloroethane), 85 percent relative humidity.

**This page left intentionally blank.**

## Appendix C EOSAEL MODULES

|        |  |
|--------|--|
| AGAUS  | Mie Scattering Code  |
| BITS   | Broad-band Integrated Transmittances                                     |
| ASCAT  | Approximate Multiple Scattering  |
| CLIMAT | Climatology  |
| CLTRAN | Transmission through Clouds  |
| COMBIC | Obscuration Model for Multiple Battlefield-Induced Contaminants          |
| COPTER | Obscuration due to Helicopter-Lofted Snow and Dust                       |
| FASCAT | Fast Algorithm for Atmospheric Scattering Calculations                   |
| FCLOUD | Transmission through Cloud of Ellipsoidal Geometry                       |
| OVRCST | Path Radiance/Contrast Beneath Overcast Conditions                       |
| FITTE  | Fire-Induced Transmission and Turbulence Effects                         |
| GRNADE | Smoke Munitions Self-Screening Applications                              |
| GSCAT  | Multiple Scattering using Gaussian Geometry                              |
| ILUMA  | Natural Illumination under Realistic Weather Conditions                  |
| IMTURB | Imaging Through Optical Turbulence                                       |
| KWIK   | Transmission Threshold Smoke Munitions Expenditures Model                |
| LASS   | Large Area Screening Systems Application                                 |
| LOWTRN | Atmospheric Transmittance and Radiance for Broadband Applications        |
| LZTRAN | Laser Transmittance-Gaseous Absorption Algorithm                         |
| MPLUME | Missile Smoke Plume Obscuration  |
| NBSCAT | Narrow Beam Multiple Scattering  |
| MSCAT  | Aerosol Multiple Scattering, Monte Carlo                                 |
| NMMW   | Near Millimeter Wave, Gaseous Absorption                                 |
| NOVAE  | Nonlinear Aerosol Vaporization and Breakdown Effects, High Energy Lasers |
| OVRCST | Contrast Transmission  |
| PFNDAT | Aerosol Phase Function Data Base   |
| RADAR  | Millimeter Wave System Performance                                       |
| REFRAC | Optical Path Bending Code for Near Earth Paths                           |
| TARGAC | Target Acquisition   |
| UVTRAN | Ultraviolet Transmission and Lidar Simulation                            |
| XSCALE | Natural Aerosol Extinction   |

**This page left intentionally blank.**

**Distribution**

**Copies**

|  |   |
|--|---|
| AEROSPACE<br>ATTN M DICKERSON<br>PO BOX 92957<br>LOS ANGELES CA 90009 2957                             | 1 |
| AEROSPACE<br>M4/954<br>ATTN C YINGER<br>PO BOX 92957<br>LOS ANGELES CA 90009                           | 1 |
| AEROSPACE CORP<br>M4/954<br>ATTN J LANGER<br>PO BOX 92957<br>LOS ANGELES CA 90009                      | 1 |
| AEROSPACE CORP<br>MS M4 944<br>ATTN J TOTH<br>PO BOX 92957<br>LOS ANGELES CA 90009 2957                | 1 |
| AFMC DOW<br>WRIGHT PATTERSON AFB OH 0334 5000  | 1 |
| AFSPC/DRFN<br>ATTN CAPT R KOON<br>150 VANDENBERG STRET STE 1105<br>WRIGHT PATTERSON AFB CO 80914 45900 | 1 |
| AIR WEATHER SERVICE<br>TECH LIBRARY FL4414 3<br>SCOTT AFB IL 62225 5458                                | 1 |

ALLEN'S TIME  
ATTN D ALLAN  
PO BOX 66  
FOUNTAIN GREEN UT 84632

1

AMC OMP/746 TS  
ATTN A CHASKO  
PO BOX 310  
HIGH ROLLS NM 88325

1

APPLIED RSRCH LAB UNIV OF TX  
ATTN B RENFRO  
PO BOX 8029  
AUSTIN TX 78713 8029

1

APPLIED RSRCH LAB UNIV OF TX  
ATTN J SAUNDERS  
PO BOX 8029  
AUSTIN TX 78713 8029

1

APPLIED RSRCH LAB UNIV OF TX  
ATTN R MACH  
PO BOX 8029  
AUSTIN TX 78713 8029

1

ARINC  
ATTN L CONOVER  
1925 AEROTECH DR STE 212  
COLORADO SPRINGS CO 80916

1

ARINC  
ATTN P MENDOZA  
4055 HANCOCK STRET  
SAN DIEGO CA 92110

1

ARL CHEMICAL BIOLOGY  
NUC EFFECTS DIV  
AMSRL SL CO  
APG MD 21010 5423

1

|   |   |
|---|---|
| ARMY ARDEC<br>SMCAR IMI I BLDG 59<br>DOVER NJ 07806 5000                                  | 1 |
| ARMY COMMUNICATIONS<br>ELECTR CTR FOR EW RSTA<br>AMSEL EW D<br>FT MONMOUTH NJ 07703 5303  | 1 |
| ARMY COMMUNICATIONS<br>ELECTR CTR FOR EW RSTA<br>AMSEL EW MD<br>FT MONMOUTH NJ 07703 5303 | 1 |
| ARMY CORPS OF ENGRS<br>ENGR TOPOGRAPHICS LAB<br>ETL GS LB<br>FT BELVOIR VA 22060          | 1 |
| ARMY DUGWAY PROVING GRD<br>STEDP 3<br>DUGWAY UT 84022 5000                                | 1 |
| ARMY DUGWAY PROVING GRD<br>STEDP MT DA L 3<br>DUGWAY UT 84022 5000                        | 1 |
| ARMY DUGWAY PROVING GRD<br>STEDP MT M<br>ATTN MR BOWERS<br>DUGWAY UT 84022 5000           | 1 |
| ARMY FIELD ARTLLRY SCHOOL<br>ATSF TSM TA<br>FT SILL OK 73503 5600                         | 1 |
| ARMY FOREGN SCI TECH CTR<br>CM<br>220 7TH STREET NE<br>CHARLOTTESVILLE VA 22901 5396      | 1 |

|  |   |
|--|---|
| ARMY INFANTRY<br>ATSH CD CS OR<br>ATTN DR E DUTOIT<br>FT BENNING GA 30905 5090               | 1 |
| ARMY MATERIEL SYST<br>ANALYSIS ACTIVITY<br>AMXSY<br>APG MD 21005 5071                        | 1 |
| ARMY MATERIEL SYST<br>ANALYSIS ACTIVITY<br>AMXSY AT<br>ATTN MR CAMPBELL<br>APG MD 21005 5071 | 1 |
| ARMY MATERIEL SYST<br>ANALYSIS ACTIVITY<br>AMXSY CR<br>ATTN MR MARCHET<br>APG MD 21005 5071  | 1 |
| ARMY MATERIEL SYST<br>ANALYSIS ACTIVITY<br>AMXSY CS<br>ATTN MR BRADLEY<br>APG MD 21005 5071  | 1 |
| ARMY MISSILE CMND<br>AMSMI<br>REDSTONE ARSENAL AL 35898 5243                                 | 1 |
| ARMY MISSILE CMND<br>AMSMI<br>REDSTONE ARSENAL AL 35898 5253                                 | 1 |
| ARMY MISSILE CMND<br>AMSMI RD AC AD<br>ATTN DR PETERSON<br>REDSTONE ARSENAL AL 35898 5242    | 1 |

|   |   |
|---|---|
| ARMY MISSILE CMND<br>AMSMI RD AS SS<br>ATTN MR H F ANDERSON<br>REDSTONE ARSENAL AL 35898 5253     | 1 |
| ARMY MISSILE CMND<br>AMSMI RD AS SS<br>ATTN MR B WILLIAMS<br>REDSTONE ARSENAL AL 35898 5253       | 1 |
| ARMY MISSILE CMND<br>AMSMI RD DE SE<br>ATTN MR GORDON LILL JR<br>REDSTONE ARSENAL AL 35898 5245   | 1 |
| ARMY MISSILE CMND<br>REDSTONE SCI INFO CTR<br>AMSMI RD CS R DOC<br>REDSTONE ARSENAL AL 35898 5241 | 1 |
| ARMY NUCLEAR CML AGCY<br>MONA ZB BLDG 2073<br>SPRINGFIELD VA 22150 3198                           | 1 |
| ARMY OEC<br>CSTE EFS<br>PARK CENTER IV<br>4501 FORD AVE<br>ALEXANDRIA VA 22302 1458               | 1 |
| ARMY RESEARCH LABORATORY<br>AMSRL<br>2800 POWDER MILL ROAD<br>ADELPHI MD 20783 1145               | 1 |
| ARMY RESEARCH LABORATORY<br>AMSRL BE E<br>BATTLEFIELD ENVIR DIR<br>WSMR NM 88002 5501             | 1 |

|  |    |
|--|----|
| ARMY RESEARCH LABORATORY<br>AMSRL BE S<br>BATTLEFIELD ENVIR DIR<br>WSMR NM 88002 5501                                | 1  |
| ARMY RESEARCH LABORATORY<br>AMSRL BE W<br>BATTLEFIELD ENVIR DIR<br>WSMR NM 88002 5501                                | 1  |
| ARMY RESEARCH LABORATORY<br>AMSRL D<br>2800 POWDER MILL ROAD<br>ADELPHI MD 20783 1145                                | 1  |
| ARMY RESEARCH LABORATORY<br>AMSRL OP CI SD TL<br>2800 POWDER MILL ROAD<br>ADELPHI MD 20783 1145                      | 1  |
| ARMY RESEARCH LABORATORY<br>AMSRL OP SD TP<br>TECHNICAL PUBLISHING<br>2800 POWDER MILL ROAD<br>ADELPHI MD 20783 1145 | 1  |
| ARMY RESEARCH LABORATORY<br>AMSRL SS SH<br>ATTN DR SZTANKAY<br>2800 POWDER MILL ROAD<br>ADELPHI MD 20783 1145        | 1  |
| ARMY RESEARCH LABORATORY<br>AMSRL IS ES<br>ATTN ALAN WETMORE<br>2800 POWDER MILL ROAD<br>ADELPHI MD 20783 1145       | 30 |

ARMY RESEARCH LABORATORY  
ELECTROMAG GROUP  
CAMPUS MAIL CODE F 0250 UNIVERSITY OF TX  
ATTN A TUCKER  
AUSTIN TX 78712

1

ARMY RESEARCH OFC  
ATTN AMXRO GS  
ATTN DR BACH  
PO BOX 12211  
RTP NC 27009

1

ARMY SATELLITE COMM AGCY  
DRCPM SC 3  
FT MONMOUTH NJ 07703 5303

1

ARMY STRAT DEFNS CMND  
CSSD SL L  
ATTN DR LILLY  
PO BOX 1500  
HUNTSVILLE AL 35807 3801

1

ARMY TOPO ENGR CTR  
CETEC ZC 1  
FT BELVOIR VA 22060 5546

1

ARMY TRADOC ANALYSIS CTR  
ATRC WSS R  
WSMR NM 88002 5502

1

ARPA  
ATTN L STOTTS  
J PENNELLA  
B KASPAR  
3701 N FAIRFAX DR  
ARLINGTON VA 22203 1714

1

|   |   |
|---|---|
| ASC OL/YUH<br>JDAM PIP<br>ATTN LT V JOLLEY<br>102 W D AVE<br>EGLIN AFB FL 32542   | 1 |
| ASHTECH INC<br>ATTN S GOUREVITCH<br>1177 KIFER RD<br>SUNNYVALE CA 94086   | 1 |
| ASST DPTY CG FOR RDE HDQTRS<br>US ARMY MATL CMND<br>AMCRD<br>ATTN COL S MANESS<br>5001 EISENHOWER AVE<br>ALEXANDRIA VA 22333 0001 | 1 |
| ATA ASSOC<br>ATTN M HARKINS<br>6800 BACKLICK RD<br>SPRINGFIELD VA 22150   | 1 |
| ATMOSPHERIC SCI DIV<br>GEOPHYSICS DIRCTRT<br>PHILLIPS LABORATORY<br>HANSCOM AFB MA 01731 5000                                     | 1 |
| BD SYSTEMS<br>ATTN J BUTTS<br>385 VAN NESS AVE #200<br>TORRANCE CA 90501  | 1 |
| CECOM<br>PM GPS<br>ATTN COL S YOUNG<br>FT MONMOUTH NJ 07703   | 1 |

|   |   |
|---|---|
| CMD (420000D(C0245))<br>ATTN DR A SHLANTA<br>NAV AIR WAR CEN WPN DIV<br>1 ADMIN CIR<br>CHINA LAKE CA 93555 6001 | 1 |
| DAMI POI<br>WASH DC 20310 1067  | 1 |
| DEAN RMD<br>ATTN DR GOMEZ<br>WASH DC 20314  | 1 |
| DEPT OF COMMERCE CTR<br>325 S BROADWAY<br>BOULDER CO 80303  | 1 |
| DEPT OF COMMERCE CTR<br>MOUNTAIN ADMINISTRATION<br>SPPRT CTR LIBRARY R 51<br>325 S BROADWAY<br>BOULDER CO 80303 | 1 |
| DEPT OF MATHEMATICAL SCIENCES<br>ATTN MDN A (MAJ DON ENGEN)<br>THAYER HALL<br>WEST POINT NY 10996 1786          | 1 |
| DEPT OF THE AIR FORCE<br>OL A 2D WEATHER SQUAD MAC<br>HOLLOWAY AFB NM 88330 5000                                | 1 |
| DMA<br>ATTN R KLOTZ<br>4211 BRIARS RD<br>ONLEY MD 20832 1814  | 1 |

DMA  
L A1  
ATTN B TALLMAN  
3200 2ND STRET  
ST LOUIS MO 63116 1

DMA  
L 41  
ATTN B HAGAN  
3200 S 2ND STRET  
ST LOUIS MO 63118 1

DMA  
L 41  
ATTN D MORGAN, F MUELLER  
3200 S 2ND STRET  
ST LOUIS MO 63118 1

DOT AFSPC/DRFN  
ATTN H SKALSKI  
150 VANDENBERG STET  
PETERSON AFB CO 80914 1

DPTY CG FOR RDE HDQTRS  
US ARMY MATL CMND  
AMCRD  
ATTN BG BEAUCHAMP  
5001 EISENHOWER AVE  
ALEXANDRIA VA 22333 0001 1

DPTY ASSIST SCY FOR RSRCH & TECHL  
SARD TT  
ATTN D CHAIT  
THE PENTAGON  
WASHINGTON DC 20310 0103 1

DPTY ASSIST SCY FOR RSRCH & TECHL  
SARD TT  
ATTN F MILTON RM  
3E479  
THE PENTAGON  
WASHINGTON DC 20310 0103

1

DPTY ASSIST SCY FOR RSRCH & TECHL  
SARDTT  
ATTN T KILLION  
THE PENTAGON  
WASHINGTON DC 20310 0103

1

DPTY ASSIST SCY FOR RSRCH & TECHL  
SARD TT  
ATTN K KOMINOS  
THE PENTAGON  
WASHINGTON DC 20310 0103

1

DPTY ASSIST SCY FOR RSRCH & TECHL  
SARD TT  
ATTN B REISMAN  
THE PENTAGON  
WASHINGTON DC 20310 0103

1

DR HANS J LIEBE  
NTIA ITS S 3  
325 S BROADWAY  
BOULDER CO 80303

1

DR JERRY DAVIS  
NCSU  
PO BOX 8208  
RALEIGH NC 27650 8208

1

DTIC  
8725 JOHN J. KINGMAN RD  
STE 0944  
FT BELVOIR VA 22060 6218

1

DUSD SPACE  
1E765  
ATTN J G MCNEFF  
3900 DEFENSE PENTAGON  
WASHINGTON DC 20301 3900

1

ELECTRONIC SYSTEMS DIV DIR  
CECOM RDEC  
ATTN J NIEMELA  
FT MONMOUTH NJ 07703

1

G GIBBONS  
859 WILLIAMETTE STRT  
EUGENE OR 97401 6806

1

GPS JOINT PROG OFC DIR  
ATTN COL J CLAY  
2435 VELA WAY STE 1613  
LOS ANGELES AFB CA 90245 5500

1

HEWLETT PACKARD CO  
ATTN J KUSTERS  
5301 STEVENS CREED BLVD  
SANTA CLARA CA 95052

1

HOLLOMAN AFB  
ATTN K WERNIE  
1644 VANDERGRIFT RD  
HOLLOMAN AFB NM 88330 7850

1

HQ AWS DOO 1  
SCOTT AFB IL 62225 5008

1

HUGHES AIRCRAFT  
ATTN R MALLA 1  
800 APOLLO AVE  
PO BOX 902  
EL SEGUNDO CA 90245

HUGHES AIRCRAFT  
ATTN S PECK 1  
800 APOLLO AVE  
PO BOX 902  
EL SEGUNDO CA 90245

HUGHES SPACE & COMM  
MS/SC/SIO/S364 1  
ATTN C SHEKLELLS  
PO BOX 92919 AIRPORT STATION  
LOS ANGELES CA 90009

INTERMETRICS INC  
ATTN J MCGOWAN 1  
615 HOPE RD BLDG 4 2ND FLOOR  
EATONTOWN NJ 07724

ITT AEROSPACE  
ATTN P BRODIE 1  
100 KINGSLAND RD  
CLIFTON NJ 07014

ITT AEROSPACE  
MS 8538 1  
ATTN L DOYLE  
100 KINGSLAND RD  
CLIFTON NJ 07014

ITT AEROSPACE  
MS 2511 1  
ATTN R PELLER  
100 KINGSLAND RD  
CLIFTON NM 07014

ITT AEROSPACE  
MS 8528  
ATTN H RAWICZ  
100 KINGSLAND RD  
CLIFTON NJ 07014

1

KERNCO  
ATTN R KERN  
28 HARBOR STRET  
DANVERS MA 01923

1

LOCKHEED MARTIN  
ATTN B MARQUIS  
1250 ACADEMY PARK LOOP 101  
COLORADO SPRINGS CO 80912

1

LOCKHEED MARTIN  
ATTN J TAYLOR  
1250 ACADEMY PARK LOOP STE 101  
COLORADO SPRINGS CO 80910

1

LORAL  
ATTN B MATHON  
700 N FREDERICK PIKE  
GAIITHERSBURG MD 20879

1

LORAL  
B PISOR  
2915 BASELINE RD 530  
BOULDER CO 80303

1

LORAL FEDERAL SYSTEMS  
ATTN R ASTALOS  
9970 FEDERAL DR  
COLORADO SPRINGS CO 80921

1

LORAL FEDERAL SYSTEMS  
ATTN M BAKER  
9970 FEDERAL DR  
COLORADO SPRINGS CO 80921

1

LORAL FEDERAL SYSTEMS  
ATTN J KANE  
9970 FEDERAL DR  
COLORADO SPRINGS CO 80921

1

METEOROLOGIST IN CHARGE  
KWAJALEIN MISSILE RANGE  
PO BOX 67  
APO SAN FRANCISCO CA 96555

1

MIL ASST FOR ENV SCI OFC  
OF THE UNDERSEC OF DEFNS  
FOR RSCH & ENGR R&AT E LS  
PENTAGON ROOM 3D129  
WASH DC 20301 3080

1

NASA SPACE FLT CTR  
ATMOSPHERIC SCIENCES DIV  
CODE ED 41 1  
HUNTSVILLE AL 35812

1

NASA MARSHAL SPACE FLT CTR  
ATMOSPHERIC SCIENCES DIV  
E501  
ATTN DR FICHTL  
HUNTSVILLE AL 35802

1

NATIONAL SECURITY AGCY W21  
ATTN DR LONGBOTHUM  
9800 SAVAGE ROAD  
FT GEORGE G MEADE MD 20755 6000

1

NAVAL AIR DEV CTR  
CODE 5012  
ATTN AL SALIK  
WARMINISTER PA 18974

1

NAVAL OCEAN SYST CTR  
CODE 54  
ATTN DR RICHTER  
SAN DIEGO CA 92152 5000

1

|   |   |
|---|---|
| NAV RSRCH LAB<br>CODE 8150/SFA<br>ATTN J BUISSON<br>4555 OVERLOOK DR SW<br>WASHINGTON DC 20375 5354 | 1 |
| NAV RSRCH LAB<br>ATTN W REID<br>4333 OVERLOOK DR SW<br>WASHINGTON DC 20375                          | 1 |
| NAV SURFACE WEAPONS CTR<br>CODE G63<br>DAHLGREN VA 22448 5000                                       | 1 |
| NAV SURFACE WARFARE CTR<br>CODE K12<br>ATTN E SWIFT<br>17320 DAHLGREN RD<br>DAHLGREN VA 22448 5100  | 1 |
| NIST<br>MS 847.5<br>ATTN M WEISS<br>325 BROADWAY<br>BOULDER CO 80303                                | 1 |
| NCAR LIBRARY SERIALS<br>NATL CTR FOR ATMOS RSCH<br>PO BOX 3000<br>BOULDER CO 80307 3000             | 1 |
| ODCSOPS<br>ATTN BG ROSE, D DSCHMIDT<br>WASHINGTON DC 20310 1001                                     | 1 |
| OIC NAVSWC<br>TECH LIBRARY CODE E 232<br>SILVER SPRINGS MD 20903 5000                               | 1 |

|  |   |
|--|---|
| ONR 331<br>ATTN H PILLOFF<br>800 N QUINCY STRET<br>ARLINGTON VA 22217                            | 1 |
| OSD<br>OUSD (A&T)/ODDDR&E(R)<br>ATTN J LUPO<br>THE PENTAGON<br>WASHINGTON DC 20301 7000          | 1 |
| OVERLOOK SYSTEMS<br>ATTN D BROWN<br>1150 ACADEMY PARK LOOP STE 114<br>COLORADO SPRINGS CO 80910  | 1 |
| OVERLOOK SYSTEMS<br>ATTN T OCVIRK<br>1150 ACADEMY PARK LOOP STE 114<br>COLORADO SPRINGS CO 80910 | 1 |
| PACIFIC MISSILE TEST CTR<br>GEOPHYSICS DIV<br>ATTN CODE 3250<br>POINT MUGU CA 93042 5000         | 1 |
| PAQ COMMCTN<br>ATTN Q HUA<br>607 SHETLAND CT<br>MILPTAS CA 95035                                 | 1 |
| PHILLIPS LABORATORY<br>PL LYP<br>ATTN MR CHISHOLM<br>HANSCOM AFB MA 01731 5000                   | 1 |
| PHILLIPS LABORATORY<br>PL LYP 3<br>HANSCOM AFB MA 01731 5000                                     | 1 |
| PL WE<br>KIRTLAND AFB NM 87118 6008  | 1 |

PRIN DPTY FOR ACQUISITION HDQTRS  
US ARMY MATL CMND  
AMCDCG A  
ATTN D ADAMS  
5001 EISENHOWER AVE  
ALEXANDRIA VA 22333 0001

1

PRIN DPTY FOR TECHLGY HDQTRS  
US ARMY MATL CMND  
AMCDCG T  
ATTN M FISSETTE  
5001 EISENHOWER AVE  
ALEXANDRIA VA 22333 0001

1

ROCKWELL CACD  
ATTN L BURNS  
400 COLLINS RD NE  
CEDAR RAPIDS IA 52398

1

ROCKWELL COLLINS  
ATTN C MASKO  
400 COLLINS RD NE  
CEDAR RAPIDS IA 52498

1

ROCKWELL DA85  
ATTN W EMMER  
12214 LAKEWOOD BLVD  
DOWNEY CA 92104

1

ROCKWELL SPACE OPS CO  
ATTN B CARLSON  
442 DISCOVERER AVE STE 38  
FALSON AFB CO 80912 4438

1

ROCKWELL SPACE OPS CO  
AFMC SSSG DET 2/NOSO/ROCKWELL  
ATTN R SMETEK  
442 DISCOVERER AVE STE 38  
FALSON AFB CO 80912 4438

1

ROCKWELL SPACE SYSTEMS  
MAILCODE 841 DA49  
ATTN D MCMURRAY  
12214 LAKEWOOD BLVD  
DOWNEY CA 90241

1

SCI AND TECHNOLOGY  
101 RESEARCH DRIVE  
HAMPTON VA 23666 1340

1

SP & TERRESTRIAL COMMCTN DIV  
AMSEL RD ST MC M  
ATTN H SOICHER  
FT MONMOUTH NJ 07703 5203

1

SPACE ENVIRONMENT LAB/NOAA  
R/E/SE  
ATTN J KUNCHES  
325 BROADWAY  
BOULDER CO 80303

1

SPECIAL ASSIST TO THE WING CMNDR  
50SW/CCX  
ATTN CAPT H BERNSTEIN  
300 O'MALLEY AVE STE 20  
FALCON AFB CO 80912 3020

1

SRI  
M/S BS378  
ATTN M MOEGLEIN  
333 RAVENSWOOD AVE  
MENLO PARK CA 94025

1

STANFORD TELECOM  
ATTN BF SMITH  
1221 CROSSMAN AVE  
SUNNYVALE CA 94088

1

STANFORD UNIVERSITY  
HELP/GP B  
ATTN D LAWRENCE  
STANFORD CA 94305 4085

1

STANFORD UNIVERSITY  
HEPL/GP B  
ATTN T WALTER  
STANFORD CA 94305 4085

1

TASC  
ATTN T BARTHOLOMEW  
1190 WINTERSON RD  
LINTHICUM MD 21090

1

TRIMBLE NAV  
ATTN L KRUCZYNSKI  
585 N MARY  
SUNNYVALE CA 94086

1

TRIMBLE NAV  
ATTN P TURNER  
585 N MARY  
SUNNYVALE CA 94086

1

USAASA  
MOAS AI  
ATTN W PARRON  
9325 GUNSTON RD STE N319  
FT BELVOIR VA 22060 5582

1

USAF ROME LAB TECH  
CORRIDOR W STE 262 RL SUL  
26 ELECTR PKWY BLD 106  
GRIFFISS AFB NY 13441 4514

1

USAF SMC/CED  
DMA/JPO ATTN M ISON  
2435 VELA WAY STE 1613  
LOS ANGELES AFB CA 90245 5500

1

USAFETAC DNE  
ATTN MR GLAUBER  
SCOTT AFB IL 62225 5008

1

US ARMY CECRL  
CECRL GP  
ATTN DR DETSCH  
HANOVER NH 03755 1290

1

USATRADOC  
ATCD FA  
FT MONROE VA 23651 5170

1

USNO  
ATTN B BOLLWERK  
5580 PIEDRA VISTA  
COLORADO SPRINGS CO 80908

1

WSMR TECH LIBRARY BR  
STEWs IM IT  
WSMR NM 88001

1

Record Copy

1

TOTAL

186